Aus dem Zentrum für Endokrinologie,
Diabetologie und Präventivmedizin
der Universität zu Köln
Direktor: Universitätsprofessor Dr. med. J. Brüning

Generation of conditional CRISPR Cas9 mediated knockout mice without off-target effects using the traffic light system

Inaugural-Dissertation zur Erlangung der Doktorwürde
der Medizinischen Fakultät
der Universität zu Köln

vorgelegt von
Shu Wang
aus Sichuan China

promoviert am 05. September 2024

Gedruckt mit Genehmigung der Medizinischen Fakultät der Universität zu Köln

2024

Dekan: Universitätsprofessor Dr. med. G. R. Fink

1. Gutachter: Universitätsprofessor Dr. med. J. C. Brüning
2. Gutachter: Universitätsprofessor Dr. rer. nat. B. Zevnik

Erklärung

Ich erkläre hiermit, dass ich die vorliegende Dissertationsschrift ohne unzulässige Hilfe Dritter und ohne Benutzung anderer als der angegebenen Hilfsmittel angefertigt habe; die aus fremden Quellen direkt oder indirekt übernommenen Gedanken sind als solche kenntlich gemacht.
Bei der Auswahl und Auswertung des Materials sowie bei der Herstellung des Manuskriptes habe ich keine Unterstützungsleistungen.
Weitere Personen waren an der Erstellung der vorliegenden Arbeit nicht beteiligt. Insbesondere habe ich nicht die Hilfe einer Promotionsberaterin/eines Promotionsberaters in Anspruch genommen. Dritte haben von mir weder unmittelbar noch mittelbar geldwerte Leistungen für Arbeiten erhalten, die im Zusammenhang mit dem Inhalt der vorgelegten Dissertationsschrift stehen.
Die Dissertationsschrift wurde von mir bisher weder im Inland noch im Ausland in gleicher oder ähnlicher Form einer anderen Prüfungsbehörde vorgelegt.
Der dieser Arbeit zugrunde liegende Versuchsaufbau wurde von mir unter der Leitung von Professor F. Thomas Wunderlich erstellt. Ich habe die Messung, Sammlung und Statistik der experimentellen Daten selbstständig durchgeführt. Die Labortechniker: Herr Patrick Jankowski und Frau Laura Kunz haben mit mir zusammengearbeitet, um die Zellkultur und Färbung von Gewebeschnitten durchzuführen.
Ich erkläre hiermit, dass ich die Ordnung zur Sicherung guter wissenschaftlicher Praxis und zum Umgang mit wissenschaftlichem Fehlverhalten (Amtliche Mitteilung der Universität zu Köln AM 132/2020) der Universität zu Köln gelesen habe und verpflichte mich hiermit, die dort genannten Vorgaben bei allen wissenschaftlichen Tätigkeiten zu beachten und umzusetzen.

Köln, Mai 2024

Shu Wang

DANKSAGUNG

Zunächst möchte ich mich bei meinem Betreuer, Prof. Dr. Jens C. Brüning, bedanken, der es mir ermöglicht hat, am MPI-MR teilzunehmen und mich als klinischer Arzt mit wissenschaftlichem Verständnis weiterzuentwickeln. Es war ein Privileg, an großartigen Konferenzen teilzunehmen, spannende Diskussionen zu führen und ihre ansteckende Begeisterung für die Wissenschaft zu teilen. Ich möchte mich auch dafür bedanken, dass ich meine eigenen Ideen einbringen kann, dass Sie selbstständig arbeiten und bei Bedarf Rat und Unterstützung erhalten. Unter Ihrer Anleitung wurde ich nachdrücklich ermutigt, eine akademische und klinische Karriere in China einzuschlagen. Ich freue mich auch, meinen Betreuern, Prof. Dr. Jens C. Brüning und Prof. Dr. F. Thomas, für ihre Unterstützung und Beratung sowie ihre Bereitschaft zur kritischen Überarbeitung der Manuskripte zu danken. Ich möchte den Menschen danken, die zum erfolgreichen Verlauf der STAT5 MASH-und sCas9-Projekte beigetragen haben: Claudia Wunderlich, Lionel Lattenist, Leonie Schroers, Peter Wienand, Patricia Schmidt, Christian Vossen, Bianca Haracska, Melika Irani, Lenzen Beate, Klingenberg, Laura Kunz, Anke Lietzau, Heike Krämer, Vivien Kohlhaas, Linyan Shen, Yiyi Zhu, Weiyi Chen, Cao Ding, Shuntaro Izawa, Putu Sicilia Subagia, Jens Alber, Christiane Schäfer, Pia Scholl, Katharina Gleich und alle Leute vom MPI-MR.

Besonderer Dank geht an Melanie J. åMittenbühler, Rui Beleza und Fenselaus Gruppe für die Bereitstellung von Plasmiden und Zellen, die es mir ermöglichten, diese zu aktualisieren und zu testen. Besonderer Dank gilt auch dem Professor Branko Zevnik für seine geduldige und sorgfältige Überprüfung des Entwurfs meiner Abschlussarbeit.

Ein besonderer Dank gilt an dieser Stelle auch allen Mitarbeitern des Büros für internationale Studierende der Universität zu Köln und des MD-Büros der Medizinischen Fakultät. Obwohl wir nie maskiert waren, haben Ihre rechtzeitigen Antworten und Antworten auf jede meiner E-Mails in den letzten drei Jahren mich als internationalen Studenten warm gemacht.

Abschließend möchte ich meiner Familie für ihre Unterstützung und Ermutigung während meines mehr als dreijährigen Auslandsstudiums danken. Ohne dich bin ich nichts. Ich möchte auch ein berühmtes Zitat von Haruki Murakami zitieren: "Wenn der Sturm vorbei ist, erinnerst du dich nicht mehr, wie du ihn verbracht hast, du bist nicht einmal sicher, ob der Sturm wirklich vorbei ist, aber du bist nicht mehr derjenige, der in den Sturm eingetreten ist."

Table of Contents

List of Figures

List of Tables

Abbreviations

Abbreviation	Meaning
°C	Degree Celsius
AAV	Adeno-associated virus
ALT	Alanine aminotransferase
AMPK	5’ adenosine monophosphate-activated protein kinase
Arg1	Arginase, liver
AST	Aspartate aminotransferase
Bcl6	B cell leukemia/lymphoma 6
BSA	Bovine serum albumin
BW	Bodyweight
Cas9	CRISPR-associated
CD	Control diet
Cd36	CD36 antigen
Cdkn1a	Cyclin-dependent kinase inhibitor 1A (P21)
Cdkn1b	Cyclin-dependent kinase inhibitor 1B
Cdkn2a	Cyclin-dependent kinase inhibitor 2A
Cdkn2b	Cyclin-dependent kinase inhibitor 2B (p15, inhibits CDK4)
cDNA	Complementary DNA
Clec4f	C-type lectin domain family 4 member F
Cish	Cytokine inducible SH2-containing protein
Col1a1	Collagen, type I, alpha 1
Col1a2	Collagen, type I, alpha 2
Cre	Cyclization Recombination Enzyme
CRISPR	Clustered regularly interspaced short palindromic repeat
CRL	Cullin-RING ubiquitin ligase
Ctgf	Connective tissue growth factor
Ctrl	Control
Cxc3rl	C-X3-C motif chemokine ligand 1

DEN	Diethylnitrosamine
DMEM	Dulbecco's Modified Eagle Medium
DMSO	Dimethylsulfoxide
DNA	Deoxyribonucleic acid
Dre	D6 site-specific DNA recombinas
dNTP	Deoxynucleoside triphosphates
E	Eosin
EDTA	Ethylenediaminetetraacetate
Egfr	Epidermal growth factor receptor
ELISA	Enzyme-linked immunosorbent assay
Emr1	EGF-like module containing, mucin-like, hormone receptor-like 1
ES-cells	Embryonic stem cells
Fabp1	Fatty acid binding protein 1, adipocyte (AP2)
Fasn	Fatty acid synthase
FFA	Free fatty acids
FGF	Human fibroblast growth factor
G6pc	Glucose-6-phosphatase catalytic subunit
GFP	Green fluorescent protein
gRNA	Guide RNA
GTT	Glucose tolerance test
h	Hour
H	Hematoxylin
HCC	Hepatocellular carcinoma
HDR	Homology-directed repair
HFD	High-fat diet
HIF	Hypoxia-inducible factor
i.p.	Intraperitoneal
IGF-1	Insulin-like growth factor 1
IL1b	Interleukin 1beta
IL6	Interleukin 6

Ifng	Interferon gamma
ITT	Insulin tolerance test
JAK	Janus kinase
KO	Knockout
loxP	Locus of crossing over x, P1
MAFLD	Metabolic dysfunction associated fatty liver disease
MASLD	Metabolic dysfunction-associated steatotic liver disease
MASH	Metabolic dysfunction-associated steatohepatitis
MEF	Mouse embryonic fibroblasts
min	Minute
ml	Milliliter
mM	Millimolar
Mmp2	Matrix metallopeptidase 2
Mmp9	Matrix metallopeptidase 9
mRNA	Messenger RNA
NaCl	Sodium chloride
NAFLD	Non-alcoholic fatty liver disease
neo	Neomycin resistance cassette
NER	Nucleotide excision repair
NHEJ	Nonhomologous end joining
NLS	Nuclear localization signal
NMR	Nuclear magnetic resonance
Nos2	Nitric oxide synthase 2, inducible
NOT	Negative on TATA
Onecut	One cut domain, family member 3
PAM	Protospacer adjacent motif
PBS	Phosphate buffered saline
Pck1	Phosphoenolpyruvate Carboxykinase 1
PCR	Polymerase chain reaction
PFA	Paraformaldehyde

Ppara	Peroxisome proliferator activated receptor alpha
qRT-PCR	Real-time polymerase chain reaction
RNA	Ribonucleic acid
rox	Rox-DNA-binding Element
rpm	Rounds per minute
RT	Room temperature
Scd1	Stearoyl-Coenzyme A desaturase 1
SD	Standard deviation
SDS-PAGE	Sodium dodecyl sulfate polyacrylamide gel electrophoresis
Sec	Second
Socs2	Suppressor of cytokine signaling 2
Srebf1	Sterol regulatory element binding factor 1
STAT5	Signal transducer and activator of transcription 5
Tgfb1	Transforming growth factor, beta 1
Timp1	Tissue inhibitor of metalloproteinase 1
TNFα	Tumor necrosis factor-alpha
tRNA	Transfer RNA
UTR	Untranslated region
V	Volt
WAT	White adipose tissue
µg	Microgram
µl	Microliter

ABSTRACT

CRISPR/Cas9 technologies can be used to disrupt genes in specific murine cell types which express Cas9 and a gRNA against the gene of interest. However, proper gRNA delivery and the genetic lesions induced by Cas9 cannot be monitored in vivo yet, and there might be off target effects of excessive Cas9/gRNA in the cell type. To this end, a ROSA26 locus-driven, self-destructing sCas9-P2A-AAVR-E2AtdTOMATO construct has been developed that can be activated by Cre- and Dre-mediated recombination. Cre/Dre-mediated excision of loxP- and rox-flanked stop cassettes lead to the compound expression of sCas9, AAVR, and tdTOMATO in cells expressing both recombinases. Specific gRNAs against sCas9/tdTomato and gene of interest are delivered via adeno-associated viruses (AAV) that will be efficiently bound by the AAV receptor AAVR co-expressed with sCas9 and tdTOMATO. Moreover, delivery of AAVs carrying U6-driven gRNAs against sCas9/td tdTomato and the gene of interest as well as Cre, Dre or Cre/Dre inducible ZsGreen cassettes indicates Cas9 activity via a red to green switch in fluorescence, owing to the self-destruction of sCas9/tdTOMATO and activation of ZsGreen expression. This novel traffic light system allows for monitoring gene editing using sCas9 to be restricted to specific cell types and to limit the off-target effects of Cas9 on the genome by self-destructing the Cas9 (sCas9) protein.

Metabolic dysfunction-associated steatotic liver disease (MASLD) is a growing health problem in many countries. The first stage of MASLD is characterized by excessive fat accumulation in hepatocytes, the main cell type of the liver followed by the second stage of inflammation, which is the stage of metabolic dysfunction-associated steatohepatitis (MASH) that can further progress to the third liver fibrosis stage. However, the molecular mechanisms driving the development of MASH are not completely understood. We investigated the role of STAT5 in MASH by analyzing hepatocyte-specific STAT5-specific knockout mice on metabolic and fibrotic MASH diets. Our data suggest that independent under which dietary regimen, hepatic STAT5-deficient ($STAT5^{LKO}$) mice exhibited increased lipid droplet deposition and inflammatory cell infiltration in the liver compared with the $STAT5^{fl/fl}$ mice. Interestingly, under fibrotic diet-fed condition, the expression of genes was markedly reduced in the $STAT5^{LKO}$ mice. On the contrary, under NCD and MASH-Ctrl conditions, $STAT5^{LKO}$ mice showed elevated fibrosis gene expression compared with Ctrl mice. Thus, hepatic STAT5 silencing may play a dual role in different dietary interventions during the development of liver disease.

1. ZUSAMMENFASSUNG

CRISPR/Cas9-Technologien können verwendet werden, um Gene in bestimmten murinen Zelltypen zu zerstören, die Cas9 und eine gRNA gegen das interessierende Gen exprimieren. Die ordnungsgemäße gRNA-Abgabe und die durch Cas9 induzierten genetischen Läsionen können jedoch noch nicht in vivo überwacht werden, und es kann zu unerwünschten Auswirkungen übermäßiger Cas9/gRNA im Zelltyp kommen. Zu diesem Zweck wurde ein ROSA26-Locus-gesteuertes, selbstzerstörendes sCas9-P2A-AAVR-E2AtdTomato -Konstrukt entwickelt, das durch Cre- und Dre-vermittelte Rekombination aktiviert werden kann. Die Cre/Dre-vermittelte Entfernung von loxP- und rox-flankierten Stoppkassetten führte zur zusammengesetzten Expression von sCas9, AAVR und tdTomato in Zellen, die beide Rekombinasen exprimieren. Spezifische gRNAs gegen sCas9/tdTomato und gegen das Gen von Interesse werden über Adeno-assoziierte Viren (AAV) übertragen, die effizient an den AAV-Rezeptor AAVR gebunden werden, der zusammen mit sCas9 und tdTomato exprimiert wird. Darüber hinaus weist die Lieferung von AAVs, die U6-gesteuerte gRNAs gegen sCas9/tdTomato und das interessierende Gen sowie Cre-, Dre- oder Cre/Dre-induzierbare ZsGreen-Kassetten tragen, auf Cas9-Aktivität über einen Rot-Grün-Schalter in der Fluoreszenz aufgrund der Selbstzerstörung von hin sCas9/ tdTomato und Aktivierung der ZsGreen-Expression. Dieses neuartige Ampelsystem ermöglicht es, die Überwachung der Genbearbeitung mithilfe von sCas9 auf bestimmte Zelltypen zu beschränken und die Off-Target-Effekte von Cas9 auf das Genom durch Selbstzerstörung des Cas9 (sCas9) -Proteins zu begrenzen.

Die metabolische Dysfunktion-assoziierte steatotische Lebererkrankung (MASLD) ist in vielen Ländern ein wachsendes Gesundheitsproblem. Das erste Stadium der MASLD ist durch eine übermäßige Fettansammlung in Hepatozyten, dem Hauptzelltyp der Leber, gekennzeichnet, gefolgt vom zweiten Stadium der Entzündung, dem Stadium der metabolischen Dysfunktions-assoziierten Steatohepatitis (MASH), das sich weiter auf die dritte Leber ausbreiten kann Fibrosestadium. Allerdings sind die molekularen Mechanismen, die die Entwicklung von MASH vorantreiben, nicht vollständig geklärt. Wir untersuchten die Rolle von STAT5 bei MASH, indem wir Hepatozyten-spezifische STAT5-spezifische Knockout-Mäuse unter metabolischer und fibrotischer MASH-Diät analysierten. Unsere Daten deuten darauf hin, dass Mäuse mit hepatischem STAT5-Mangel ($STAT5^{LKO}$) unabhängig von der Ernährungsweise im Vergleich zu $STAT5^{fl/fl}$-Mäusen eine erhöhte Ablagerung von Lipidtröpfchen und eine Infiltration entzündlicher Zellen in der Leber aufwiesen. Interessanterweise war die Expression von Genen bei $STAT5^{LKO}$-Mäusen unter fibrotischer Ernährung deutlich reduziert. Im Gegenteil, unter NCD- und MASH-Ctrl-Bedingungen zeigten $STAT5^{LKO}$-Mäuse im Vergleich zu Ctrl-Mäusen eine erhöhte Fibrose-Genexpression. Daher kann die hepatische STAT5-

Stummschaltung bei verschiedenen diätetischen Eingriffen während der Entwicklung einer Lebererkrankung eine doppelte Rolle spielen.

2. INTRODUCTION

This doctoral thesis is divided into two parts.

Part I: Generation of conditional CRISPR/Cas9 mediated knockout mice without off-target effects using the novel traffic light system

Part II: Investigating the role of STAT5 in MASH

2.1. Genetic Engineering

Conditional mutagenesis based on the Cre/loxP system has enabled researchers to define the function of specific genes in a cell type and/or inducible manner[1]. The Cre/loxP system was the gold standard provided by expert researchers to investigate gene function until recently, when the novel, revolutionizing technology called clustered regularly interspaced short palindromic repeats (CRISPR)/CRISPR-associated (Cas) was developed. This technology enables the easy editing of the genome and learning more about specific gene functions in health and disease.

2.1.1. Cre/loxP and Dre/rox System

In the Cre/loxP system, P1 bacteriophages express the Cre recombinase capable of recombining specific loxP sites[2]. The Cre/loxP system plays an important role in regulating the life cycle of bacteriophage P1. This system was successfully used to edit genes in vivo in mice by the generation of countless Cre-driver mice and mice carrying loxP-flanked essential exons of genes (floxed mice)[3]. In detail, two components of this system must be assembled to produce a conditional knockout mouse: First, mice in which the loxP sites are inserted on both sides of a specific locus, usually flank one or several exons in the gene of interest (GOI). Secondly, to excise the sequence between the loxP sites, the cells or animals must simultaneously express the Cre recombinase. Both Cre-driver and floxed mouse lines have been separately generated by conventional embryonic stem cell (ES) targeting or conventional transgenesis approaches[4, 5]. Finally, knockout mice for the respective GOI are generated by intercrossing Cre and floxed mice. A tissue-specific or inducible promoter can control the Cre gene to generate tissue-specific conditional knockout mice[4, 6, 7].

Dre (D6 site-specific DNA recombinase) is also a tyrosine recombinase discovered from a phage that recognizes a 32bp DNA sequence rox consisting of two 14bp reverse palindromic sequences and a 4bp intermediate spacer sequence[8, 9]. Dre recombinase and Cre recombinase are specific, Dre recombinase cannot recognize the loxP site, and Cre recombinase cannot recognize rox site. So Cre-loxp and Cre-rox are independent and complementary systems. We can use them to edit two different genes in the same cell simultaneously or separately.

One way to control the expression of the GOI in a tissue-specific way is to introduce a loxP-flanked stop cassette before the GOI that can be excised by Cre recombinase in a tissue-specific way. The ROSA 26 locus, ubiquitously expressed but not translated into a protein, is commonly used as a safe harbor to introduce genes or foreign transgenes[10-12]. Moreover, other recombinase systems have been developed upon successfully using the Cre/loxP system, among which the Dre/rox system has demonstrated similar efficiency[13]. Combination of these recombinase systems allows for more cell type-specific activation of transgenes by utilizing overlapping promoters that drive expression of Cre and Dre with effector transgenes whose expression is prevented by two STOP cassettes that are flanked by loxP and rox sites, respectively[14]. Thus, Cre/loxP and Dre/rox technology are powerful tools for studying gene functions *in vitro* and *in vivo*. However, introducing the specific genetic manipulation to generate Cre, Dre, or loxP, rox sites via ES cell gene targeting is time- and resource-consuming and can last for several months.

2.1.2. CRISPR/Cas9 System

The CRISPR/Cas9 system is derived from the immune systems of bacteria and archaea, which protect them against bacteriophage infections by cleaving foreign DNA[15]. In detail, it consists of short, repeated, conserved sequences, separated by unique spacers, which are usually derived from viral or plasmid DNA and the Cas9 nuclease[16, 17]. When infected with viral DNA, Cas recognizes and cleaves the foreign DNA at specific protospacer adjacent motifs (PAM) within the viral genome[18, 19]. Afterward, the cleaved protospacers are incorporated into a CRISPR array without the PAM sequence and are referred to as spacers. In addition, the spacers are transcribed into CRISPR RNA precursors (pre-crRNA) and hybridize with transactivating CRISPR RNA (tracrRNA)[18, 19]. In the next step, endogenous RNase II cleaves the pre-crRNA-tracrRNA complex, resulting in mature crRNA[18, 19]. The mature crRNA binds to the Cas9 protein, guiding it to the complementary foreign DNA. Cas9 mediates the cleavage of the DNA double-strand, preventing virus replication and activity[16, 20]. As of 2013, the CRISPR/Cas system has been engineered for genome editing[21]. However, the CRISPR Cas9 system can also be utilized in mammalian cells, providing an easy and fast effort to disrupt genes *in vivo.* For this purpose, Cas9 nuclease and guide RNA (gRNA), which consists of crRNA and tracrRNA, are expressed or delivered into the target organism[22]. It is easy, quick, and resource-saving to clone the gRNA since it is only around 20 bp in size. By expressing both Cas9 and gRNA, double-strand breaks are facilitated at gRNA-defined, specific locus of the GOI[23]. Then, double-strand breaks are repaired by nonhomologous end joining (NHEJ) or homology-directed repair (HDR) **(Fig.1)**. It is common for NHEJ to result in the insertion of mismatches, which ultimately can cause the knockout of the targeted gene[24, 25].

On the other hand, HDR is a precise DNA repair mechanism that requires a DNA template for proper repair, which is why it is limited to the G2 and S phases of the cell cycle, where a

homologous DNA sequence is present in the nucleus. Using CRISPR/Cas9, knock-ins are created by adding pre-designed DNA repair templates containing homologous arms. HDR then uses these templates to repair DNA double-strand lesions induced by Cas9[24]. Thus, inserting the desired DNA sequence into the target locus is possible. However, the creation of targeted knock-in via CRISPR/Cas9 remains challenging due to the low efficiency with which large DNA inserts can be properly inserted[22, 26, 27]. It has been demonstrated that the CRISPR/Cas system can generate knockouts and knock-ins and modulate processes such as gene regulation, epigenetic modifications, and chromatin remodeling[19]. In combination, the CRISPR/Cas system represents a powerful tool for editing genomes. This system is particularly advantageous because it allows rapid generation of mutants without time-consuming and resource-intense ES-cell targeting.

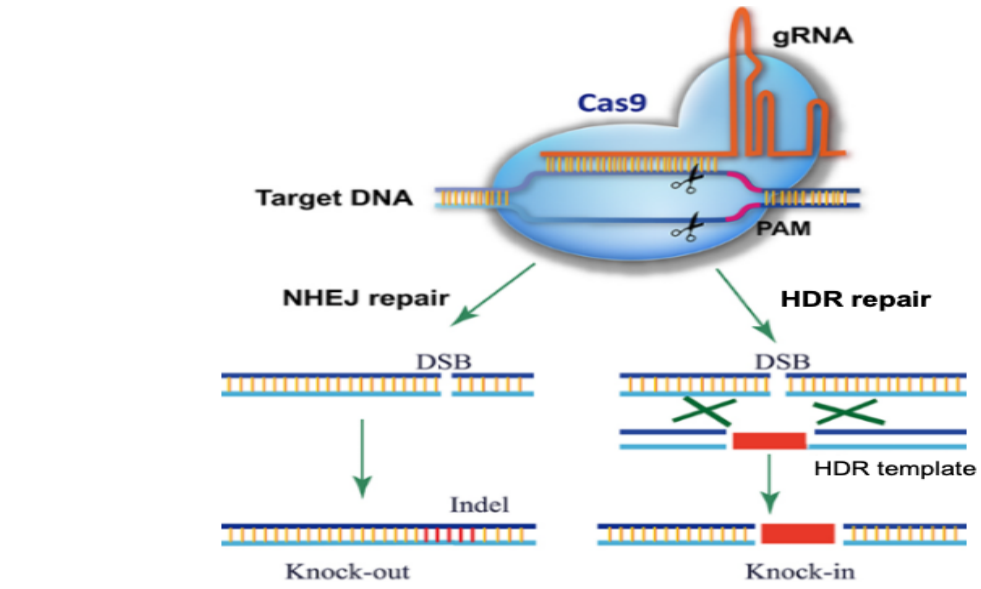

modified from Ding et al., 2016

Figure 1: Schematic of CRISPR Cas9/gRNA genome editing. Base pairing between the gRNA and DNA directs Cas9 to its DNA target. A PAM motif downstream of the gRNA-binding region is required for Cas9 recognition and cleavage. Cas9/gRNA cuts both strands of the target DNA, triggering endogenous DSB repair. During a knockout experiment, the DSB is repaired using the error-prone NHEJ pathway, which introduces an inDel at the DSB site, which knocks out the gene's function. In a knock-in experiment, the DSB is repaired by HDR using the donor template, resulting in the donor DNA sequence integrating into the site of the DSB.

2.2. Conditional CRISPR Cas9 Mediated Gene Inactivation in Vivo Using ROSA26 Cas9 Mice

Recently, conditional Cas9-expressing mouse strains have been generated that allow for easy gene inactivation in a cell type and/or inducible manner[28]. For, Cas9 was targeted into the

rosa26 locus, but a loxP prevents its expression flanked stop cassette **(Fig.2)**. Thus, intercrossing with Cre mouse strains will result in cell type specific Cre mediated excision of the stop cassette and Cas9 expression in these cells. Subsequently, the gene-specific gRNA must be delivered in vivo so that both components Cas9 and the gRNA are in these cells. This will result in the guidance of Cas9 to the specific genomic site targeted by the gRNA to induce a double strand break to disrupt gene function ultimately. Thus, such a CRISPR/Cas9 approach of conditional gene inactivation is relatively easy to perform and much faster than generating a loxP-flanked gene of interest mouse line intercrossed to homozygosity together with the Cre strain, etc.

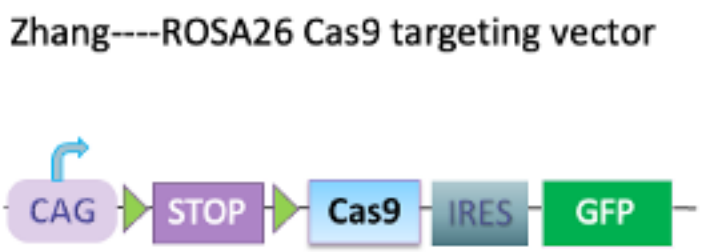

Figure 2: Zhang-ROSA26 Cas9 targeting vector. CAG = chicken beta-actin promoter, triangle = loxP sites, IRES= Internal Ribosome Entry Site, GFP= Green Fluorescent Proteins.

However, the conditional CRISPR/Cas9 approach has several limitations: **1.** Viral delivery will result in high gRNA expression that increases the risk of off-target effects. **2.** The genetic lesion induced by Cas9 composes only single nucleotides that will be difficult to monitor. **3.** Delivery of the gRNA is difficult, there have been attempts to use viruses for gRNA delivery, but not all cell types can be infected.

When Cas9 and gRNA expression are high, the specificity of CRISPR Cas9 is diminished, and Cas9 protein might cleave other targets, known as off-target effects. A first report used ROSA26 fl Cas9 IRES GFP mice crossed to AgrP Cre and AAV mediated delivery of gRNA to knock out the leptin receptor in AgrP neurons. In contrast to a previous report that described unaltered bodyweight gain using classical Cre/loxP approach to inactivate leptin receptor (Lepr) in AgrP neurons, such CRISPR Cas9 mediated conditional Lepr knock-out mice were morbidly obese[29] (**Fig.3 A, B, C**). Thus, this discrepancy might be derived from off-target effects of the CRISPR/Cas9 system in Agrp neurons that cannot be monitored even after sacrificing the animals (**Fig.3 D**).

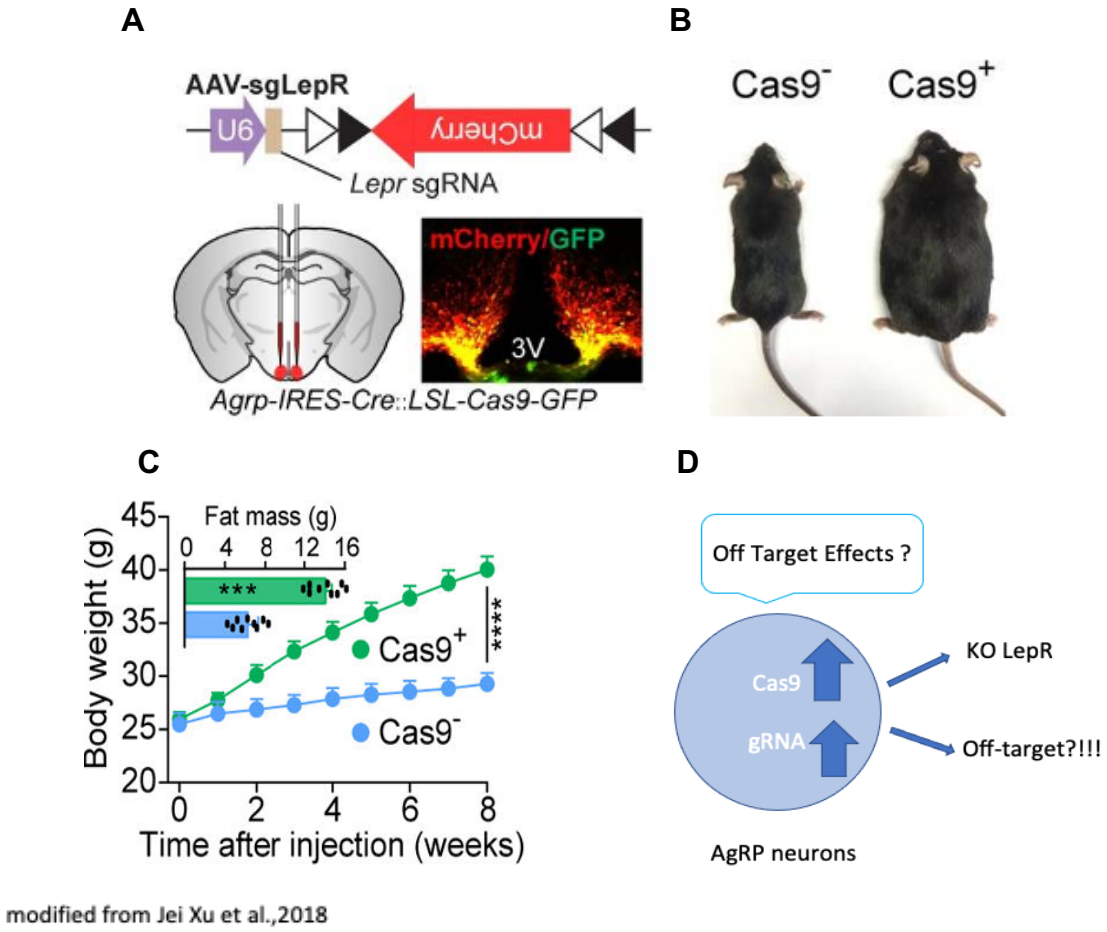

Figure 3: Off-target effects in Lepr KO mouse. (A) Schematic diagram of AAV pU6-sgRNA^{Lepr}: pEF1α-FLEX-mCherry (AAV-sgLepR) injected bilaterally into the ARC of Agrp-IRES-Cre: LSL-Cas9-GFP mice and mCherry: GFP co-immunostaining. (B) Representative littermates. (C) body weight and analysis of fat mass. (D) off-target effects occurred.

Current approaches using ROSA26 Cas9 mice and viral gRNA delivery cannot determine the efficacy of CRISPR/Cas9 in single cells, since the genomic lesion only composes single nucleotides and even these might be different between the cells. While antibody staining of tissues will be the gold standard for determination of gene inactivation using this technique, the single nucleotide deletions mediated by the double strand break repair might even not impact mRNA stability such that researchers are unable to examine gene inactivation on RNA level using qPCR or RNAscope.

gRNAs can be delivered to cell type specific Cas9 expressing mice by viruses such as adeno or adeno-associated viruses. However, the viruses are unable to infect every cell with the same efficiency. Thus, researchers went back and isolated primary B cells from cas9 expressing mice and infected them ex vivo with adenoviruses to knock out specific genes. On the other hand, AAVs with different tropisms might help to deliver gRNAs to specific tissues or cells of Cas9 expressing mice in vivo. This might be effective in the brain since AAV viruses are used

quite commonly there to deliver transgenes. Nevertheless, there is no universal way to deliver gRNAs to Cas9 expressing mice.

Taken together, there is urgent technical need to clarify universal delivery of gRNAs, to reduce potential off-target effects and to investigate whether CRISPR/Cas9 has worked using ROSA26 Cas9 mouse lines.

2.2.1. Generation of Conditional CRISPR Cas9 Mediated Knock-Out Mice Without Off-Target Effects Using the Traffic Light System

In our previous work, we generated a self-destructing Cas9 (sCas9) ROSA26 targeting vector that contained a ROSA26 short and a long arm of homology, a CMV early enhancer/chicken beta-actin promoter (CAG), and two STOP cassettes, of which one was flanked by loxP flanked, and the other flanked by rox sites. These two STOP cassettes allow for tissue-specific intersectional expression of sCas9. In addition, a E2A driven tdTOMATO reporter gene is inserted downstream of the sCas9, and a woodchuck hepatitis virus posttranscriptional regulatory element, which enhances gene expression **(Fig.4 A)**. Thus, upon Cre and Dre mediated excision of stop cassettes, sCas9 and tdTomato are expressed in the defined cell type. sCas9 on the genomic level is defined such that in 5' of Cas9 cDNA, there is 20 nt +PAM inserted specific for and copied from the tdTomato cDNA. These 20 nt + PAM allowed us to generate a gRNA against tdTomato and sCas9 (gRNATomato) to be included into dual U6 driven gRNA cassettes (one against tdTomato sCas9 the other against a specific gene of interest) that upon delivery by AAV will not only destroy the gene of interest but also Cas9 and tdTomato to ultimately reduce off target effects **(Fig.4 B)**. Therefore, this technical gimmick will solve problem 1. E.g. reduce off target effects of CRISPR/Cas9 described in the previous paragraph. Furthermore, using this gimmick, upon successful CRISPR/Cas9 mediated genomic editing, cells will lose tdTomato red fluorescence and cannot be monitored by fluorescence microscopy.

2.2.2. Generation of gRNAs and gAAVs

To circumvent this, we modified the AAV carrying the dual U6gRNA cassettes such that we included ZsGreen reporter cDNAs driven by the CAG promoter whose expression was prevented by loxP, rox or loxP and rox-flanked mini stop cassettes **(Fig.4 C)**. Thus, our novel sCas9 mouse line, combined with the generated AAV, forms the traffic light system that visualizes gene editing in vivo by switching red fluorescent sCas9 cells to green, as well as AAV-infected knockout cells in small populations where other methods fail to detect gene editing. Moreover, the genomic effects of constant Cas9-mediated cleavage, which normally affect off-target sites, are reduced in this system when using sCas9. An enhanced specificity Cas9 (espCas9 1.1) was used and modified here to generate a mouse line with the highest Cas9 specificity and efficiency[30]. Unfortunately, when we examined the Cre, Dre or Cre/Dre activatable ZsGreen AAVs in vivo, we observed that the mini stop cassettes failed to prevent

ZsGreen expression, e.g. all infected cells were green fluorescent independent whether they expressed Cre, Dre, or Cre and Dre. Thus, we urgently need to conditionally activate ZsGreen from AAVs by other ways to visualize specific gene editing using our traffic light system.

A R26 fl rx sCas9 tdTomato

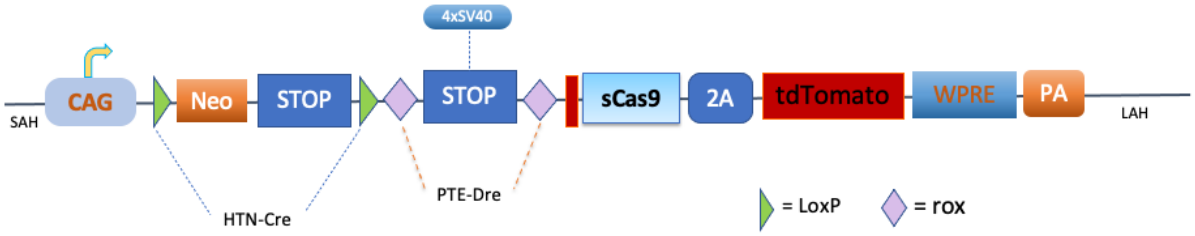

B Cellular subpopulation specific sCas9 expressing mouse

C Melanie's gAAV constructs

Figure 4: sCas9 ROSA26 targeting vector and gRNA plasmids built by Melanie. (A) R26 fl rx sCas9 tdTomato mouse line. (B) sCas9 mouse that expresses sCas9 and tdTomato in the cellular subpopulation of interest. (C) gAAV containing ZsGreen, gRNA against the GOI, and gRNA against the tdTomato/sCas9. SAH = short arm of homology, CAG = chicken beta-actin promoter, triangle = loxP sites, diamond = rox sites, Neo = neomycin, red bock = self-destructing element, 2A = self-cleaving, WPRE = woodchuck hepatitis virus posttranscriptional regulatory element, PA = poly A peptide, LAH = long arm of homology, GOI = gene of interest, PGK = mouse phosphoglycerate kinase 1 promoter.

To monitor the effectiveness of CRISPR/Cas9, we created the traffic light system: Cre and Dre-mediated excision of the two stop cassettes leads to the expression of sCas9 and tomato. Making cells that express sCAS9 also emit red fluorescence. In addition, a 20 nt sequence from tomato was inserted 5' to the sCas9 gene. This allows for the inactivation of both the tomato and sCAS9 genes when the gRNA of the tomato is expressed.

2.3. NAFLD is Now MASLD in 2023

As a result of a multi-year consensus process involving professional associations, patient advocacy groups, and other stakeholders, the name NAFLD has been changed to MASLD[28]. There has been a push for a change to reduce stigma among patients. It is now more evident from scientific research that the pathogenesis of obesity is driven by metabolic dysfunction and steatosis (fat accumulation) rather than inflammation[31, 32]. According to genetic studies, steatosis is one of the major causes of this disease[33]. It was for this reason that a more biologically accurate name was requested.

When other potential causes of fatty liver disease have been excluded, MASLD applies to all types of fatty liver disease involving metabolic dysfunction. It includes obesity, diabetes, hypertension, and lipid disorders[34]. Specific diagnostic criteria are provided for adults and children when defining “metabolic dysfunction.” The term “steatotic” emphasizes the importance of fat accumulation as an underlying pathology. The basis for this is the enhanced understanding of how steatosis contributes to disease progression. The term "metabolic dysfunction" also emphasizes the metabolic roots instead of a primary inflammatory disorder. Alcohol-related liver disease and other specific forms of fatty liver retain their distinct names and are not called MASLD[32]. However, the transition still has challenges: The long name is cumbersome. Shorthand versions like “metabolic liver disease” may be needed for practical use. Despite attempts to reduce stigma, the words “fatty” and “steatotic” may still carry negative connotations in some sociocultural contexts. Updating medical coding, medical education, and clinical systems like Epic will take years. MASLD will likely persist in documents and systems for some time. Measuring the impact of stigma will require further study. Surveys on patient perceptions should be repeated in the MASLD era.

2.4. Metabolic Dysfunction Associated with Steatotic Fatty Liver Disease and Metabolic Dysfunction Steatohepatitis

Metabolic Dysfunction Associated with Steatotic Liver Disease (MASLD) is a growing health problem in developing and developed countries. The first stage of MASLD is characterized by excessive fat accumulation in hepatocytes, the main cell type of the liver, to the extent of more than 5% liver fat, called liver steatosis[35]. Signs of the second stage are inflammation, which – if non-alcohol abuse is diagnosed – is the stage of metabolic dysfunction associated with steatohepatitis with hepatic necroinflammation and underlying fibrosis (MASH); it can progress to a third stage in which liver fibrosis is added to liver fat accumulation and subsequent inflammation[36]. Finally, the disease can progress to liver cirrhosis, which is irreversible damage caused by ongoing fibrosis and inflammation and loss of functional liver tissue due to changes in tissue architecture. MASH is a form of MASLD in which the patients have metabolic dysfunction associated with steatotic liver disease with hepatic necroinflammation and underlying fibrosis. About 20% of all MAFLD patients progress to MASH[37]. Pharmaceutical

therapies for MASLD or MASH are limited, but clinical trials are conducted. However, diet intervention in the first stage of MASLD can reverse fatty liver and the progression of MASLD[37, 38].

2.5. The Molecular Mechanisms Driving the Development of MASH

There is still a lack of understanding of the mechanisms contributing to MASH's development. A key event in the progression from fatty liver to MASH is the death of hepatocytes due to excessive fat accumulation. The increase in hepatocyte fat content will induce different cellular stressors, e.g., ER stress and/or lipotoxicity, which induce hepatocyte cell death. Hepatocyte death leads to the recruitment and activation of immune cells such as macrophages. The recruited immune cells will release pro-inflammatory cytokines, further enhancing hepatocyte cell death[39]. The release of cytokines further stimulates hepatic stellate cells to differentiate into activated hepatic stellate cells (AHSC), which are responsible for extracellular matrix buildup by secreting collagens and other molecules leading to scar formation[40]. Thus, AHSCs are responsible for fibrosis during MASH and the development of liver cirrhosis.

2.5.1. TWEAK- NIK- (Non-Canonical NF- κB) Pathway

Tumor necrosis factor-like weak inducer of apoptosis (TWEAK) is increased during MASLD[41]. TWEAK activates the non-canonical NF-κB pathway, one of the main inflammatory pathways, by binding to its receptor Fn14. Thereby NF-κB, inducing Kinase (NIK, also known as MAP3K14), is activated, leading to the expression of NF-κB signaling controlled genes[42]. NIK induces p100 phosphorylation via the activation of the kinase IKKα10,13[43, 44]. Comparatively to the rapid and transient activation of the canonical NF-κB pathway, the non-canonical NF-κB pathway is characteristically slow and persistent. Typical Inducers of the non-canonical NF-B pathway are ligands of members of the tumor necrosis factor receptor superfamily (TNFR). As originally believed to be an important signaling pathway for lymphoid organ development and B cell maturation, that pathway has been recently shown to play a role in different aspects of innate and adaptive immunity. It is also believed that the pathogenesis of inflammatory conditions can also be attributed to dysregulated non-canonical NF-κB activation.

2.5.2. Growth Hormone- JAK-STAT Pathway

Several extracellular signals, including cytokines, hormones, and growth factors, are rapidly transduced into cellular and molecular responses through the evolutionarily highly conserved Janus kinase (JAK) / STAT signaling pathway[45, 46]. Unbalanced JAK/ STAT signal transduction is associated with developing various pathologies, from inflammatory diseases to cancer. In mammals, four JAK tyrosine kinases (JAK1-3 and TYK2) and seven STAT transcription factors (STAT1-4, 5A, 5B, and 6) are involved in the transduction of signals from transmembrane receptors, which lack intrinsic tyrosine kinase activity [45, 47].

One of the molecules signaling through the JACK-STAT pathway is the growth hormone (GH). This single-chain peptide is synthesized and released into the bloodstream by the anterior pituitary somatotrophs. Additionally, GH may be expressed in other tissues, possibly acting in an autocrine or paracrine manner in the surrounding environment. GH's important negative feedback mechanism that regulates its secretion involves its main downstream effector, IGF-1, which stimulates hypothalamic somatostatin secretion and directly affects pituitary somatotrophs[48]. Several additional factors have been reported to counteract GH release, such as obesity and hyperglycemia. At the same time, dietary restriction/fasting, hypoglycemia, acute stress, and exercise have been associated with an increase in GH production[49, 50]. GH's metabolic functions include optimization of body composition and adaptation to energy shortage, enhancing adipose tissue lipolysis and overall fatty acid oxidation while promoting protein synthesis or decreasing protein breakdown depending on the actual energy status[49, 51]. Furthermore, GH directly and indirectly influences systemic glucose metabolism by antagonizing insulin function, inhibiting glucose oxidation, and stimulating hepatic gluconeogenesis.

Several signaling pathways have been demonstrated to mediate GH's diverse functions at the cellular level. An initial step in the signaling process involving GH binds to the widely expressed GH receptor (GHR), which then activates the receptor-associated kinase JAK2 **(Fig. 6)**. Upon activation of JAK2, downstream signaling molecules such as ERK, JNK, and STATs are activated[52, 53]. It has been shown that GHR activates STAT1 and STAT3. However, STAT5 appears to be the major downstream target of GHR[54, 55]. In several body parts, homeostatic processes are regulated by the transduction of signals through STAT5. As a result of these processes, the immune system, breast, and liver epithelial cells are most significantly affected[56, 57].

STAT5 is composed of two isoforms, STAT5A and STAT5B. STAT5A is the predominant. STAT5A is the predominant isoform in the mammary glands[58]. Alternatively, STAT5B is more abundant in liver epithelial cells, which confers many of GH's functions and supports the expression of several GH-controlled sexual dimorphic genes[59]. It has been demonstrated that the Janus-activated kinase (JAK)-signal transducer and activator of transcription (STAT) pathway is an extremely rapid membrane-to-nucleus signaling system that mediates cytokine signals in mammals[60, 61]. STAT5 (STAT5a and STAT5b) are highly homologous proteins encoded by two genes and activated by Janus-activated kinases (JAK) downstream of cytokine receptors. Many hematopoietic and nonhematopoietic cytokines and growth factors activate STAT5 proteins via the JAK-STAT pathway. There is a crucial role for STAT5 proteins in regulating vital cellular functions, such as proliferation, differentiation, and survival[62]. STAT5a is the major STAT5 isoform in the mammary gland, whereas STAT5b is the major STAT5 isoform in the liver, and it is 91% similar in the human STAT5a and STAT5b[63].

Hepatic STAT5 indirectly regulates systemic GH availability and liver sensitivity to GH by expressing IGF-1 and SOCS2[64-66]. Recent studies using liver-specific STAT5 knockout mice have further provided substantial evidence that GH-activated STAT5 has important functions in controlling hepatic lipid metabolism and hepatocyte regeneration[64, 67]. In this way, STAT5 may contribute to developing fatty liver diseases.

2.5.3. Crosstalk between GH /JAK2/ STAT5 and TWEAK/NIK Signals in Human HCC

We have previously conducted GH and GH/TWEAK stimulation experiments in HepG2 cells derived from human HCC, revealing that GH-induced STAT5 activation is blunted when TWEAK is activated, as well as NIK expression at the mRNA and protein levels in human HCC. The analysis of pSTAT5 showed that STAT5 activation is significantly blunted in HCC grade 3, along with the highest degree of NIK immunoreactivity[68]. Furthermore, we analyzed the global gene expression of samples obtained from matched non-tumor and tumor (HCC) biopsies. We found that 43.7% of the overlapping genes had STAT5 binding motifs in their promoters, including the genuine STAT5 targets IGF1, SOCS2, Onecut1, etc. As a result, we assume that the inhibition of JAK2/STAT5 by NIK is conserved between mice and humans[68]. The results of our study suggest that hepatic NIK deficiency may be explained by improved STAT5 signaling, proving that NIK is an inhibitor of STAT5. While the inhibitory function of NIK was not directly responsible for affecting STAT5, it did inhibit JAK2 upstream. As a result of the phosphorylation of JAK2 S633 by NIK, STAT5 signaling is impaired, but not those of STAT3 or STAT1. NIK's specificity on the JAK2/STAT5 axis could be explained by the limited signaling capacity of the growth hormone receptor (GHR), which is exclusively dependent on JAK2 activity to activate STAT5[69, 70]. Therefore, the specific inhibitory effects of NIK on GH-induced STAT5 could result from the critical dependency of the GHR on JAK2.

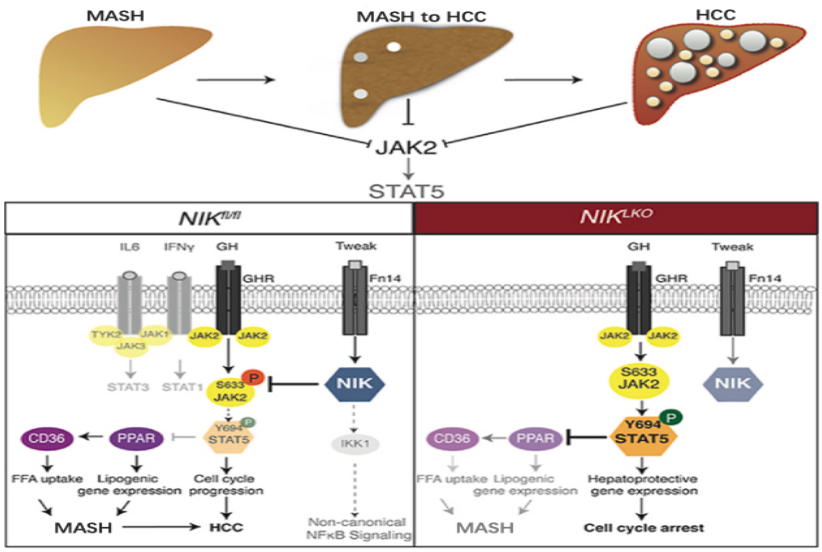

Figure 5. Hepatocyte-specific NIK Knock-out prevents MASH (previous findings of our lab). Hepatocyte-specific NIK^{LKO} mice protect these mice from MASH if fed MASH-inducing diets. This is due to inhibitory phosphorylation carried out in $NIK^{fl/fl}$ animals on JAK2 by NIK, which renders JAK2 inactive and thereby inhibits the following phosphorylation of STAT5, which is then unable to induce hepatoprotective gene expression.

2.6. Objectives

Even if the CRISPR/Cas9 system is highly specific, high expression of both proteins will lead to off-target effects where unspecific cleavage might occur and destabilize the mouse genome or inactivate other genes. These off-target effects have often been reported, and they cannot be neglected since additional unwanted cleavage of the mouse genome might mask or alter the phenotype of CRISPR/Cas9-mediated knock-out mice. Thus, it would be highly desirable to have a mouse strain that enables Cre/loxP and Dre/rox mediated expression of Cas9 with self-inactivating capacity. To circumvent off-target effects and monitor the effectiveness of CRISPR/Cas9, we have previously created the traffic light system to visualize gene editing of targeted gene. However, the previous approach that contained min stop cassettes in front of ZsGreen failed/was leaky. My first aim was to generate Cre, Dre and Cre/Dre activatable ZsGreen cassettes into the AAV carrying the dual U6 driven gRNA cassettes. Upon successful generation and testing in vitro in MEFs, I realized that my modified AAVs were able to infect MEFS, but not ES cells in vitro. Therefore next, I aimed to modify the previous R26-fl-rx-sCas9E2AtdTomato construct such that I inserted a receptor for AAV2 (AAVR) to be expressed in addition to sCas9 and tdTomato to enable efficient AAV2 uptake. The novel R26-fl-rx-sCas9P2A-AAVR-E2AtdTomato targeting vector had been successfully cloned and will be transfected soon.

Moreover, in previous work, our lab investigated the role of NIK during MASH and found that a hepatocyte-specific knockout of NIK in mice protects from MASH development. Single-nucleus RNA seq(snRNA-Seq) of the hepatocytes of NIK knockout mice revealed an upregulation of JAK-STAT signaling. Further investigations revealed that in $NIK^{fl/fl}$ animals, NIK phosphorylates JAK2 and thereby inhibits JAK2 kinase activity, preventing the phosphorylation and activation of downstream STAT5[68]. Thus, my next aim was to investigate whether the role of STAT5 is consistent with NIK observed during MASH via examining hepatocyte specific STAT5 knock out mice in dietary models of MASH.

3. MATERIALS AND METHODS

3.1. Materials

3.1.1. Chemicals

Table 1: Chemicals

Chemical	Supplier
β-Mercaptoethanol	Applichem, Darmstadt, Germany
0.9% saline (sterile)	Berlin Chemie, Berlin, Germany
Acetonitrile (ACN)	Sigma-Aldrich, Seelze, Germany
Agarose (ultrapure)	Invitrogen, Karlsruhe, Germany
Ampicillin	Applichem, Darmstadt, Germany
Bovine serum albumin (BSA)	Sigma-Aldrich, Seelze, Germany
Chloroform	Merck, Darmstadt, Germany
Dimethylsulfoxide (DMSO)	Merck, Darmstadt, Germany
1,4-Dithiothreitol (DTT)	Applichem, Darmstadt, Germany
Eosin	Applichem, Darmstadt, Germany
Ethanol, absolute	Applichem, Darmstadt, Germany
Ethidium Bromide- solution 1%	Applichem, Darmstadt, Germany
Ethylenediaminetetraacetate (EDTA)	Applichem, Darmstadt, Germany
Formic Acid	Sigma-Aldrich, Seelze, Germany
Glucose (20%)	Bela-Pharm, Vechta, Germany
Glycerol	Serva, Heidelberg, Germany
Glycine	Applichem, Darmstadt, Germany
Hematoxylin	Applichem, Darmstadt, Germany
HEPES	Applichem, Darmstadt, Germany
Insulin	Sanofi, Frankfurt, Germany
Isopropanol	Roth, Karlsruhe, Germany
Kanamycin	Applichem, Darmstadt, Germany
LB, Medium and Agar	Applichem, Darmstadt, Germany
Magnesium chloride	Merck, Darmstadt, Germany

Memanol	Roth, Karlsruhe, Germany
Mitomycin C	Sigma-Aldrich, Seelze, Germany
N-Nitrosodimethylamine	Sigma-Aldrich, Seelze, Germany
Nitrogen (liquid)	Linde, Pullach, Germany
Paraformaldehyde (PFA)	Sigma-Aldrich, Seelze, Germany
Phenol	Roth, Karlsruhe, Germany
Sodium chloride	Applichem, Darmstadt, Germany
Sodium citrate	Merck, Darmstadt, Germany
Sodium dodecyl sulfate (SDS)	Applichem, Darmstadt, Germany
Sodium hydroxide	Applichem, Darmstadt, Germany
Tissue freezing medium	Jung, Heidelberg, Germany
Tris Hydroxymethyl Aminomethane (Tris)	Applichem, Darmstadt, Germany
Tween 20	Applichem, Darmstadt, Germany
Western blocking reagent	Roche, Mannheim, Germany

3.1.2. Buffers and Solutions

Table 2: Buffers and solutions

Buffer/Solution	**Composition/Supplier**
Anode buffer 1	0.3 M Tris 20% (v/v) Methanol
Anode buffer 2	25 mM Tris 20% (v/v) Methanol
Antibody Solution	5% (v/v) Roche Western Blocking Reagent in TBS-T
Buffer A	0.1% Formic acid Milli-Q water
Buffer B	80% Acetonitrile 0.1% Formic acid
Cathode buffer	40 mM 6-Aminohexanoic acid 0.01% (v/v) SDS 20% (v/v) Methanol
Cell freezing medium	10%DMSO in FCS
Cell lysis buffer	10 x Cell Lysis Buffer (Cell signaling) 1 mM PMSF Protease inhibitor tablets, 1 in 10 ml (Roche) PhosStop, 1 in 10 ml (Roche)
ES-cell culture medium	DMEM with L-glutamine (Gibco) 15% FCS (Biochrom AG) 1 mM Sodium pyruvate (Gibco)

	1 x Non-essential Amino Acids (Gibco) 100U/ml Pen-Strep (Gibco) 10 U/ml LIF 0.1 mM p-Mercaptoethanol 2 mM L-Glutamine
ES-cell lysis buffer	10 mM Tris, pH 7.5 10 mM EDTA 0.5% Sarkosyl 10 mM Sodium chloride 1/25 Proteinase K
Laemmli Sample Buffer (4x)	Bio-Rad,#1610747 10% β-Mercaptoethanol
MACSQuant running buffer	Miltenyi Biotech,#130-092-747
MEF-culture medium	DMEM with L-Glutamine (Gibco) 10%FCS (Biochrom AG) 1 mM Sodium pyruvate (Gibco) 1x Non-essential Amino Acids (Gibco) 100 U/ml Pen-Strep (Gibco)
meRIP Elution Buffer	5 mM Tris-HCL pH 7.5 1 mM EDTA 0.05% SDS
Opti-MEM	Gibco#31985062
Double phosphate buffered saline (DPBS)	Gibco,#14190169
Prehybridization buffer	M Sodium chloride 50 mM Tris HCL 10% Dextran Sulfate%SDS 250 ug Salmon spermidine in ddH_2O
RIPA Buffer	10x RIPA Buffer (Cell signaling) 1 mM PMSF Protease inhibitor tablets, 1 in 10 ml (Roche) PhosStop, 1 in 10 ml (Roche)
SCC, 20x	3 M Sodium chloride 0.3 M Tris sodium citrate dihydrate in ddH_2O
SDS-PAGE electrophoresis buffer (10x)	0.25 M Tris 2M Glycine 35 mM SDS
Stripping Solution	0.7% β-Mercaptoethanol 2%(v/v) SDS
TAE (50x)	2 M Tris 50 mM EDTA
Tail-Lysis-Buffer	100mM Tris-HCl, pH 8.5 200 mM NaCl 5 mM EDTA 0.2%(w/v)SDS 1:100 Proteinase K
TBS (10x)	1.47 M NaCl 0.2 M Tris, pH 7.4
TBS-Tween (1x)	1x TBS 0.1%Tween20
TE-Buffer	10 mM Tris-HCL, pH 7.4 10 mM EDTA, pH 7.8 RNaseA (1:1000)

Trypsin 0.5%	Gibco, #15400054
Trypsin 2.5%	Gibco, #15090046
Western Blot blocking solution	10%(v/v) Roche Western Blocking Reagent in TBS-T

3.1.3. Kits

Table 3: Kits

Kit	Supplier
DreamTaq Green PCR Master Mix (2X)	Thermo Scientific, Schwerte, Germany
PrimeScript™ RT Master Mix (Perfect Real Time)	#RR036A, Takara Bio,Shinga, Japan
Ladderman DNA labeling kit	Takara Bio,Shinga, Japan
Magnetic mRNA isolation kit	NEB,Frankfurt am Main, Germany
MAX Efficiency Stbl2™ Competent Cells	Thermo Scientific,Schwerte, Germany
Invitrogen™ One Shot™ Stbl3™ Chemically Competent E. coli	Thermo Scientific,Schwerte, Germany
NucleoBond® Xtra Midi/Maxi kit	Macherey-Nagel, Düren, Germany
PeqGold, Plasmid Miniprep kit	Peqlab, Erlangen,Germany
Pierce® BCA Protein assay kit	Thermo Scientific,Schwerte, Germany
QIAEX II gel extraction kit	Qiagen, Hilden,Germany
RNeasy extraction kit	Qiagen, Hilden, Germany
Lipofectamine®2000 DNA Transfection Reagent kit	Thermo Scientific, Schwerte, Germany

3.1.4. Enzymes

Table 4: Enzymes

Enzymes	Dilution	Buffer	Supplier
Proteinase K	1:100	Tail Lysis Buffer	Roche
RNaseA	1:1000	TE-Buffer	Peqlab
Trypsin	1:100	ABC	Sigma-Aldrich

3.1.5. Marker and Ladder

Table 5: Protein and DNA Ladder

Standard	Company
GeneRuler™ DNA ladder mix	ThermoScientific, SchwerteGermany

PageRuler™ Protein ladder	ThermoScientific, SchwerteGermany

3.2. Methods

3.2.1. Molecular Biology

3.2.1.1. Isolation of Genomic DNA

Tail or ear biopsies were taken at postnatal day (p) 18-25 and digested at 56 °C overnight in 500 pl tail lysis buffer containing 180 pg/ml proteinase K. To precipitate the DNA, 500 µl isopropanol was added, subsequently, samples were vortexed briefly and centrifuged for 10 minutes at 17,000 g. The DNA pellet was washed in 500 µl 70% ethanol and dried at room temperature (RT). The DNA was resuspended in a TE buffer containing 10 µg/ml RNaseA and stored at RT.

3.2.1.2. Polymerase chain reaction

Genomic DNA isolated from biopsies was used to perform polymerase chain reaction (PCR). Primers are listed in Table 6. DNA polymerase and DreamTaq PCR MasterMix (ThermoScientific) were used to perform the PCR. For each reaction (25 µl), 50 ng DNA, 25 µM dNTP mix, 25 pMol of respective primers, and 1 unit DNA polymerase were used. PCR programs were adjusted to primer and amplicon length. The different PCR programs are listed in Table 7. Amplified DNA was separated according to the molecular mass using 1-2% agarose gels containing Ethidium Bromide or peqGREEN dye.

Table 6: Genotyping Primer

Mouse Line	Primer	Sequence
Alfp-Cre	AlfpCre_831 AlfpCre_699 OMPC1 OMPC2	5'-TCC AGA TGG CAA ACA TAC GC-3' 5'-GTG TAC GGT CAG TAA ATT GGA C-3' 5'-GTG TAC GGT CAG TAA ATT GGA C -3' 5'-AAA GGC CTC TAC AGT CTA TAG-3'
STAT5$^{fl/fl}$	Stat5-1 Stat5-2	5'-AGC AGC AAC CAG AGG ACT AC-3' 5'-AAG TTA TCT CGA GTT AGT CAG G-3'
ROSA-CAGs	5Rosatyp TyprevcAGs Typ forwrev	5'-CGT TTG CGG GGA TGG GCG GCC-3' 5'-TGT CGC AAA TTA ACT GTG AAT C-3' 5'-GAT AAC AAC TCA GAG CGA CTT T-3'
sCas9 fl;rx/fl;rx	5Rosatyp TyprevcAGs Typ forwrev	5'-CGT TTG CGG GGA TGG GCG GCC-3' 5'-TGT CGC AAA TTA ACT GTG AAT C-3' 5'-GAT AAC AAC TCA GAG CGA CTT T-3'

Table 7: PCR-Programs

PCR	Temperature	Time
Alfp-Cre	94 °C 94 °C 60 °C 72 °C 72 °C 4 °C	3 min 30 sec 30 sec 30 sec 10 min ∞
Stat5$^{fl/fl}$	94 °C 94 °C 56 °C 72 °C 72 °C 4 °C	5 min 30 sec 30 sec 1min 5 min ∞
ROSA-CAGs	94 °C 94 °C 60 °C 72 °C 72 °C 4 °C	3 min 30 sec 45 sec 1.5 min 10 min ∞
sCas9 fl;rx/fl;rx	94 °C 94 °C 54 °C 72 °C 72 °C 4 °C	4 min 30 sec 30 sec 45 sec 10 min ∞

3.2.1.3. Quantitative Real-Time PCR (qRT-PCR)

3.2.1.3.1. mRNA Isolation

From mice liver tissue: + 1 ml Trizol, homogenized in 2 ml eppis. Homogenize Tissue: Use beads (one per sample) and tissue homogenizer; frequency: 300 1/s; time 2 min if necessary, longer. After homogenizing the centrifuge full-speed for 10 mins at 4°C to pellet cell debris, transfer to new eppis and incubate 5 min, then add 200 µl Chloroform, vortex thoroughly, and incubate 2 min at RT, Centrifuge 12.000g, 4°C. Take 250 µl from the aqueous phase and transfer to the new eppis; add 250 µl (or the same amount) of 70% Ethanol in DEPC-Water. Vortex thoroughly and incubate for 10 min at RT. Transfer to spin columns and centrifuge 8000g 15 sec, then wash with 350 µl RW1 and centrifuge 8000g 15 sec, Incubate each column with DNAse I (DNAse I + 550 µl dH_2O), then combine DNAse I with RDP-Buffer in a ratio of (1:7), add 80 µl DNAse I solution per sample, incubate 30 min at RT, wash with 350 µl RW1 and centrifuge 8000g 15 sec, wash twice with 500 µl RPE and centrifuge 8000g 15 sec, then change column receptor tubes and centrifuge 2 min full-speed, change to normal 1.5 ml eppis,

add 30 µl RNAasefree-Water and Incubate 2 min then centrifuge 1min full-speed and measure concentration at NanoDrop

3.2.1.3.2. cDNA synthesis and qRT-PCR

RNA samples were diluted to 200 ng/µl. Then, use the PrimeScriptTM RT Master Mix (Perfect Real Time) kit to prepare the reverse-transcription reaction solution on ice:

---

1. <Per reaction>

Reagent	Volume	Final conc.
5X PrimeScript RT Master Mix (Perfect Real Time)	2 *µl*	1X
total RNA*		
RNase Free dH_2O	up to 10 *µl*	

2. Perform the reverse-transcription reaction after gently mixing the reaction solution.

37 °C 15 min (reverse-transcription)

85 °C 5 sec (for heat inactivation of reverse transcriptase)

4 °C

Afterwards, RNA was reversely transcribed into cDNA, and qRT-PCR was performed. Next, it was amplified using Takyon Low Rox Probe 2x Master Mix dTTP Blue with the respective TaqMan Probes listed in Table 8. Target mRNA expression was measured with the QuantStudioM 7 Flex Real-Time PCR System (Applied Biosystems), and the samples were normalized to a housekeeping gene. The calculations were performed using the comparative method[71].

Table 8: TaqMan Probes for qRT-PCR

Probe	**Order number**
Arg1	Mm00475988_m1
Bcl6	Mm00477633_m1
Cd36	Mm00432403_m1
Cdkn1a	Mm01303209_m1
Cdkn1b	Mm01257348_m1
Cdkn2a	Mm01257348_m1
Cdkn2b	Mm07295536_m1
Clec4f	Mm00443934_m1

Cish	Mm00515488_m1
Col1a1	Mm00801666_m1
Col1a2	Mm00483888_m1
Ctgf	Mm01192932_g1
Egfr	Mm00433023_m1
Emr1	Mm00802530_m1
Fabp1	Mm00444340_m1
Fasn	Mm00662319_m1
G6pc	Mm00839363_m1
Igf1	Mm00439560_m1
IL1b	Mm01336189_m1
IL6	Mm00446190_m1
Ifng	Mm00801778_m1
Mmp2	Mm00439506_m1
Mmp9	Mm00442991_m1
Nos2	Mm00440502_m1
Onecut	Mm00839394_m1
Pck1	Mm00451023_m1
Ppara	Mm00440939_m1
Scd1	Mm00772290_m1
Socs2	Mm01236704_m1
Srebf1	Mm00550338_m1
Tgfb1	Mm01178820_m1
Timp1	Mm00441818_m1
TNFα	Mm00443258_m1

3.2.2. Biochemistry

3.2.2.1. Protein Extraction

3.2.2.1.1. Protein Extraction from Cells

To extract the sCas9 protein with RIPA buffer. Frozen sCas9-ES cells were resuspended in 100 µl cell lysis buffer, frozen in liquid nitrogen, and thawed on ice thrice. To remove the cell

debris, the samples were centrifuged at 17,000 g for 10 min at 4 °C. The supernatant was transferred into a fresh tube, and the protein concentration was determined (3.2.2.1.2)

3.2.2.1.2. Bicinchoninic Acid Solution Assay (BCA)

To determine protein concentration, a bicinchoninic acid solution assay was performed according to the manufacturer's instructions (Pierce BCA Protein Assay Kit, #23225). Absorptions were measured at 595 nm using a plate reader (FilterMax F5 Multi-Mode Microplate Reader, Molecular devices), and an Albumin standard curve was used to determine sample concentration.

3.2.2.2. Western Blot Analysis

3.2.2.2.1. Sodium Dodecyl/Sulfate-Polyacrylamide Gel Electrophoresis (SDS-PAGE)

Proteins were separated according to their molecular mass using SDS-PAGE.4x Laemmli buffer containing 10% β-Mercaptoethanol was added to 10-50 µg of total protein and boiled at 95 °C for 10 minutes.Afterwards,protein lysates were loaded on 10%,12%,or 4-15% gradient gel (casted or precast SDS Criterion™ TGX™, Bio Rad). Gel electrophoresis was performed in 1xSDS running buffer at 80-200 V for 1-2 hours. PageRuler Prestained Protein Ladder (ThermoScientific) was used as the marker.

3.2.2.2.2. Immunoblotting

Separated proteins were transferred to PVDF-membranes (Bio-Rad) at 100 mA for 1 hour by using a semi-dry blotting system (peqlab) or by using a fast-blot chamber for 7 minutes (Trans-Blot* Turbo, Bio-Rad). After transfer, the membrane was blocked in either a 5% blocking solution (Roche) or 5% nonfat milk in 1x TBS-T for 1 hour at RT. Primary antibody incubation was performed overnight at 4 °C. Subsequently, the membrane was washed three times in 1x TBS-T for 5-10 minutes at RT and incubated with a secondary antibody for 1 hour at RT. Next, the membrane was washed three times with 1x TBS-T (5-10 min at RT) and incubated for 1 min with SuperSignal West Dura Extended Duration Substrate (ThermoFisher). The luminescence detection was performed using a fusion image (Vilber). Membrane stripping was done in 1x stripping solution for 30 minutes at 56C. Antibodies used in this study are listed below (**Table 9**).

Table 9: Antibodies

Antibodies	Type	Dilution	Supplier
Calnexin	Mouse, monoclonal	1:10000	Sigma-Aldrich, Seelze Germany
FLAG (F7425)	Rabbit, polyclonal	1:1000	Sigma-Aldrich,

			Seelze Germany
FLAG M2 (F3165)	Mouse, monoclonal	1:1000	Sigma-Aldrich, Seelze Germany
FLAG clone SIG 1-25 (F2555)	Rabbit, monoclonal	1:1000	Sigma-Aldrich, Seelze Germany

3.2.3. Cellular Biology

3.2.3.1. Cell Culture

Cells were maintained in an incubator with 95% humidity, 37 °C, and 5% CO_2 saturation. For sustaining culture, cells were split when confluent monolayers were formed by washing with PBS and subsequently treating with 0.5% Trypsin for 5 min. The culture medium was used to stop the trypsin reaction, and cells were centrifuged at 1200 rpm. Cell pellets were resuspended in a culture medium, and cells were seeded as required. Cells were frozen in the cell freezing medium containing 10% DMSO and stored at -80 °C. For long-term storage, cells were transferred to liquid nitrogen. All procedures were performed under a sterile hood.

3.2.3.1.1. Transient plasmid transfection and AAV infection

Before transfection, $2x10^5$ tdTOMATO positive MEFs were seeded on 6-well plates. Cells were approximately 80% confluent on the day of transfection. According to the manufacturer's instructions, PGK-Cre/and PTE-Dre were performed with Lipofectamine™ 2000 Transfection Reagent (Invitrogen). The transfection mixture was removed after 24 hours of incubation and replaced with the normal MEF culture medium. Next, 2 µl AAVs (2a, 2b, 2c) were added to the plates severally. After 24 hours of incubation, cells were observed with the fluorescence microscope and took photos.

3.2.3.1.2. Embryonic stem cell culture

Cell culture plates were coated with 0.2% gelatin (Merck Darmstadt) in PBS for 30 min at 37 °C. Afterward, Mitomycin C (Merck Darmstadt) treated MEFs were seeded on coated cell culture plates in a confluent monolayer. Subsequently, Bruce4 embryonic stem (ES)-cells were seeded on non-dividing MEFs to maintain ES-cell pluripotency. ES-cell culture medium was changed daily, and cells were passed at 80% confluency.

3.2.3.1.3. Embryonic stem cell transfection and clonal isolation

Before transfection, the 40 µg ROSA26 sCas9-AAVR targeting vector was linearized with AsisI (ThermoScientific), precipitated with isopropanol, washed with 70% ethanol, and resuspended in 400 µl PBS. 4 hours before transfection, the culture medium was exchanged. Subsequently, 10^7 cells were harvested using 0.5% trypsin, and the pellet was resuspended in 400 µl PBS. ES-cells and linearized vectors were transferred into an electroporation cuvette and electroporated with 230 V and 450 µFd in a GenePulser (Bio-Rad, München, Germany).

Transfected ES-cells were seeded on 10 cm dishes and screened for successful targeting via G418 selection (300 µg/ml) for 10 days.
After the G418 selection, colonies were picked. Therefore, ES-cells were washed twice with PBS, and each clone was transferred to a separate well of a 96-well plate containing 25 µl trypsin. Clones were incubated for 5 minutes at 37 °C to separate the colony into single cells. 100 µl culture medium was added to stop the trypsin reaction, and cells were split on three 96-well plates.

3.2.3.2. Immunohistochemistry and Staining

3.2.3.2.1. H&E Staining

Before dewaxing the 4 µm thick paraffin-embedded liver sections into the 70 °C incubator for 15 min, Next, xylene and alcohol (from high to low concentration) were dewaxed, and tap water was washed. The slices into hematoxylin staining for 3 min and washed with tap water the slices were stained in eosin staining solution for 1 min and washed with tap water. For dehydration and sealing, put the slices in 95% alcohol for 2 min in turn; Anhydrous ethanol for 2 min; Xylene for 2 min is dehydrated and transparent, and dried slightly, in the end, sealed with a resinous medium.

3.2.3.2.2. Sirius Red Staining

De-wax and hydrate paraffin liver sections. Stain nuclei with hematoxylin and wash the slides for 10 minutes in tap water. Stain in micro-Sirius red (Solution A) for one hour. Then, wash the slides in two changes of acidified water (Solution B). Remove most water from the slides by shaking. Dehydrate in three changes of 100% ethanol. Clear in xylene and mount in a resinous medium.

3.2.3.2.3. Oil Red O Staining

Cryosections of livers were fixed in formalin and washed in tap water for 10 min. Next, liver sections were rinsed with 60% isopropanol and stained for 15 min with an Oil red O working solution. After rinsing with 60% isopropanol, hematoxylin and eosin staining were performed to visualize nuclei and cytoplasm.

3.2.4. Mouse Experiments

3.2.4.1. Animal Care

The experiments were authorized by the local government authorities and overseen by the animal welfare committee of the University of Cologne. EU guidelines kept mice (Mus musculus Genetic Background C57B//6N).
The mice were exposed to a 12-hour light/12-hour dark cycle and housed at 22-24 °C in a specific-pathogen-free animal facility. The access to water and food was unlimited. Depending on the experimental set-up, mice were fed one of the following diets:

1.Normal chow diet (NCD, Ssniff, R/M-H low phytoestrogen)
2.CDAA diet (Ssniff, E15666 CDAA, Choline free, LARD+1% Cholesterol ¦ Low Met)
3.MASH control diet (Ssniff, E15767-040 low sugar)
4.MASH diet (Ssniff, E15766-340, 20 kJ% Fructose, High trans FA).
The body weights of experimental animals were monitored weekly.

3.2.4.2. Insulin Tolerance Test (ITT)

Insulin sensitivity was determined by an insulin tolerance test. Before the experiment, blood glucose levels were determined by punctuating the tail vein using a Contour-NextR blood glucose meter and Contour-Next® test stripes. Afterward, mice were injected i.p. with insulin (0.75 U insulin/g BW), and blood glucose was measured at 15, 30, and 60 minutes after injection.

3.2.4.3. Glucose Tolerance Test (GTT)

To analyze the reaction of mice to hyperglycemic stimuli, a glucose tolerance test was performed. Before the experiment, the mice were fasted for 6 hours. Fasted blood glucose was determined by punctuating the tail vein using a Contour-NextR blood glucose meter and Contour-Next® test stripes. Next, mice were injected i.p. with glucose (2 mg/g BW), and blood glucose levels were measured 15, 30, 60, and 120 minutes after injection.

3.2.4.4. Cheek Bleeding and Serum Analysis

Blood samples were collected from the submandibular vein by using a lancet. Subsequently, blood was centrifuged for 30 minutes at 17000 g at 4 °C, and serum was stored at -20 °C.
Alanine aminotransferase (ALT) and aspartate aminotransferase (AST) levels were determined to monitor liver damage in the serum. Additionally, serum triglyceride and cholesterol levels were analyzed. Therefore, the serum was diluted 1:10 in 0.9% saline and analyzed by the central lab of the University Hospital in Cologne.

3.2.4.5. Micro-CT System

Total fat and lean mass were measured using a Micro-CT (AL-R307-IVIS)

3.2.4.6. Organ Preparation

Mice were sacrificed at the end of the experiment using the Decapitation method. First, epididymal white adipose tissue (WAT) and liver weights were determined. Carotid artery blood was taken, and the liver, WAT, hypothalamus, and pituitary were snap-frozen in liquid nitrogen. The organs were stored at -80 °C until further analysis.

3.2.5. Genetic Engineering

To amplify DNA sequences, a high-fidelity PCR Master mix was used. High-fidelity PCR was performed with 50 pmol of each primer and 50 ng of DNA template in a total volume of 50 µl. Primers used for amplification and sequencing are listed below in (**Table 10)**. The PCR

program was adapted to primer melting temperature and the size of the amplicon (1 min elongation time/kb of amplicon). Amplified sequences were inserted into the pGEM-T-Easy vector system (PromegaMadison, WI USA) and sequenced by GATC (Eurofins, Hamburg, Germany). The sequencing reaction contained approximately 500 DNA (20 ng/pl). 20 µl of 10 µM custom sequencing primers were sent separately to GATC.

If not stated otherwise, restriction enzymes used in this study were obtained from NEB. Before gel extraction, 10 µg of DNA was digested in a total volume of 50 pl for vector linearization or restriction digestion. To analyze correct fragment insertion,100-500 pg DNA was digested in a total volume of 10 pl. Subsequently, vectors were dephosphorylated using shrimp alkaline phosphatase (NEB). 0.8-1% agarose gels (UltraPure Agarose, Life Technologies) containing Ethidium Bromide were run in 1xTAE buffer to separate DNA fragments. Fragments with the correct size were isolated, and gel extractions were performed using the QIAEX II gel extraction kit according to the manufacturer's instructions. Ligation was performed with T4 ligase for 1 h at RT or overnight at 4 °C. Generated vectors were introduced into self-made, competent E coli cells (Stbl2/C3019H) via heat shock for 25 or 45 seconds at 42 °C. Bacteria were cultured in LB-medium or on LB-agar plates containing respective antibiotics for selection (Ampicillin 50 µg/ml, Kanamycin 25 µg/ml) at 30 °C or 37 °C. Mini-and maxi-preparations of plasmids from bacterial cultures were performed according to the manufacturer's instructions (PeqGold, Plasmid Miniprep Kit on NucleoBond®Xtra Midi/Maxi).

Table 10: Cloning and sequencing primers

Primer Name	**Sequence**
CAG-Flex-mcherry-seq	AAT-AAA-CAA-GTT-AAC-AAC-AAG-AG

Table 11: Synthesized fragments

Double U6 gRNA
Catgtcaattggagggcctatttcccatgattccttcataatttgcatatacgatacaaggctgttagagagataattgga
attaatttgactgtaaacacaaagatattagtacaaaattacgtgacgtagaaagtaataatttcttgggtagtttgcagt
tttaaaattatgttttaaaatggactatcatatgcttaccgtaacttgaaagtatttcgatttcttggctttatatatcttgtgga
aaggacgaaacaccgggtcttcgagaagacctgttttagagctagaaatagcaagttaaaataaggctagtccgtt
atcaacttgaaaaagtggcaccgagtcggtgctttttttgagggcctatttcccatgattccttcatatttgcatatacgat
acaaggctgttagagagataattggaattaatttgactgtaaacacaaagatattagtacaaaatacgtgacgtaga
aagtaataatttcttgggtagtttgcagttttaaaattatggttttaaaatggactatcatatgcttaccgtaacttgaaagtat
ttcgatttcttggctttatatatcttgtggaaaggacgaaagctcgRNATOMATOgttttagagctagaaatagc
aagttaaaataaggctagtccgttatcaacttgaaaaagtggcaccgagtcggtgctttttttggccaggtacc

STAT3 gRNA

CAC-CGG-AGC-GAC-AGC-TTC-CCC-A-5’

AAA-CTA-GGG-AAG-CTG-TCG-CTC-TAC-C-3’

POMC gRN

CAC-CGA-GAT-TCT-GCT-ACA-GTC-GCT-C-5’

AAA-CGA-GCG-ACT-GTA-GCA-GAA-TCT-3’

Lox-STOP-lox-rox-STOP-rox zsGreen

cATAACTTCGTATAGCATACATTATACGAAGTTATGACCCTGGAAGGTGCCACT
CCCACTGTCCTTTCCTAATAAAATGAGGAAATTGCGACCCTGGAAGGTGCCAC
TCCCACTGTCCTTTCCTAATAAAATGAGGAAATTGCATAACTTCGTATAGCATA
CATTATACGAAGTTATTAACTTTAAATAATTGGCATTATTTAAAGTTAgccaccatg

AAVR

ATGGAGAAGAGGCTGGGAGTCAAGCCAAATCCTGCTTCCTGGATTTTATCAGGATATT
ATTGGCAGACATCTGCGAAGTGGTTGAGAAGCCTGTACCTGTTTTATACTTGCTTTTG
CTTCAGCGTTCTGTGGTTGTCAACAGATGCCAGTGAGAGCAGGTGCCAGCAGGGGAA
GACACAATTTGGAGTTGGCCTGAGATCTGGGGGAGAAAATCACCTCTGGCTTCTTGA
AGGAACCCCCTCTCTCCAGTCATGTTGGGCTGCCTGCTGCCAGGACTCTGCCTGCCA
TGTCTTTTGGTGGCTAGAAGGGATGTGCATTCAGGCAGACTGCAGCAGGCCCCAGAG
CTGCCGGGCTTTTAGGACACACTCCTCCAATTCCATGCTGGTGTTTTTAAAAAAATTC
CAAACTGCAGATGATTTGGGCTTTCTACCTGAAGATGATGTACCACATCTTCTGGGGC
TAGGTTGGAACTGGGCATCTTGGAGGCAGAGCCCACCCAGAGCTGCACTCAGACCT
GCTGTATCTTCCAGTGACCAGCAGAGCTTAATCAGGAAGCTTCAGAAGAGAGGTAGT
CCCAGTGACGTAGTTACACCTATAGTGACACAGCATTCTAAAGTGAATGACTCCAACG
AATTAGGTGGTCTGACTACCAGTGGCTCTGCAGAGGTCCACAAGGCGATTACAATTTC
CAGTCCCCTAACCACAGACCTGACTGCAGAGCTGTCTGGTGGGCCAAAGAATGTATC
AGTGCAACCTGAAATATCAGAGGGTCTTGCTACTACGCCCAGCACTCAACAAGTAAAA
AGTTCTGAGAAAACCCAGATTGCTGTCCCCCAGCCAGTGGCTCCCTCCTACAGTTAT
GCTACCCCTACCCCCCAGGCCTCTTTCCAGAGCACCTCAGCACCATACCCAGTTATA
AAGGAACTGGTGGTATCTGCTGGAGAGAGTGTCCAGATAACCCTGCCTAAGAATGAA
GTTCAATTAAATGCATATGTTCTCCAAGAACCACCTAAAGGAGAAACCTACACCTACG
ACTGGCAGCTGATTACTCATCCTAGAGACTACAGTGGAGAAATGGAAGGGAAACATT
CCCAGATCCTCAAACTATCGAAGCTCACTCCAGGCCTGTATGAATTCAAAGTGATTGT
AGAGGGTCAAAATGCCCATGGGGAAGGCTATGTGAACGTGACAGTCAAGCCAGAGC
CCCGTAAGAATCGGCCCCCCATTGCTATTGTGTCACCTCAGTTCCAGGAGATCTCTTT
GCCAACCACTTCTACAGTCATTGATGGCAGTCAAAGCACTGATGATGATAAAATCGTT

CAGTACCATTGGGAAGAACTTAAGGGGCCTCTAAGAGAAGAGAAGATTTCTGAAGATA
CAGCCATATTAAAACTAAGTAAACTCGTCCCTGGGAACTACACTTTCAGCTTGACTGT
AGTAGACTCTGATGGAGCTACCAACTCTACTACTGCAAACCTGACAGTGAACAAAGCT
GTGGATTACCCCCCTGTGGCCAACGCAGGCCCCAACCAAGTGATCACCCTGCCCCAA
AACTCCATCACCCTCTTTGGGAACCAGAGCACTGATGATCATGGCATCACCAGCTATG
AGTGGTCACTCAGCCCAAGCAGCAAAGGGAAAGTGGTGGAGATGCAGGGTGTTAGA
ACACCAACCTTACAGCTCTCTGCGATGCAAGAAGGAGACTACACTTACCAGCTCACA
GTGACTGACACAATAGGACAGCAGGCCACTGCTCAAGTGACTGTTATTGTGCAACCT
GAAAACAATAAGCCTCCTCAGGCAGATGCAGGCCCAGATAAAGAGCTGACCCTTCCT
GTGGATAGCACAACCCTGGATGGCAGCAAGAGCTCAGATGATCAGAAAATTATCTCAT
ATCTCTGGGAAAAAACACAGGGACCTGATGGGGTGCAGCTCGAGAATGCTAACAGCA
GTGTTGCTACTGTGACTGGGCTGCAAGTGGGGACCTATGTGTTCACCTTGACTGTCA
AAGATGAGAGGAACCTGCAAAGCCAGAGCTCTGTGAATGTCATTGTCAAAGAAGAAAT
AAACAAACCACCTATAGCCAAGATAACTGGGAATGTGGTGATTACCCTACCCACGAGC
ACAGCAGAGCTGGATGGCTCTAAGTCCTCAGATGACAAGGGAATAGTCAGCTACCTC
TGGACTCGAGATGAGGGGAGCCCAGCAGCAGGGGAGGTGTTAAATCACTCTGACCA
TCACCCTATCCTTTTTCTTTCAAACCTGGTTGAGGGAACCTACACTTTTCACCTGAAAG
TGACCGATGCAAAGGGTGAGAGTGACACAGACCGGACCACTGTGGAGGTGAAACCT
GATCCCAGGAAAAACAACCTGGTGGAGATCATCTTGGATATCAACGTCAGTCAGCTAA
CTGAGAGGCTGAAGGGGATGTTCATCCGCCAGATTGGGGTCCTCCTGGGGGTGCTG
GATTCCGACATCATTGTGCAAAAGATTCAGCCGTACACGGAGCAGAGCACCAAAATG
GTATTTTTTGTTCAAAACGAGCCTCCCCACCAGATCTTCAAAGGCCATGAGGTGGCAG
CGATGCTCAAGAGTGAGCTGCGGAAGCAAAAGGCAGACTTTTTGATATTCAGAGCCT
TGGAAGTCAACACTGTCACATGTCAGCTGAACTGTTCCGACCATGGCCACTGTGACT
CGTTCACCAAACGCTGTATCTGTGACCCTTTTTGGATGGAGAATTTCATCAAGGTGCA
GCTGAGGGATGGAGACAGCAACTGTGAGTGGAGCGTGTTATATGTTATCATTGCTAC
CTTTGTCATTGTTGTTGCCTTGGGAATCCTGTCTTGGACTGTGATCTGTTGTTGTAAGA
GGCAAAAAGGAAAACCCAAGAGGAAAAGCAAGTACAAGATCCTGGATGCCACGGATC
AGGAAAGCCTGGAGCTGAAGCCAACCTCCCGAGCAGGCATCAAACAGAAAGGCCTTT
TGCTAAGTAGCAGCCTGATGCACTCCGAGTCAGAGCTGGACAGCGATGATGCCATCT
TTACATGGCCAGACCGAGAGAAGGGCAAACTCCTGCATGGTCAGAATGGCTCTGTAC
CCAACGGGCAGACCCCTCTGAAGGCCAGGAGCCCGCGGGAGGAGATCCTGTAG

4. RESULTS

Our previous attempt to establish the traffic light system failed where red sCas9 and tomato expressing cells switch their color to green upon successful AAV infection and gene editing due to inefficient prevention of ZsGreen expression in the AAV independent of Cre and/or Dre mediated recombination. Most probably, the loxP and rox flanked stop mini cassettes were leaky since all AAV infected cells were green. Furthermore, these mini stop cassettes were chosen since for AAV packaging, the DNA fragment limitation should not proceed more than 5 kb between ITRs. To circumvent the usage of large stop cassettes that prevent ZsGreen expression in our traffic light system, we made use of the Flex and frex systems, where ORF of ZsGreen is placed in opposite orientation to the CAG promoter. To this end, we generated three AAV constructs 2a, 2b and 2c: the construct 2a contain Cre activatable CAG promoter driven inverted ZsGreen gene flanked by mutant and wt loxP site as well as an U6 promoter-driven gRNA of tdTomato and a U6 driven gRNA against the gene of interest (can be cloned by Bbs1). When expressed in cells that express the sCas9 and tomato in addition to Cre, the construct 2a will deliver the gRNA against the gene of interest (GOI) and the gRNA against tdTomato / sCas9. These gRNA will induce inactivation of the GOI as well as tdTomato and sCas9 gene thereby preventing the emission of red fluorescence. In addition, the ZsGreen gene will flipped be the CRE recombinase, thereby emitting green fluorescence. This switch from emitting red fluorescence to green is termed the traffic light system and allows for quick control of CRISPR Cas9 efficiently (**Fig.6**). For the construct 2b the inverted ZsGreen gene had been flanked by mutant and wt rox sites whereas in construct 2c the complete ZsGreen cassette is flexed but in addition the ZsGreen is divided into two parts separated by an intron containing frex sites such that proper ORF of ZsGreen can be only achieved upon Cre and Dre mediated inversion.

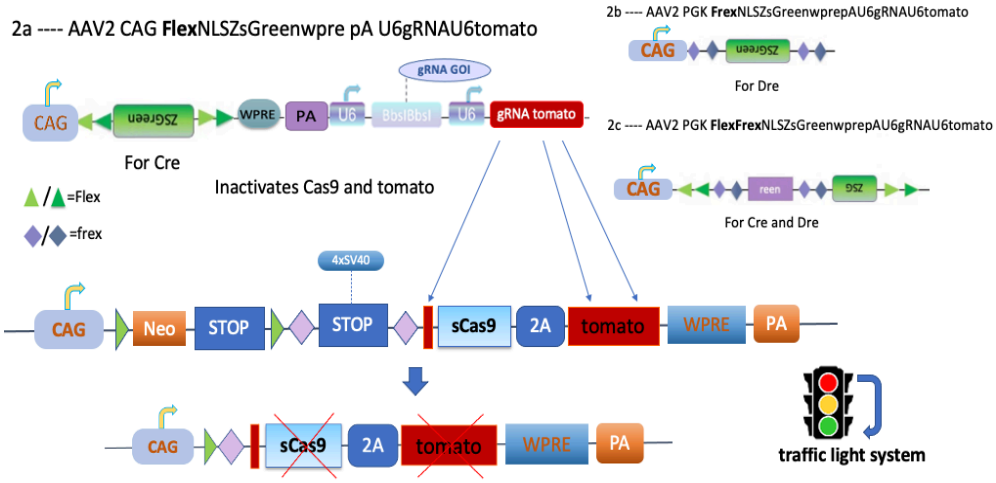

Figure 6: Generation of reporter AAV2 expressing gRNAs (2a, 2b, 2c) 2a=CAG FlexNLSZsGreenwprepAU6gRNAU6tomato,2b=CAGfrexNLSZsGreenwprepAU6gRNAU6to

mato, 2c=CAGFlexfrexNLSZsGreenwprepAU6gRNAU6tomato, CAG=chicken-beta-actin promoter, PGK= human phosphoglycerate kinase promoter

4.1. Generation of Cre-, Dre- and Cre/Dre-activatable AAV viruses with double U6 gRNA cassettes

2a, 2b and 2c constructs were described earlier and were purchased from thermos fisher gene arts company **(Fig.6)**. To insert those three plasmids in pAAV backbone, the pAAV plasmid was digested with BamH I and Mfe I restriction enzymes **(Fig.7 A)**. The 3,9 kb band corresponding to the digested backbone containing the CAG promoter, iTRs, the AmpR gene and plasmid sequence was then isolated. In parallel, plasmid 2a' was also digested with restriction enzymes Bam I, Mfe I, and Sca I. The 2,46 kb band corresponding to 2a was then inserted into the digested AAV backbone using conventional T4 ligase mediated cloning techniques **(Fig.7 B, C)**. The construct and presence of ITRs was validated by digestion with Sma I, successful constructs showing 2.58, 2.57 and a 1.1 kb band (**Fig.7 C).** This 2a plasmid **(Fig.7 D)** was used as backbone upon restriction enzyme mediated release of flex ZsGreen to generate 2b and 2c from 2b' and 2c' **(Fig.7 E, F)**. In short, 2a, 2b' and 2c' were digested with EcoR I and BamH I (**Fig.7 G)**. Digested 2b' and 2c' were inserted in digested 2a using T4 ligase to generate 2b and 2c plasmids. The constructs were validated by digestion with Sma I, successful constructs showing a 1.1 kb band (**Fig.7 H).** Plasmids 2a, 2b and 2c were sent to Vector Biolabs company for packaging into AAV2 capsids.

A

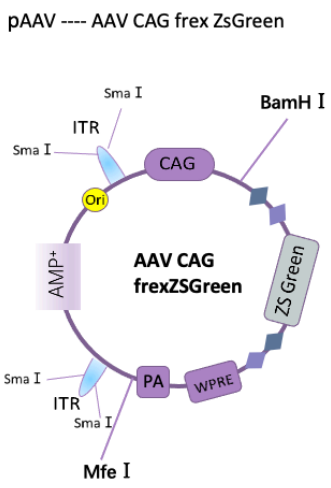

B

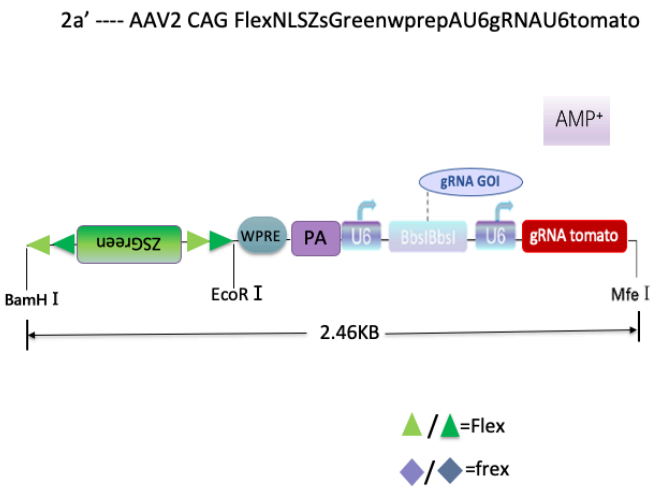

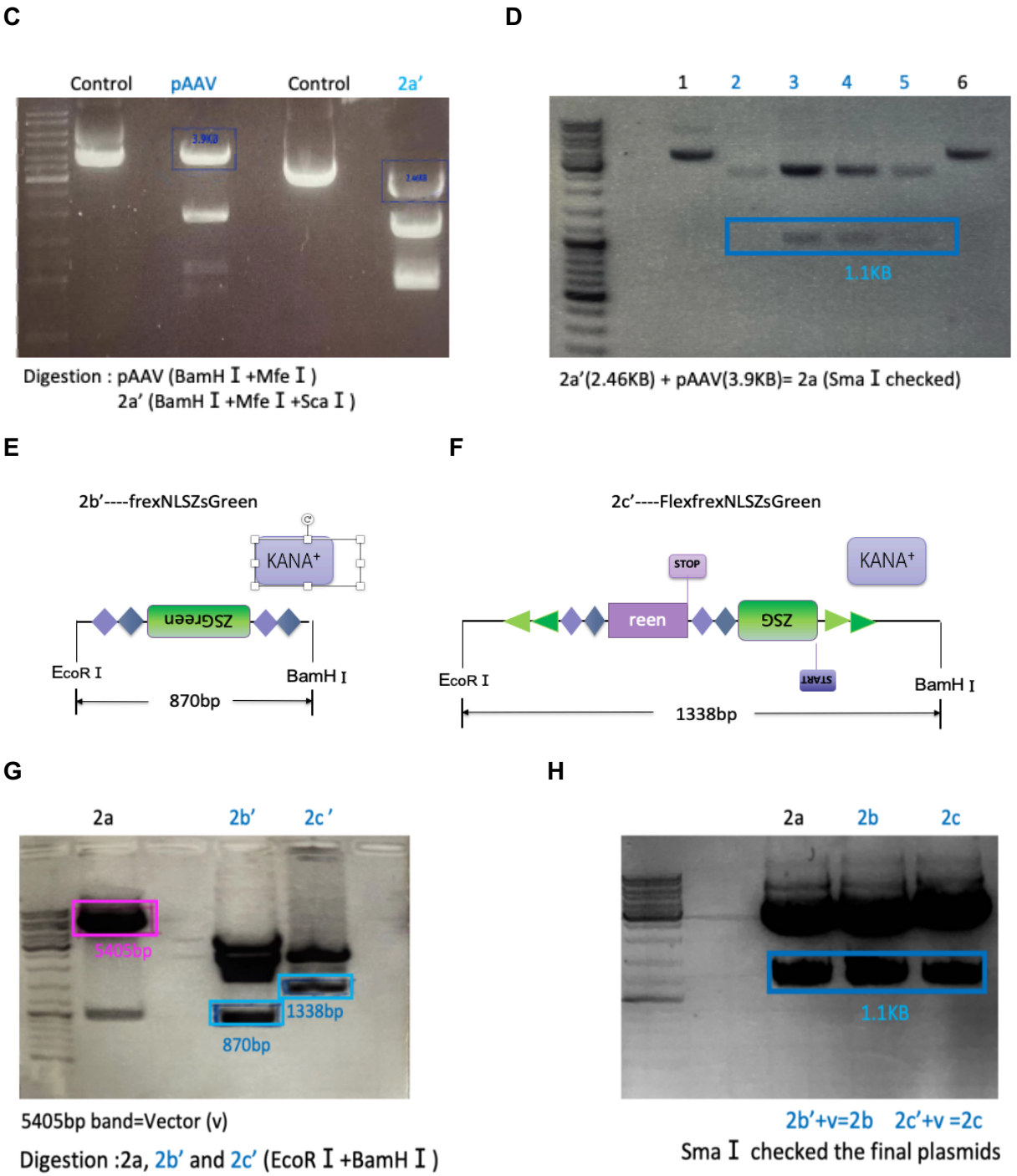

Figure 7: Generation of 2a, 2b, and 2c and checked the plasmids with Sma I. (A) pAAV backbone constructs (B) 2a' constructs (C) Digestion pAAV and 2a'of different restriction enzymes to obtain target bands (D) Sma I checked the 2a plasmid has the correct bands (E) 2b' constructs (F) 2c' constructs (G) EcoR I and BamH I digested 2a, 2b' and 2c' obtain target bands (H) Sma I checked the 2a, 2b and 2c plasmids have the correct bands.2a= CAG FlexNLSZsGreenwprepAU6gRNAU6tomato(6378bp),2b=CAGfrexNLSZsGreenwprepAU6gRNAU6tomato (6275bp), 2c= CAG FlexfrexNLSZsGreenwprepAU6gRNAU6tomato (6743bp).

4.1.1. Test the AAV2s (2a, 2b, 2c) in tdTOMATO MEFs

To ensure the previously generated viruses are functional, mouse embryonic fibroblasts MEFs) derived from the Ai9 line carrying a CAG driven loxP flanked stop cassette preventing tdTomato expression were transfected with plasmids expressing Cre, Dre or Cre and Dre using Lipo2000 method **(Fig.8 A)**. 48h later, those cells were infected with AAV2 of 2a, 2b, or 2c types.

Red fluorescence was only observed when cells were transfected with Cre or Cre/Dre plasmids. Green fluorescence was observed upon infection of 2A AAV of Cre transfected **(Fig.8 B)** whereas green fluorescence of Dre transfected cells was observed only upon infection with AAV2b. Strikingly, the green fluorescence of AAV 2c infected cells was only found when they were transfected with Cre and Dre expressing plasmids. Thus, this indicates that all three plasmids and AAVs are functional.

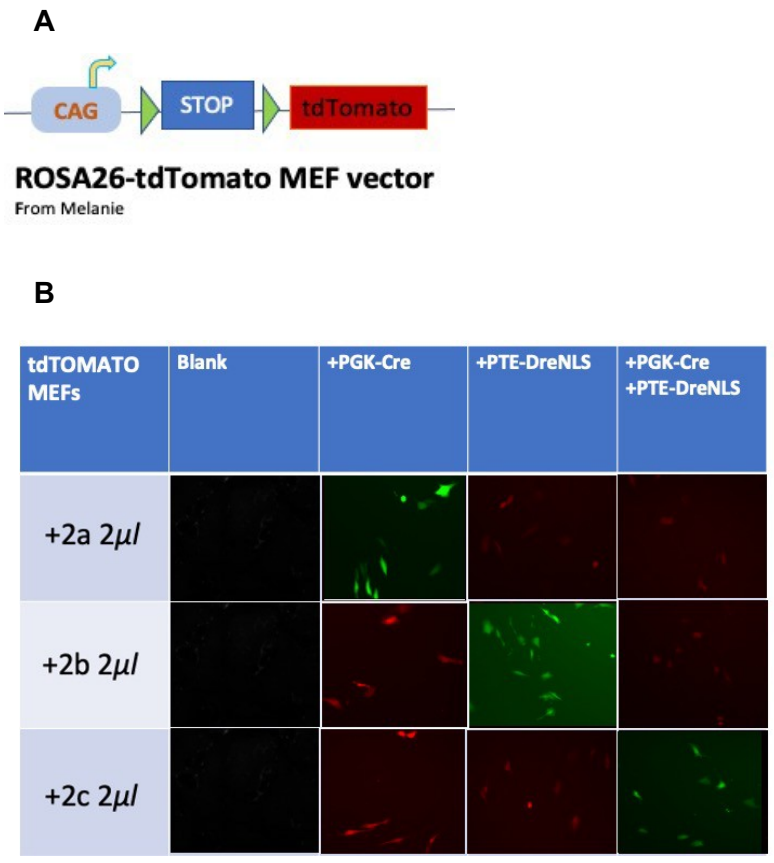

Figure 8: Examination of AAV functionalities using floxed tomato MEFs. (A) Schematic picture of Ai9 construct in MEFs. (B) Ai9 derived MEFs were transfected with either PGKCre, pTEDreNLS or with both. 48h after transfection, cells were infected with 2 µl of 2a, 2b, and 2c AAVs.

4.1.2. Examination of Traffic Light System in ES Cells

In the next step, we aimed at examining whether the traffic light system works in ES cells. Patrick Jankowski, technician in our group, had transiently transfected ES cells containing the sCas9 construct in their R26 locus with Cre and Dre expressing plasmids to excise the loxP and rox flanked stop cassette. While A1 and G4 clones showed no red fluorescence. A3 ES cells showed sCAS9 and tomato expression as revealed by fluorescence microscopy and western blot analysis **(Fig.9 A, B)**. Thus, A3 ES clone was used for further AAV infection procedures.

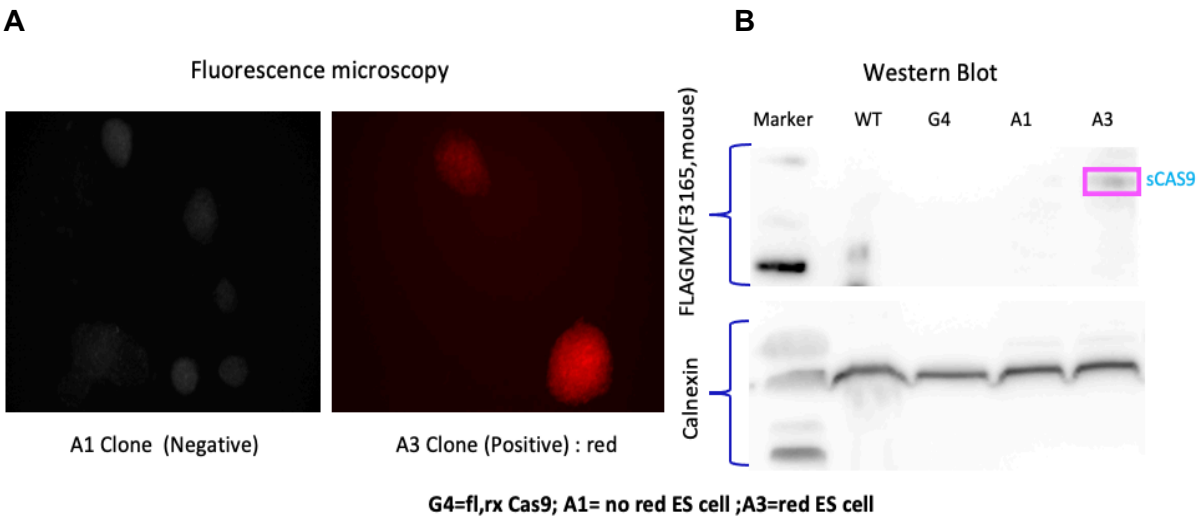

Figure 9: Successful expression of sCAS9 and tomato in ES cells upon Cre and Dre-mediated excision of STOP cassettes. (A) fluorescence microscopy (B) Western Blot using lysates from WT, G4 A1 and A3 clones with Cas9 and calnexin antibodies. This revealed that A3 clone has sCas9 expression.

4.1.3. Investigate AAV2 (2a) Efficiency in A3 sCas9 Tomato Expressing ES Cells

Our goal is to generate mouse lines that enables Cre/loxP and Dre/rox mediated expression of Cas9 with self-inactivating capacity. To ensure that the traffic light system works, we added HTNCre to A3 ES clone emitting red fluorescence. One day later, we infected these cells with the Cre activatable 2a virus. However, only the MEFs turned green, whereas the ES cells kept emitting red fluorescence, indicating that the infection was successful in MEFs but not in ES cells. **(Fig.10 A)**.

A

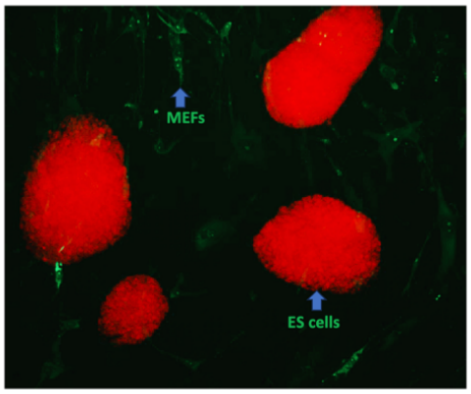

B

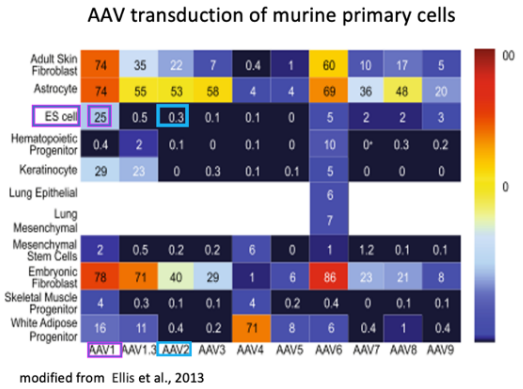

Figure 10: AAV2 (2a) infected sCas9 expressing A3 ES cells. (A) Only the MEFs were infected. (B) Efficiency of infection of ES cells by different serotypes of AAVs.

Our difficulties in infecting ES cells with AAV2 (2a) could be due to the choice of the AAV serotype. AAV2 (0.3%) is known to have a particularly low infection rate toward ES cells whereas AAV1 (25%) is the most effective serotype to transduces cells (**Fig.10 B**)[72].

4.1.4. Examination of Off-Target Effects in ES Cells Using STAT3 gRNA

Since AAV1 is most effective in infecting ES cells, we aimed at investigating whether our traffic light system works with AAV1 serotype packed plasmids. Furthermore, we have used a new strategy. In addition to relying on color changes, we will rely on ES differentiation status as well. ES cells maintain their pluripotency via LIF/Stat3 axis – thus ES cells grow in media supplemented with LIF. When STAT3 is activated by LIF, ES cells cannot differentiate. On the other hand, when provided with gRNA against STAT3, ES cells differentiate even when stimulated with LIF, which is easily visible in the microscope. Three new plasmids are needed to apply this new strategy:

1. Plasmid a containing gRNA against STAT3 and a flex mCherry reporter gene. When infected by this virus ES cells expressing tdTOMATO, Cre, and sCas9 should emit red fluorescence and be differentiated (**Fig.11 A**).
2. Plasmid b (AAV2a with gRNA STAT3) contains gRNA against STAT3, gRNA against tdTOMATO, and a flex ZsGreen reporter gene. When infected by this virus ES cells expressing tdTOMATO, Cre, and sCas9 should stop emitting red fluorescence, start emitting green fluorescence, and be differentiated (**Fig.11 B**).
3. Plasmid c (AAV 2a) containing gRNA against tdTOMATO and a flex ZsGreen reporter gene. When infected by this virus ES cells expressing tdTOMATO, Cre, and sCas9 should stop emitting red fluorescence, and start emitting green fluorescence **but not** be differentiated (**Fig.11 C**).

Plasmids A (without gRNA insertion) was obtained from Fenselau group. Plasmids A and B were digested with restriction enzyme Bbs I and the gRNA against STAT3 was inserted to create plasmids a and b. The ITRs of the three constructs were validated by digestion with Sma I, with successful constructs b and c showing a 1,1 kb band and successful construct a showing a 750 bp band **(Fig.11 D)**. gRNA insertion was verified by sequencing. Subsequently, plasmids A, B, and C were sent to Vector Biolabs company for packaging into AAV1 serotype.

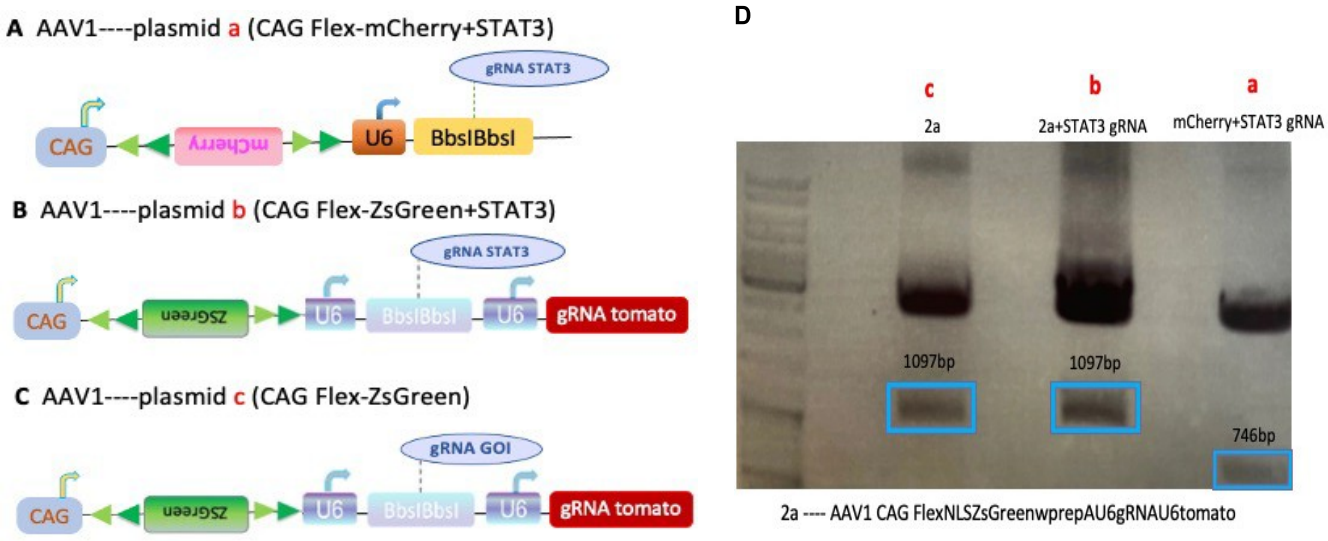

Figure 11: Generation of AAV1 (a, b, c) expressing gRNA STAT3 or GOI. (A) a= CAG Flex-mCherry-U6-gRNA STAT3- U6gRNAtomato=mCherry+STAT3 (B) b= CAG Flex-ZsGreen-U6-gRNA STAT3-U6gRNAtomato=2a+STAT3 (C) c= CAG Flex-ZsGreen-U6-gRNA GOI (blank)-U6gRNAtomato=2a (D) a=insert the STAT3 gRNA into the Bbs I sites of Flex-mCherry, b= insert the STAT3 gRNA into the Bbs I sites of 2a, c= 2a

4.1.5. Test AAV1s (a, b, c) in ES Cells

To examine whether the AAV1 packed plasmids worked, A3 ES cells expressing tdTomato, Cre, and sCas9 were infected. When infected with AAV1 (a) the ES cells remained not differentiated and emitted red fluorescence indicating that the infection was not successful **(Fig.12 A)**. Of note, when infected with AAV1 a, MEFs but not ES cells expressed mCherry, whereas AAV1 b and c infected MEFs, emitted green light, indicating successful infection rates in MEFs but not es cells that remained tomato red and undifferentiated **(Fig.12 B, C)**. Thus, even when packed with previously published AAV1 serotype, our traffic light system cannot be tested in ES cells since they are not infected by AAVs.

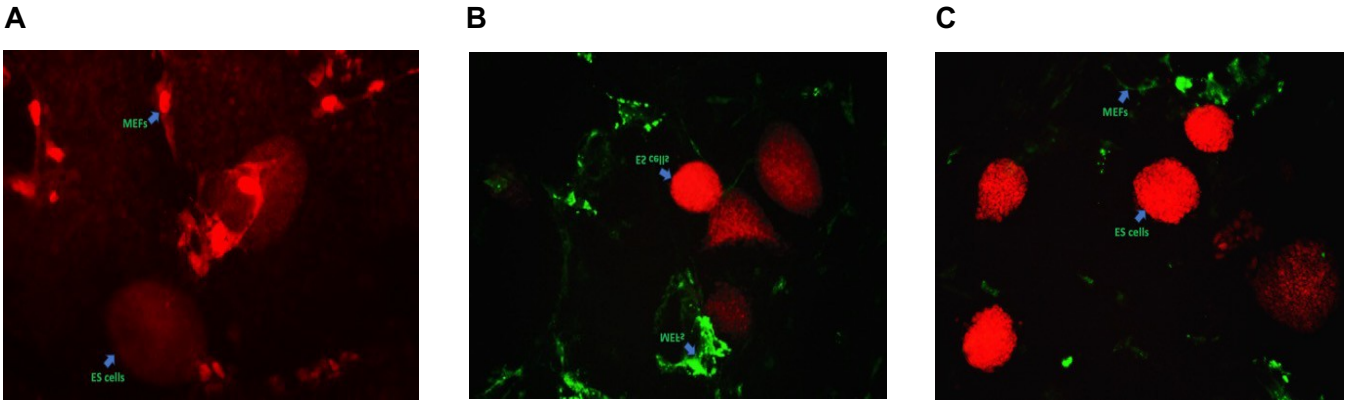

Figure 12: AAV1s (a, b, c) infected sCas9 ES cells & tdTomato MEFs. (A) AAV1a (mCherry +STAT3), (B) AAV1b (2a+STAT3), (C) AAV1c (2a).

Our difficulties to infect ES cells with AAV could be circumvent with a new strategy consisting of in over expressing AAV receptor (AAVR). Indeed, it has been described that overexpression of AAVR dramatically increases the infection rate by AAV2 **(Fig.13)** [73]. So, our next step would be to generate a novel traffic light construct that in addition to sCas9 and tomato expresses the AAVR upon Cre and Dre mediated recombination.

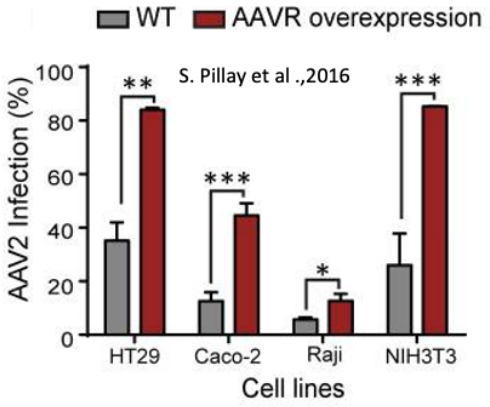

Figure 13: Cells that overexpress AAVR increase the susceptibility of AAV2.

4.1.6. Modification of Conditional R26 Targeting Vector of sCas9E2AtdTomato with P2AAAVR Cassette

Next, we wanted to generate a conditional R26 TV encoding sCas9 AAVR and tdTomato. A plasmid containing the 5' end of the sCAS9 gene, a P2A peptide, and the AAVR gene was purchased from Thermo Fisher gene arts and inserted into the pre-existing R26 fl rx sCas9E2AtdTomato plasmid via digestion with restriction enzymes Kfl I and Fse I. This led to the generation of a plasmid expressing sCas 9, AAVR under the control of a CAG promotor, a rox-flanked stop cassette, and a loxP-flanked stop cassette (**Fig.14 A**). The construct was validated by digestion with EcoR I successful showing 8400, 4303, 3610, and 960 bp bands (**Fig.14 B**).

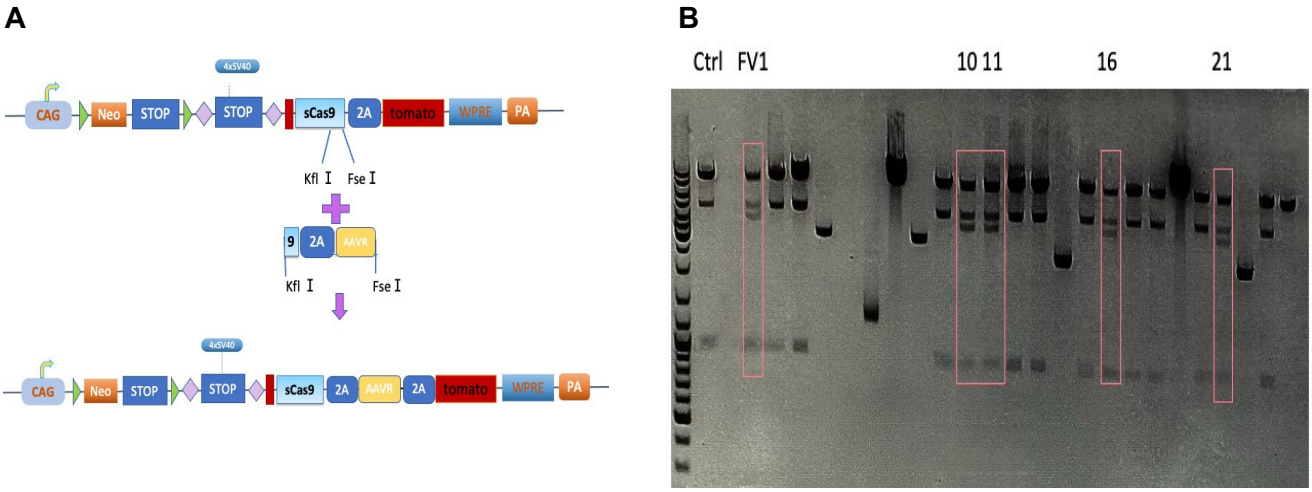

Figure 14: sCas9E2A-AAVR Final ROSA26 targeting Vector. (A) Insert AAVR into the sCas92A-tomato plasmid. (B) EcoR I checked Miniprep sCas9-2A-AAVR Final Vector. Final Vector 1, 10, 11, 16, 21 have correct bands.

In the future, we will transfect ES cells with this plasmid and infect them with our AAV2. AAVR is only for AAV2 viruses to hopefully create *in vitro* our traffic light system **(Fig.15)**.

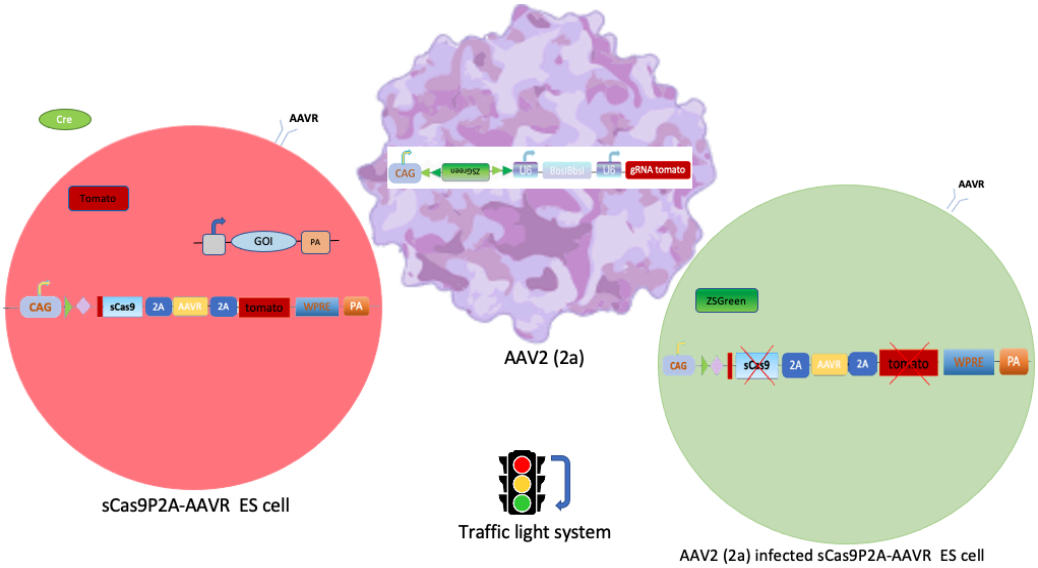

Figure 15: Traffic lights system operation diagram in sCas9-2A-AAVR ES cells.

4.2. The Role of STAT5 in MASH

In previous work, our lab investigated the role of NIK during MASH and found that a hepatocyte-specific knock-out of NIK in mice protects from MASH development. Single-nucleus RNA seq (snRNA-Seq) of the hepatocytes of NIK ^{KO} mice revealed an upregulation of JAK-STAT signaling in NIK ^{KO} mice[68]. Further investigations revealed that in NIK$^{fl/fl}$ animals, NIK phosphorylates JAK2 and thereby inhibits JAK2 kinase activity, preventing the phosphorylation and activation of downstream STAT5. This increases free fatty acid uptake, lipogenic gene expression, and MASH[68]. This mechanism is absent in NIK KO animals as NIK

does not phosphorylate JAK2 due to the knock-out. Thus, in NIK ^{KO} animals, STAT5 is activated and can inhibit free fatty acid uptake and lipogenic gene expression and instead induce hepatoprotective gene expression, leading to protection from MASH[68].

4.2.1. Alfp-Cre Expression is Sufficient to Deplete Hepatic STAT5 Expression

STAT5$^{fl/fl}$ mice were obtained from "European Conditional Mouse Mutagenesis Program" (EUCOMM). To inactivate STAT5 specifically in the liver, STAT5$^{fl/fl}$ mice[74] were intercrossed with Alfp-Cre expressing mice[75], allowing for hepatocyte-specific Cre-mediated STAT5 inactivation from the embryonic stage. Thereby, the STAT5 gene was specifically removed in hepatocytes (STAT5^{LKO}). These hepatocyte-specific knock-out animals (STAT5^{LKO}) will be compared to control animals with floxed STAT5 (STAT5$^{fl/fl}$). MASH will be induced by feeding a MASH- or CDAA- (Choline deficient high-fat diet) diet to the animals for 20 weeks, starting 6 weeks after birth. The MASH diet consists of 40% coming from lard with 2% cholesterol and a high sugar content (34.2%). Feeding this diet to mice leads to the development of histological and metabolic properties of human MASH with diffuse fibrosis but without cirrhosis. In contrast, the CDAA diet, enriched with 1% cholesterol and butter fat, induces macrovascular steatosis after 3 weeks and fibrosis after 16 weeks in mice. Both diets have their control counterparts against which they will be compared MASH or CDAA control diet, respectively **(Fig.16)**. The experiment will be performed twice with each time 20 knockout and 20 control animals (STAT5$^{fl/fl}$) resulting in 4 cohorts of 20 transgenic vs. 20 floxed animals to assess the role of STAT5 in hepatocytes.

During the feeding period, insulin and glucose tolerance will be assessed by insulin and glucose tolerance tests (ITT, GTT) to monitor the progression of NASH. ITTs and GTTs will be performed at weeks 12 and 22 and weeks 13 and 23, respectively. Additionally, the blood of each mouse will be collected at weeks 5, 9, 14, 19, and 24 to measure the activity of liver transaminases (ALT, AST), which reflects the level of liver injuries and MASH progression. At week 25 micro computed tomography (MicroCT) will be performed to analyze the fat content and its distribution in the animals' bodies. At week 26, the mice will be sacrificed. The liver will be harvested for further analysis. Furthermore, the hepatic immune cell population and their activation state will be analyzed by FACS. The organs will also be analyzed by qPCR and western blot analyses for the progression of MASH and expression of inflammatory cytokines like Tweak, IL6, and TNFa. In addition to this, we will perform transcriptomic analysis of the livers from control and experimental animals to investigate potential changes in signaling pathways, especially in the JAK-STAT signaling pathway.

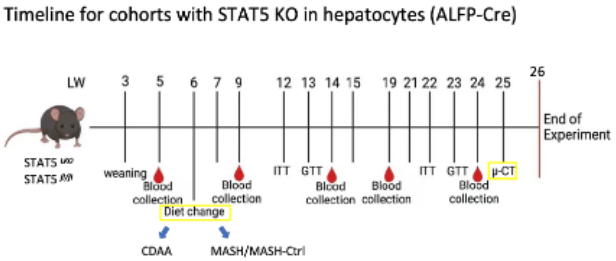

Figure 16: Generation of hepatic STAT5 knock-out mice (STAT5LKO). (A) Generation of hepatic STAT5 knock-out mice. Hepatocyte-specific deletion of loxP flanked STATA5a/b was mediated by Alfp-Cre mediated recombination. (B) Timeline for cohorts with STAT5 KO in hepatocytes (ALFP-Cre). ITT = Insulin tolerance test, GTT = Glucose tolerance test, CDAA = Choline deficient high-fat diet, NASH = 40% kcal fat with 2% cholesterol and 34.2% sugar diet.

4.2.2. STAT5^{LKO} Mice are Smaller in Size and Suffer from Steatosis

Our previous results point towards the role of STAT5 in hepatocytes, as it is affected by NIK activity via JAK2 phosphorylation[68]. To investigate whether STAT5 inactivation in the liver affects metabolism and fibrosis, we created STAT5^{LKO} mice by intercrossing STAT5$^{fl/fl}$ mice with Alfp-Cre mice. STAT5^{LKO} mice show impaired expression of STAT5 target genes in the liver **(Fig.17 A, B)**. The NCD-fed mice with hepatic STAT5 deficiency showed a significantly reduced body length after 26 weeks of age **(Fig.17 C)**. Serum ASAT, ALAT, triglyceride, and cholesterol levels were measured at 26 weeks of age. The triglyceride, cholesterol, and ASAT levels were the same in the two genotypes. In contrast, the serum levels of ALAT were significantly increased in STAT5^{LKO} mice compared to STAT5$^{fl/fl}$ mice **(Fig.17 D)**.

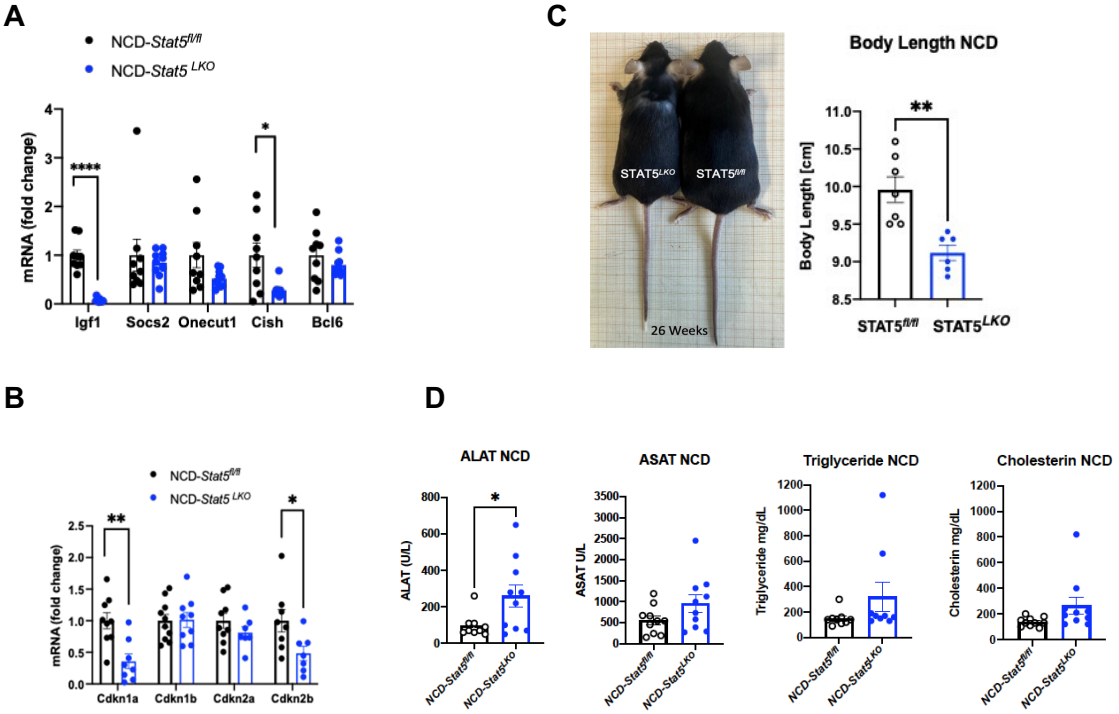

Figure 17: Hepatic STAT5 deficiency reduces STAT5 gene expression and body length and increases serum ALAT in NCD-fed mice. (A) Expression of STAT5 target genes in mice's liver (n = 8-10). (B) Expression of Cell cycle STAT5 target genes in mice's liver (n = 8-10). (C) Representative images show the significantly reduced body length of STAT5^{LKO} mice compared with those of STAT5fl/fl mice (n = 6-7). (D) Serum ALAT and ASAT levels of Ctrl and STAT5^{LKO} mice at 26 weeks of age; triglyceride and cholesterol levels of Ctrl and STAT5^{LKO} mice at 26 weeks of age (n = 8-10). (Two-tailed unpaired t-test. Mean ± SEM, p* ≤ 0.05, p** ≤ 0.01, p*** ≤ 0.001, p**** ≤ 0.0001).

Next, we aimed to investigate whether hepatic stat5 deficiency affects steatosis. The HE and Oil red O Staining showed that compared with the control group, the hepatocytes of STAT5^{LKO} mice were arranged loosely and showed many fat vacuoles, hepatocyte steatosis, and inflammatory cell infiltration **(Fig.18 A, B)** Oil-red O Staining quantitated by Fiji shows the liver of STAT5^{LKO} mice had significantly more fat droplets than the control group **(Fig.18 C)**. Liver qPCR showed that compared to the wild-type, fat-associated genes (CD36, Scd1, Fasn, Srebf1) expression was increased significantly in STAT5^{LKO} mice **(Fig. 18D)**. Thus, without further challenge, STAT5^{LKO} mice are smaller and suffer from steatosis most probably via the impairments of negative pituitary/hypothalamic/liver feedback axis via GH/Igf1.

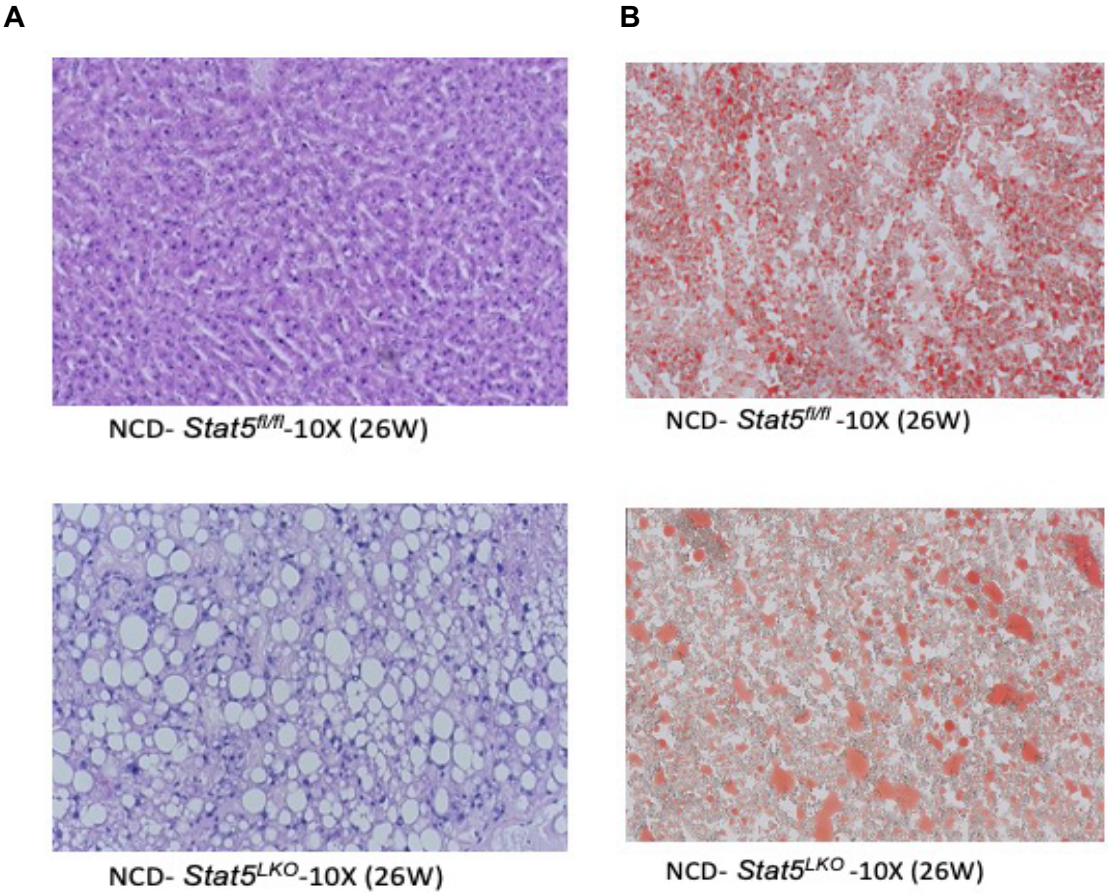

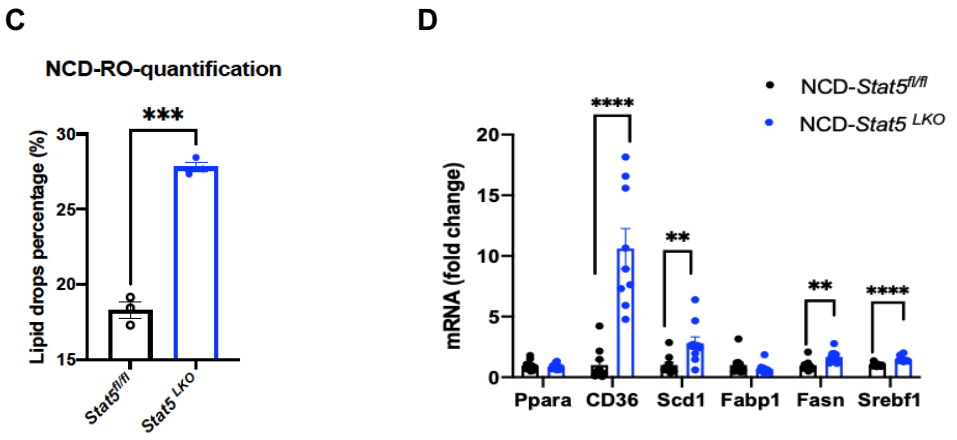

Figure 18: Hepatic STAT5 deficiency aggravates hepatocyte lipidosis and increase fat gene expression in NCD-fed mice. (A) HE stains in mice's liver: STAT5$^{fl/fl}$ (WT) and STAT5^{LKO} (TG) mice (26 weeks). NCD-WT: Normal hepatocytes were closely arranged in a strip shape and had no cell edema and steatosis; NCD-TG: hepatocytes were loosely arranged with mild edema and steatosis. (B) Oil red O staining in mice's liver: normal chow diet (NCD) of STAT5$^{fl/fl}$ (WT) and STAT5^{LKO} (TG) mice (26 weeks). NCDWT: A small number of punctated red-stained lipid droplets; NCD-TG: A portion of red-stained lipid droplets was blocky. (C) Oil-red O Staining Analysis by Fiji: 16bit, threshold from 0-142. (D) Expression of Fat genes in mice's liver (n = 8-10). (Two-tailed unpaired t-test. Mean ± SEM, p* ≤ 0.05, p** ≤ 0.01, p*** ≤ 0.001, p**** ≤ 0.0001)

Inflammatory genes (TNFα, IFNγ, IL1β) expression was significantly increased in STAT5^{LKO} mice compared to control mice **(Fig.19 A)**. Macrophage target gene (Clec4f, Nos2) expression was significantly increased in STAT5^{LKO} mice compared to STAT5$^{fl/fl}$ mice **(Fig.19 B)**. The expression of fibrosis (Timp1, Tgfb1, Col1a1, Col1a2) was significantly higher than in the control mice **(Fig.19 C)**. taken together, these experiments demonstrate that hepatic STAT5 inactivation promotes inflammation and fibrosis.

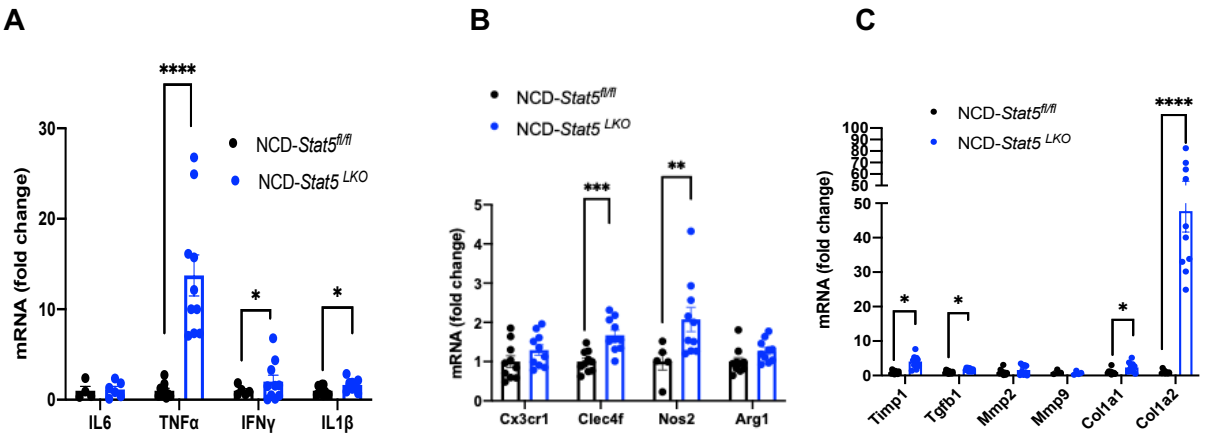

Figure 19: Hepatic STAT5 deficiency increases some of inflammatory and fibrosis gene expression in NCD-fed mice. (A) HE stains in mice's liver: STAT5$^{fl/fl}$ (WT) and STAT5^{LKO} (TG)

mice (26 weeks). NCD-WT: Normal hepatocytes were closely arranged in a strip shape and had no cell edema and steatosis; NCD-TG: hepatocytes were loosely arranged with mild edema and steatosis. (B) Oil red O staining in mice's liver: normal chow diet (NCD) of $STAT5^{fl/fl}$ (WT) and $STAT5^{LKO}$ (TG) mice (26 weeks). NCD-WT: A small number of punctated red-stained lipid droplets; NCD-TG: A portion of red-stained lipid droplets was blocky. (C) Oil-red O Staining Analysis by Fiji: 16bit, threshold from 0-142. (D) Expression of Fat genes in mice's liver (n = 8-10). (Two-tailed unpaired t-test. Mean ± SEM, p* ≤ 0.05, p** ≤ 0.01, p*** ≤ 0.001, p**** ≤ 0.0001).

4.2.3. $STAT5^{LKO}$ Mice Exposed to the MASH Diet Show Largely Unaltered Phenotypic Changes

Then, we wanted to investigate whether Stat5lko mice show worsened liver fat accumulation, inflammation, or fibrosis. Therefore, we exposed cohorts of $STAT5^{LKO}$ and ctrl mice to MASH and MASH-Ctrl diets. Liver qPCR showed that in $STAT5^{LKO}$ mice, the expression of almost all STAT5 target genes (Igf1, Onecut1, Cish, Cdkn1a) were significantly decreased compared with the control mice, except Bcl6, which is inversely regulated to STAT5 **(Fig.20 A, B)**. When fed with the MASH-Ctrl diet group, the weight of $STAT5^{LKO}$ mice was not significantly different from control mice ($STAT5^{fl/fl}$), though obviously with a tendency towards decreased BW **(Fig.20 C)**. Upon MASH diet feeding, the weight of $STAT5^{LKO}$ mice decreased significantly compared to that of control mice ($STAT5^{fl/fl}$) **(Fig.20 D)**. In MASH-Ctrl and MASH-fed mice, the final body was significantly decreased in STAT5 knockout mice **(Fig.20 E)**. In addition, at 25 weeks of age, the µCT revealed that $STAT5^{LKO}$ mice showed a significant reduction in fat percentage under the MASH-Ctrl fed condition **(Fig.20 F)**. Concordantly, the final WAT was significantly decreased in STAT5 knockout mice in MASH-Ctrl and MASH-fed mice **(Fig.20 G)**.

A **B**

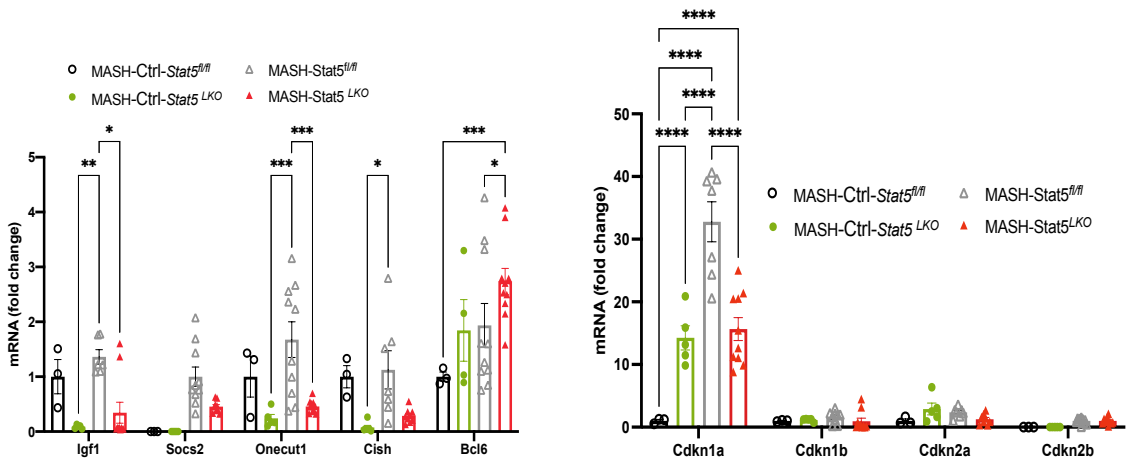

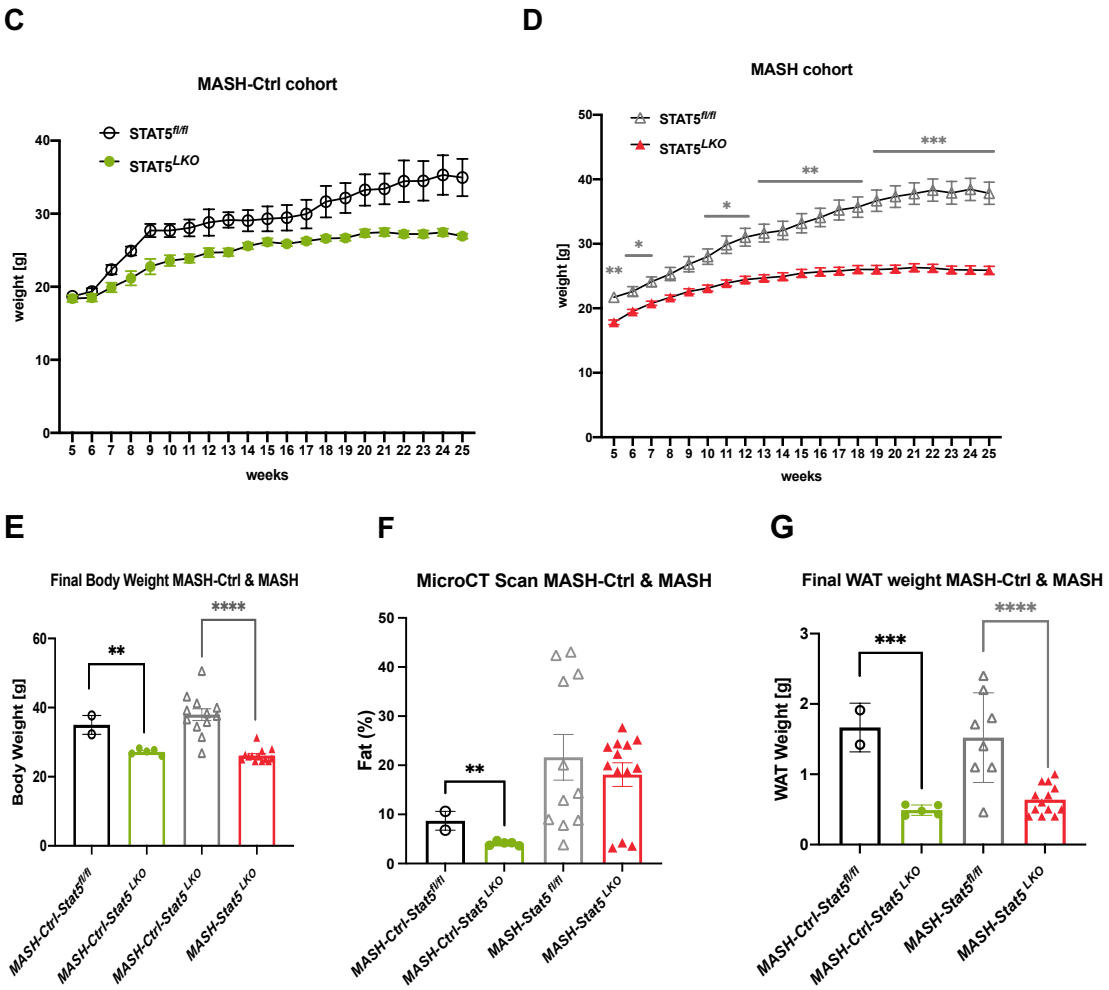

Figure 20: The expression of STAT5 target genes decreased in mice's liver, and body weight and fat distribution were reduced in STAT5LKO mice under MASH-Ctrl / MASH conditions. (A) Expression of STAT5 target genes in mice's liver (MASH-Ctrl-fed mice: n = 3-5, green column; MASH-fed mice: n = 8-10, red column). (B) Expression of cell cycle STAT5 target genes in mice's liver (MASH-Ctrl-fed mice: n = 3-5, green column; MASH-fed mice: n = 8-10, red column). (C) Body weight curve of Ctrl and STAT5^{LKO} mice in MASH-Ctrl cohort (n = 3-7). (D) Body weight curve of Ctrl and STAT5^{LKO} mice in MASH cohort (n = 10-11). (E) Final body weight of Ctrl and STAT5^{LKO} mice in MASH-Ctrl -fed mice (n = 3-5, green column); mice in MASH-fed mice (n = 8-11, red column). (F) Fat percentage of Ctrl and STAT5^{LKO} mice at 26 weeks of age (MASH-Ctrl-fed mice: n = 3-5, green column; MASH-fed mice: n = 8-11, red column). (G) Final WAT weight of Ctrl and STAT5^{LKO} mice in MASH-Ctrl -fed mice (n = 3-5, green column); mice in MASH-fed mice (n = 8-11, red column). (Ordinary two-way ANOVA; two-tailed unpaired t-test. Mean ± SEM, p* ≤ 0.05, p** ≤ 0.01, p*** ≤ 0.001, p**** ≤ 0.0001).

4.2.4. Aminotransferase Reveal Largely Altered Upon MASH-Ctrl and MASH-fed STAT5^{LKO} Mice

Upon sacrificing the animal cohorts, we investigated macroscopic appearance of livers of mice. In MASH-Ctrl-fed condition, STAT5^{LKO} animals' liver appeared bigger than STAT5$^{fl/fl}$ animals

(Fig.21 A). However, there was no significant difference in the appearance of mice livers between the STAT5$^{fl/fl}$ and STAT5^{LKO} animals under MASH-fed condition **(Fig.21 B)**. Under MASH-Ctrl-fed condition, compared with the control group, the hepatocytes of STAT5^{LKO} mice were arranged loosely and showed hepatocyte steatosis, and inflammatory cell infiltration. However, mice fed the MASH diet developed hepatocyte necrosis and steatosis regardless of hepatocyte STAT5 inactivation **(Fig.21 C)**. Serum triglyceride and cholesterol levels did not differ between MASH-Ctrl and MASH mice. However, under the MASH-Ctrl condition, serum ALAT concentration was significantly increased in STAT5^{LKO} mice at 26 months of age compared to control mice, indicating increased liver damage in STAT5 deficient animals. In contrast, under MASH-fed conditions, serum ASAT and ALAT in STAT5^{LKO} mice were decreased (**Fig.21 D)**.

Collectively, hepatic Stat5 inactivation increases steatosis and liver inflammation whose progression is not more pronounced when exposed to MASH diet feeding.

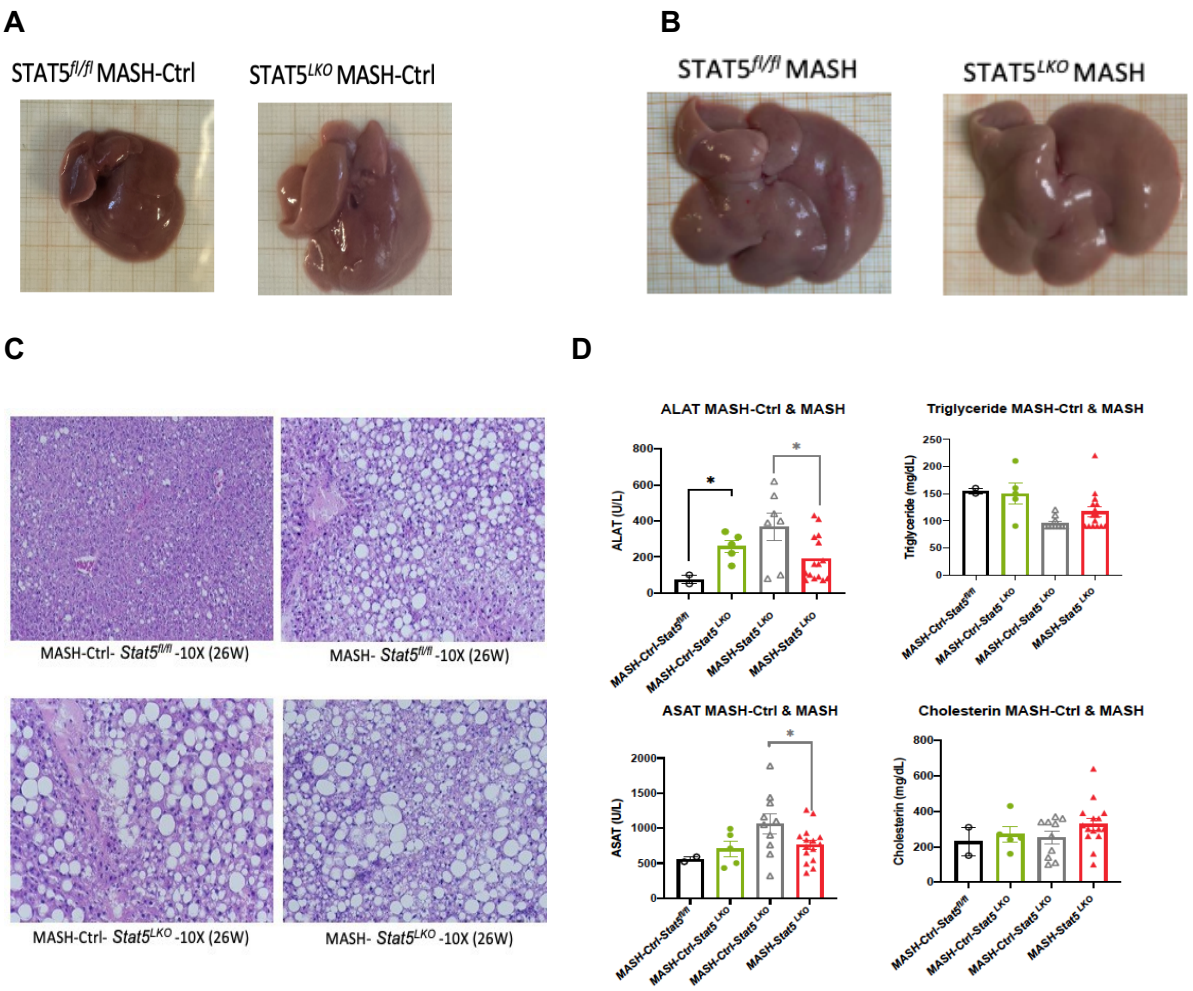

Figure 21: STAT5^{LKO} mice's liver shows oilier, aminotransferase revealed largely altered under MASH-Ctrl / MASH conditions. (A) Representative images show that under MASH-Ctrl-fed condition, STAT5^{LKO} mice's liver is oilier than control mice. (B) Representative images show that MASH-fed mice livers from both genotypes did not differ significantly in appearance.

(C) HE stains in mice's liver: MASH-Ctrl diet of STAT5*fl/fl* (WT) and STAT5*LKO* (TG) mice (26 weeks); MASH diet of STAT5$^{fl/fl}$ (WT) and STAT5^{LKO} (TG) mice (26 weeks). (D) Serum ALAT and ASAT levels of Ctrl and STAT5^{LKO} mice at 26 weeks of age (MASH-Ctrl-fed mice: n = 3-5, green column; MASH-fed mice: n = 8-10, red column). Serum triglyceride and cholesterol levels of Ctrl and STAT5^{LKO} mice at 26 weeks of age (MASH-Ctrl -fed mice: n = 3-5, green column; MASH-fed mice: n = 8-10, red column. (Ordinary two-way ANOVA; two-tailed unpaired t-test. Mean ± SEM, p* ≤ 0.05, p** ≤ 0.01).

4.2.5. STAT5^{LKO} Mice Shows Significant Hepatic Steatosis Under MASH-Ctrl-fed Condition

In the MASH feeding group, there was no significant difference in the deposition of lipid droplets in hepatocytes of both genotypes of mice. However, STAT5^{LKO} mice showed more red lipid droplets than the control mice under MASH-Ctrl-fed condition **(Fig.22 A)**. This is consistent with the results of Fiji analysis **(Fig.22 B)**. Liver qPCR showed that compared to the wild-type, fat-associated genes (Pparαγ, Scd1, Fasn, Srebf1) expression were increased significantly in STAT5^{LKO} mice under MASH-Ctrl and/or MASH dietary conditions **(Fig.22 C)**.

These experiments reveal again that STAT5 deficiency under ctrl diet conditions increase ectopic fat deposition in the liver, that is not more pronounced when mice are exposed to MASH diet feeding. Conclusively, it seems that MASH diet feeding recapitulates STAT5 deficiency under ctrl diet feeding or in other words: MASH diet decreases STAT5 activity.

A

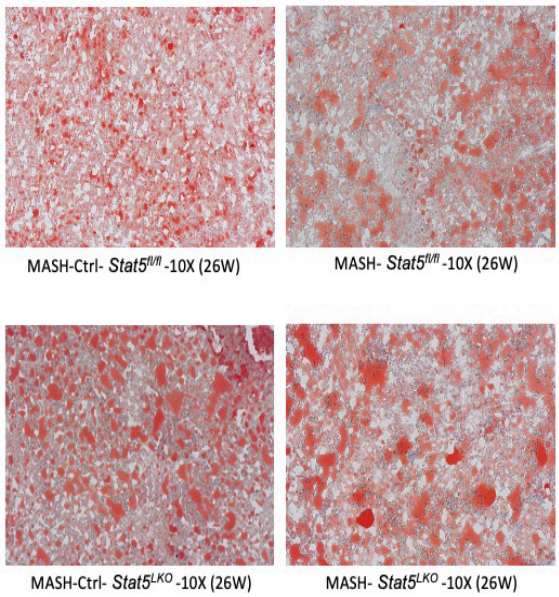

B

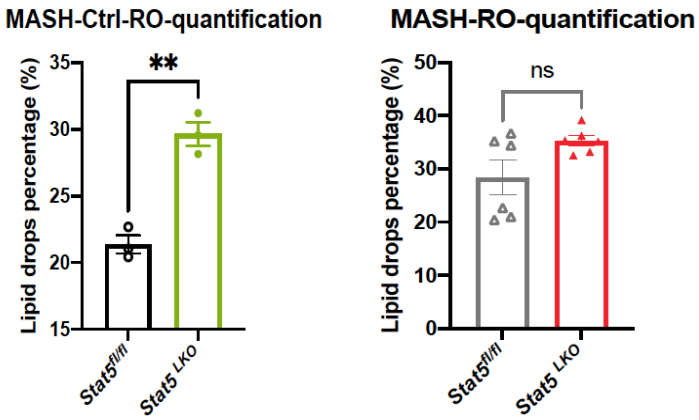

C

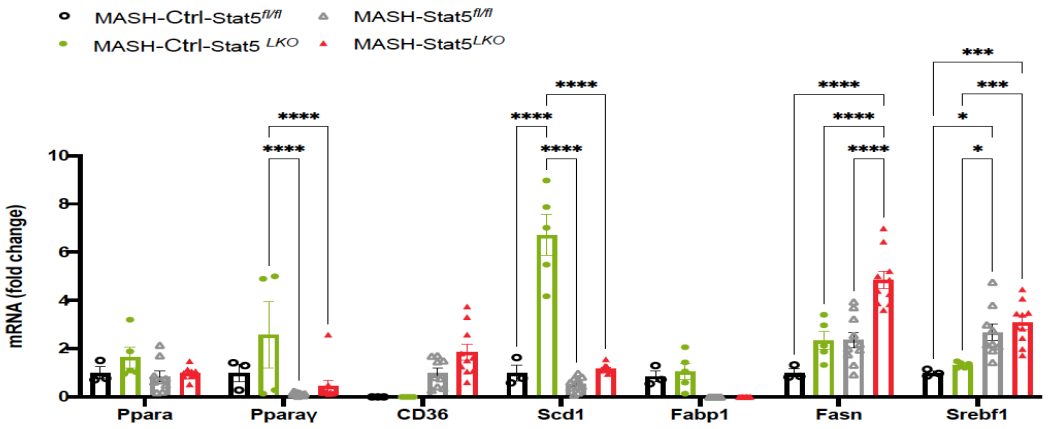

Figure 22: STAT5LKO mice's liver shows significant hepatic steatosis under MASH-Ctrl-fed condition. (A) Oil red O staining in mice's liver: MASH-Ctrl diet of STAT5$^{fl/fl}$ (WT) and STAT5^{LKO} (TG) mice (26 weeks). MASH-Ctrl-WT: A small number of punctate, red-stained lipid droplets; MASH-Ctrl-TG: A part of the red-stained lipid droplets was blocky; MASH diet of STAT5$^{fl/fl}$ (WT) and STAT5^{LKO} (TG) mice (26 weeks). Both genotypes showed large areas of massive, red-stained lipid droplets. (B) Oil-red O Staining Analysis by Fiji: 16bit, threshold from 0-142 (C) Expression of Fat genes in mice's liver (MASH-Ctrl-fed mice: n = 3-5, green column; MASH-fed mice: n = 9-10, red column). (Ordinary two-way ANOVA; two-tailed unpaired t-test. Mean ± SEM, p* ⩽ 0.05, p** ⩽ 0.01, p*** ⩽ 0.001, p**** ⩽ 0.0001).

4.2.6. STAT5^{LKO} Mice Reveal Expression of Inflammatory and Fibrosis Genes Altered Upon MASH-Ctrl and MASH-fed Conditions

Next, we aimed at investigating whether hepatic stat5 deficiency alters hepatic micromilieu. To this end, we performed qPCR for inflammatory mediators, macrophage specific and fibrosis genes. Inflammatory genes (IL6) expression was largely unaltered **(Fig.23 A),** but Nos2 (marker for M1 inflammatory macrophages was increased in ctrl mash fed STAT5^{LKO} mice as well as similarly in mash diet fed livers. Infiltrating Macrophage indicated by Cx3cr1 expression was comparably increased in MASH diet-fed livers when compared to MASH-Ctrl-fed mice **(Fig.23 B)**. Moreover, the expression of fibrosis (Timp1, Mmp2, Col1a1) was increased in STAT5^{LKO} livers than in the control mice **(Fig.23 C)**. Conclusively, under the MASH diet, hepatic STAT5 deficiency might promote M1 macrophage polarization, which might affect hepatic stellate cells to increase fibrosis.

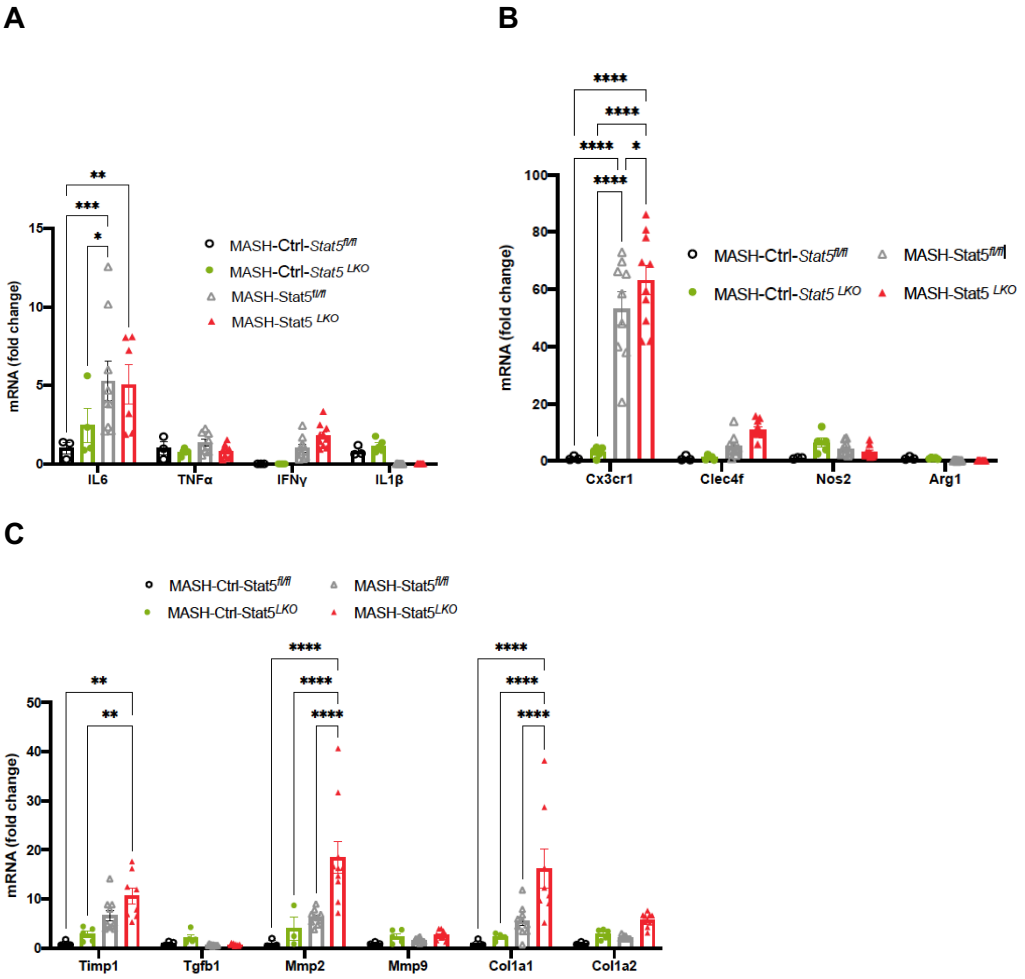

Figure 23: Inflammatory, Macrophage target and fibrosis genes reveal altered under MASH-Ctrl / MASH-fed STAT5LKO mice. (A) Expression of Inflammatory genes in mice's liver (MASH-Ctrl-fed mice: n = 3-5, green column; MASH-fed mice: n = 8-10, red column). (B) Expression of macrophage target genes in mice's liver (MASH-Ctrl-fed mice: n = 3-5, green column; MASH-fed mice: n = 8-10, red column). (C) Expression of Fibrosis genes in mice's liver (MASH-Ctrl-fed mice: n = 3-5, green column; MASH-fed mice: n = 8-10, red column). (Ordinary two-way ANOVA; two-tailed unpaired t-test. Mean ± SEM, p* ⩽ 0.05, p** ⩽ 0.01, p*** ⩽0.001, p**** ⩽ 0.0001).

4.2.7. STAT5^{LKO} Mice Show Unaltered Insulin Sensitivity and Glucose Homeostasis

Insulin tolerance (ITT) and glucose tolerance tests (GTT) were performed at 12, 13 ,22, and 23 weeks[76-78]. The results show that ITT was unaltered between the genotypes **(Fig.24 A)**. However, after 13 weeks and 23 weeks of age, the GTT data revealed slightly enhanced glucose tolerance in STAT5^{LKO} mice compared to controls under MASH-Ctrl and MASH dietary conditions **(Fig.24 B)**. In addition, liver qPCR showed that compared to the MASH-Ctrl diet, gluconeogenesis gene (Pck1) expression was decreased significantly in STAT5$^{fl/fl}$ and

STAT5^{LKO} mice under MASH dietary condition, but G6pc expression in STAT5^{LKO} mice was increased under MASH-Ctrl-fed condition **(Fig.24 C)**.

A

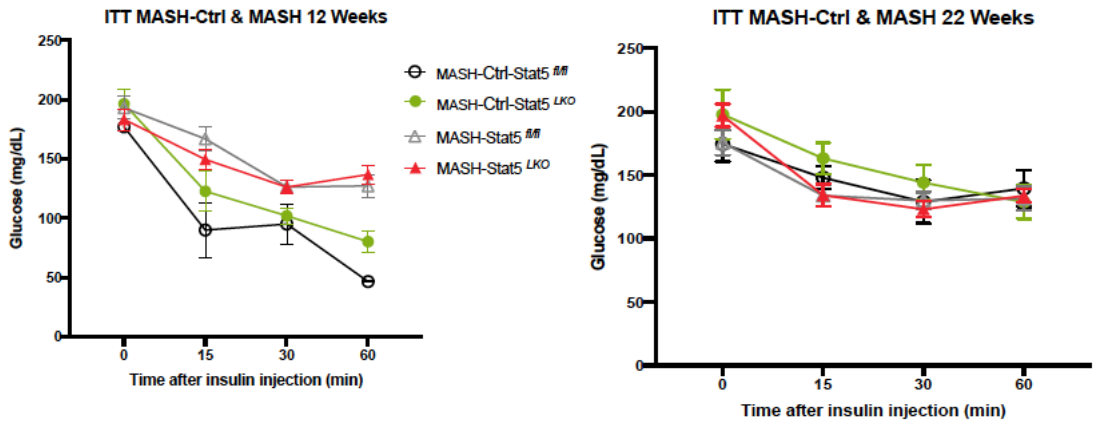

B

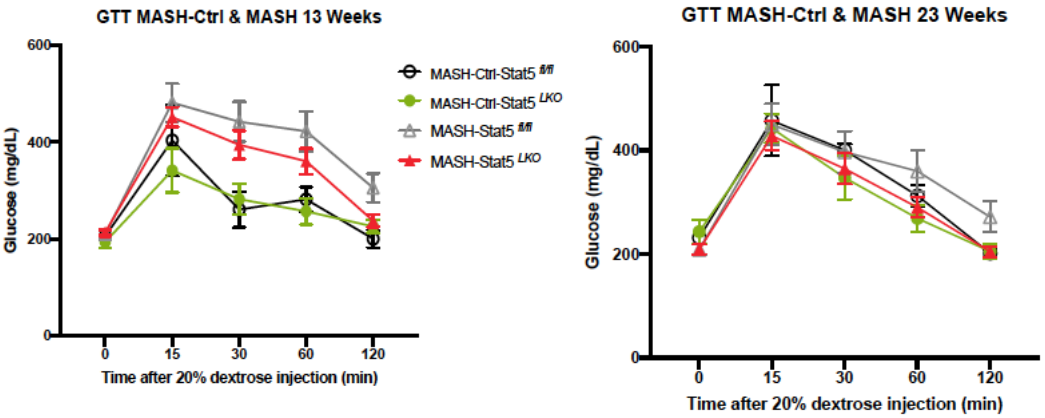

C

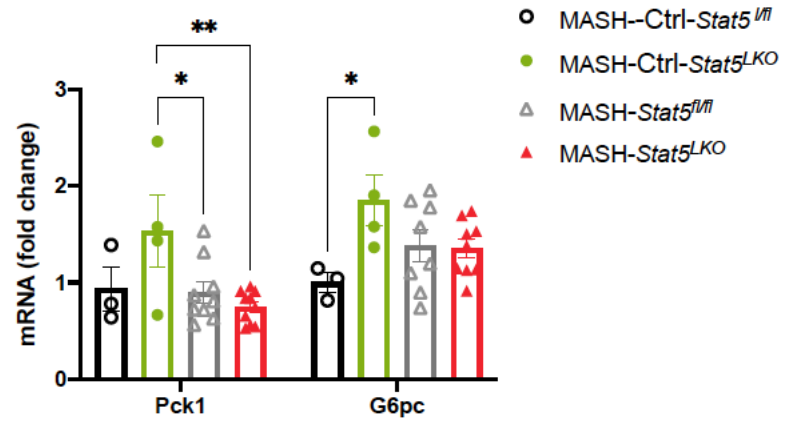

Figure 24: ITT and GTT have hardly changed under MASH-Ctrl and MASH dietary conditions. (A) Insulin tolerance was determined at 12 and 22 weeks (MASH-Ctrl-fed mice: n = 3-5, black and green lines; MASH-fed mice: n = 8-10, grey and red lines). (B) Glucose tolerance was determined at 13 and 23 weeks of age (MASH-Ctrl-fed mice: n = 3-5, black and

green lines; MASH-fed mice: n = 8-10, grey and red lines). (C) Expression of gluconeogenesis genes in mice's liver (MASH-Ctrl-fed mice: n = 3-5, black and green column; MASH-fed mice: n = 8-10, grey and red column). (Ordinary two-way ANOVA; two-tailed unpaired t-test. Mean ± SEM, p* ⩽0.05, p** ⩽ 0.01, p*** ⩽ 0.001, p**** ⩽ 0.0001).

Taken together, it seems that hepatic STAT5 deficiency fails to alter the development of insulin resistance or changes in glucose homeostasis.

4.2.8. Feeding STAT5^{LKO} Mice a Fibrotic Diet Increases Premature Lethality

Since we have observed affected fibrosis in hepatic stat5 deficient mice, we aimed at investigating fibrosis via dietary regimen. For, mouse cohorts were fed a choline deficient high fat diet that ultimately leads to fibrosis in ctrl mice. The expression of most STAT5 target and cell cycle STAT5 target genes in STAT5^{LKO} mice, such as Igf1, Socs2, Onecut1, Cish, Cdkn1b, and Cdkn2b were significantly decreased compared with the control mice, except Bcl6 that is inversely correlated with stat5 **(Fig.25 A, B)**. Thus, we conclude from this experiment that we have an efficient STAT5 knock out in the liver. The CDAA-fed STAT5^{LKO} mice showed a significant reduction in body weight after 8 weeks of age. However, this experiment had to be terminated prematurely due excessive mortality and bodyweight loss in STAT5^{LKO} mice **(Fig.25 C, D)**. The final body weight (BW) and white adipose tissue (WAT) weight were reduced significantly in CDAA-fed mice with hepatic STAT5 deficiency **(Fig.25 E, F)**.

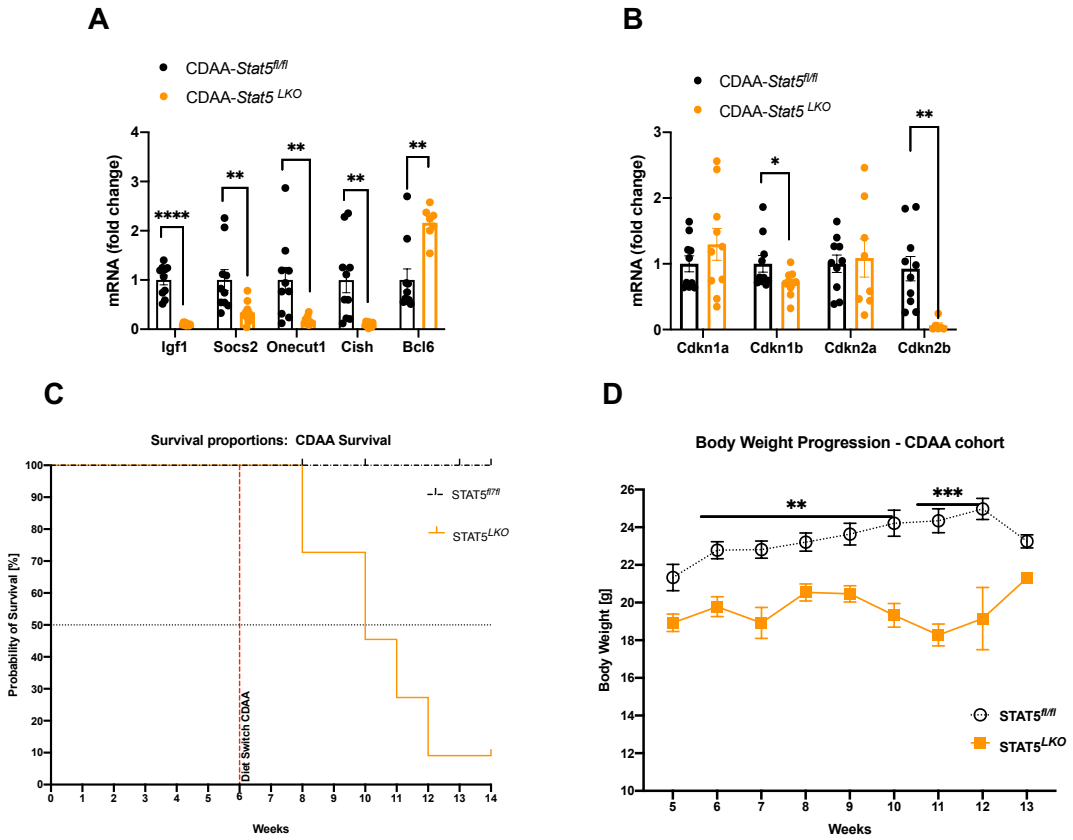

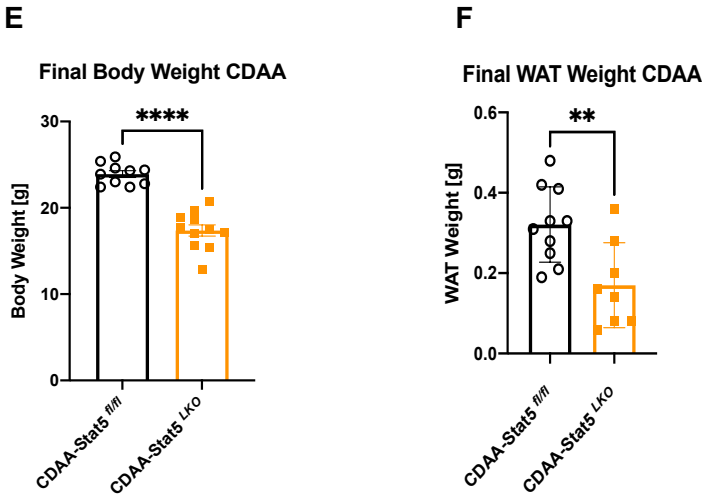

Figure 25: Increased lethality and Body weight loss in CDAA-fed STAT5LKO mice. (A) Expression of STAT5 target genes in mice's liver (n = 8-10). (B) Cell cycle STAT5 target genes are expressed in mice's liver (n = 8-10). (H) Insulin tolerance was determined at 12 weeks (n = 6-7). (C) Survival curve of Ctrl and STAT5^{LKO} mice (n = 10-11). (D) Body weight curve of Ctrl and STAT5^{LKO} mice (n = 10-11). (E) Final body weight of Ctrl and STAT5^{LKO} mice in CDAA-fed mice (n = 8-11). (F) Final WAT weight of Ctrl and STAT5^{LKO} mice in CDAA-fed mice (n = 8-11). (Ordinary two-tailed unpaired t-test. Mean ± SEM, p* ≤ 0.05, p** ≤ 0.01, p*** ≤ 0.001, p**** ≤ 0.0001).

4.2.9. STAT5^{LKO} Mice Exposed to CDAA-diet Show Altered Liver Appearance and Blood Triglyceride/Cholesterol levels

In contrast to control mice, STAT5^{LKO} mice showed apparent evidence of steatosis **(Fig.26 A).** HE stains showed that mice fed the CDAA diets developed hepatocyte necrosis and steatosis regardless of hepatocyte STAT5 inactivation **(Fig.26 B)**. In contrast, hepatic STAT5 deficiency failed to affect ALAT and ASAT in the serum of CDAA mice **(Fig.27 C)**. However, triglyceride and cholesterol levels were both significantly increased in the serum of STAT5^{LKO} mice **(Fig.26 D)**. These experiments demonstrate that feeding STAT5^{LKO} mice a CDAA diet affects liver morphology and fat uptake.

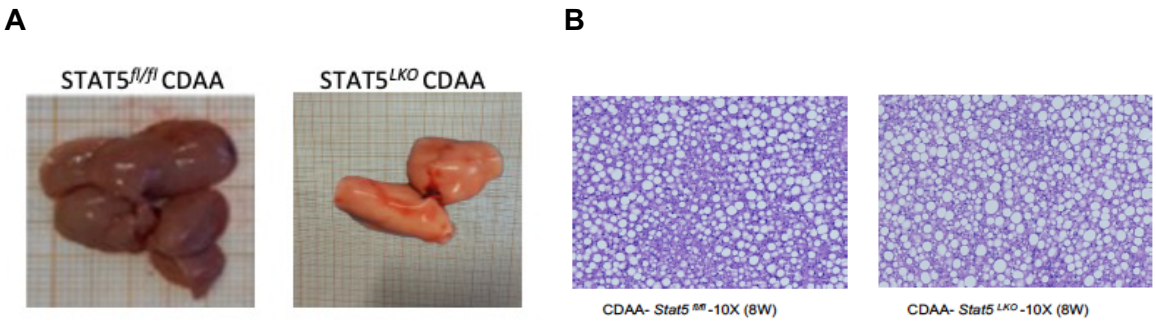

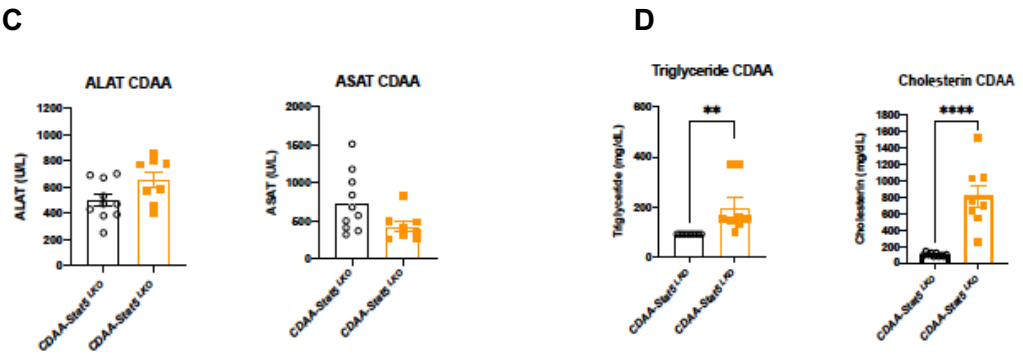

Figure 26: Body composition reveal largely altered upon CDAA-fed STAT5^{LKO} mice. (A) Representative images show that under CDAA-fed condition, STAT5^{LKO} mice liver is oilier than control mice. (B) HE stains in mice's liver: STAT5$^{fl/fl}$ (WT) and STAT5^{LKO} (TG) mice (8 weeks). (C) Serum ALAT and ASAT levels of Ctrl and STAT5^{LKO} mice at 26 weeks of (n = 9-10). (D) Serum triglyceride and cholesterol levels of Ctrl and STAT5^{LKO} mice at 26 weeks of age (n = 8-10). (Ordinary two-tailed unpaired t-test. Mean ± SEM, p* ≤ 0.05, p** ≤ 0.01, p*** ≤ 0.001, p**** ≤ 0.0001).

4.2.10. The Livers of Mice with Both Genotypes Had Significant Lipid Droplet Deposition Upon CDAA-fed Condition

Furthermore, there was no significant difference in the deposition of lipid droplets in hepatocytes of both genotypes of mice (**Fig.27 A, B)**. In addition, qPCR showed that compared to the wild-type, there was no significant difference in the expression of fat-related genes between STAT5$^{fl/fl}$ and STAT5^{LKO} mice under the choline-deficient fed condition (**Fig.27 C)**.

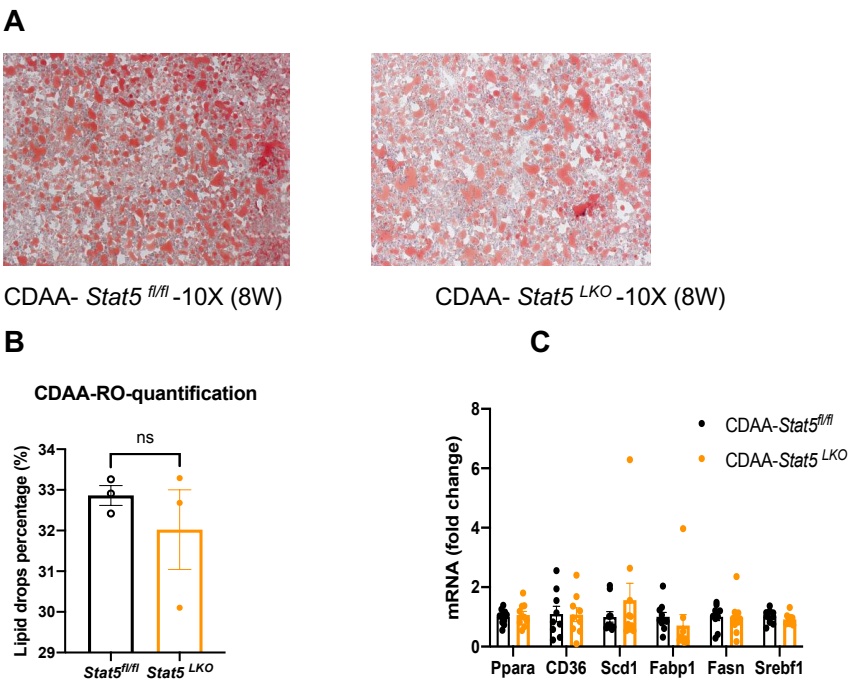

Figure 27: There was no significant difference in the deposition of lipid droplets in hepatocytes of both genotypes of mice. (A) Oil red O stains in mice's liver: STAT5$^{fl/fl}$ (WT)

and STAT5^{LKO} (TG) mice (8 weeks). (B) Oil-red O Staining Analysis by Fiji: 16bit, threshold from 0-142. (G1) Expression of Fat genes in mice's liver (n = 8-10). (C) Expression of Fat genes in mice's liver (n = 8-10). (G2) Expression of Inflammatory genes in mice's liver (n = 8-10). (Ordinary two-tailed unpaired t-test. Mean ± SEM).

4.2.11. STAT5^{LKO} Mice Reveal Expression of Inflammatory Genes Altered Upon CDAA-fed Condition

While the expression of hepatic inflammation genes such as TNFα, IFNγ, IL6, and IL1β was unaltered **(Fig.28 A)**, it seemed that there were fewer infiltrating macrophages expressing Cx3cr1 in STAT5^{LKO} mice, which in turn showed increased polarization towards the M2 Arg1-expressing phenotype **(Fig.28 B)**. Taken together, hepatic STAT5 deficiency in the fibrosis model seems to polarize macrophages towards M2, which might ameliorate fibrosis.

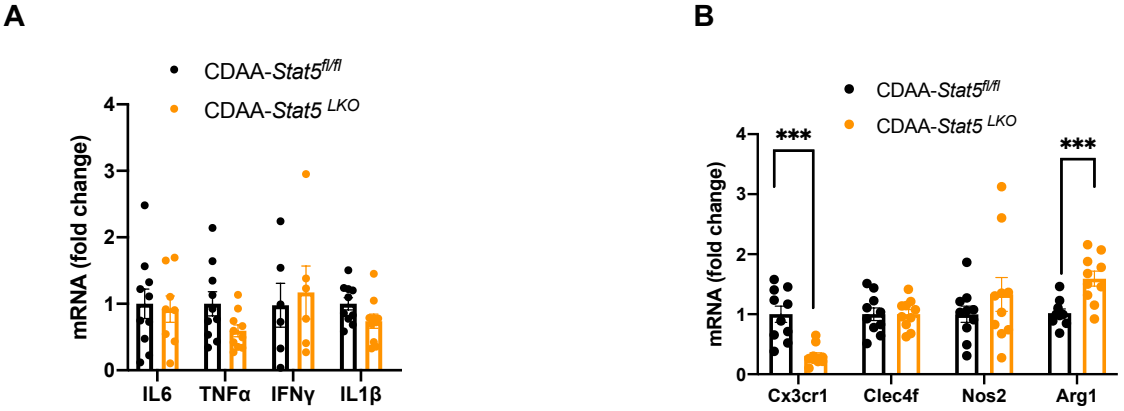

Figure 28: Expression of fibrosis gene (Cx3cr1) altered upon CDAA-fed condition. (A) Expression of Inflammatory genes in mice's liver (n = 8-10). (B) Expression of macrophage target genes in mice's liver (n = 8-10). (Ordinary two-tailed unpaired t-test. Mean ± SEM, p* ≤ 0.05, p** ≤ 0.01, p*** ≤ 0.001).

4.2.12. STAT5^{LKO} Mice Reveal Expression of Fibrosis Genes Altered Upon CDAA-fed Condition

To test this, we performed Sirius red staining of livers of mice. Red-dyed collagen fibers can be seen in both STAT5^{LKO} and the STAT5$^{fl/fl}$ mice, but reduced in STAT5^{LKO} mice (**Fig.29 A, B)**. Concomitantly, under choline deficient fed STAT5^{LKO} mice compared to the control mice, the expression of all genes associated with fibrosis was remarkably reduced **(Fig.29 C)**. Thus, these experiments clearly demonstrate that hepatic stat5 deficiency ameliorates fibrosis in CDAA diet fed conditions.

A

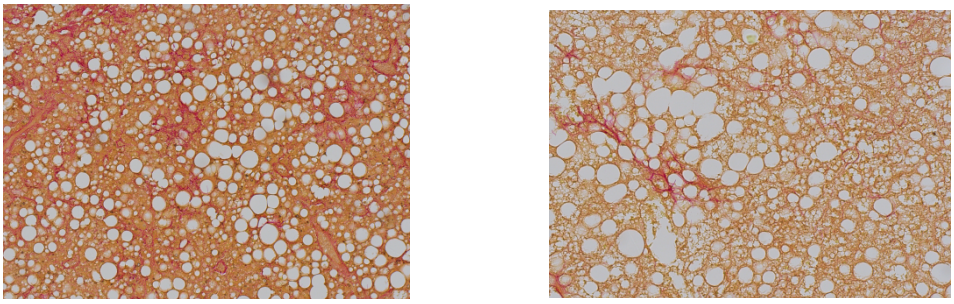

CDAA- *Stat5* $^{fl/fl}$ -10X (8W)

CDAA- *Stat5* ^{LKO} -10X (8W)

B

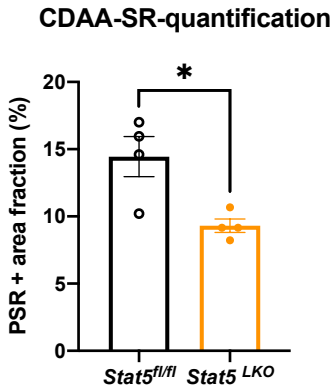

C

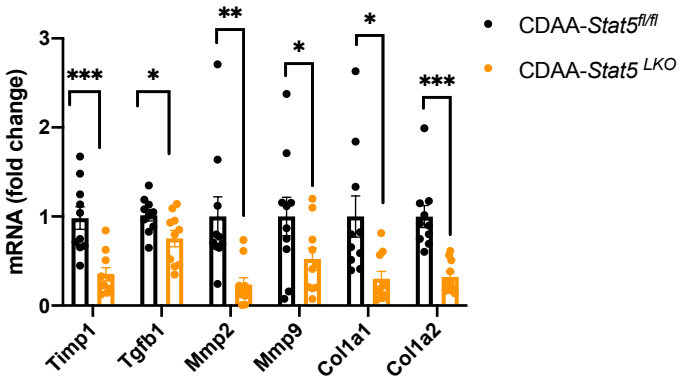

Figure 29: Expression of fibrosis genes altered upon CDAA-fed condition. (A)Sirius Red Stains in mice's liver: STAT5$^{fl/fl}$ (WT) and STAT5^{LKO} (TG) mice (8 weeks). (B) Sirius Red Staining Analysis by Fiji: 16bit, threshold from 0-156. (C) Expression of fibrosis genes in mice's liver (n = 8-10). (Two-tailed unpaired t-test. Mean ± SEM, p* ≤ 0.05, p** ≤ 0.01, p*** ≤ 0.001).

5. DISCUSSION

5.1. Generation of the Novel, sCas9-2A-AAVR Mouse Line to Target Cellular Subpopulations Without Off-Target Effects

Numerous studies have been conducted on the function of genes in vivo because of the ability to edit the mammalian genome conditionally. As a result of the characterization of conditional knockout and knock-in mice, scientists were able not only to unravel essential basic molecular mechanisms but also to translate these findings into human therapeutics[79, 80]. Genome editing is an important basic and translational research tool to investigate gene functions in health and disease.

Currently, Cre/loxP and Dre/rox recombinase-based systems and the CRISPR/Cas9 system provide countless opportunities for specifically editing the mouse genome. Particularly, when these two systems are combined in a mouse with Cre-dependent Cas9 expression, it is possible to express Cas9 conditionally (Platt et al., 2014). Combination of these recombinase systems allows for more cell type-specific activation of transgenes by utilizing overlapping promoters that drive expression of Cre and Dre with effector transgenes whose expression is prevented by two STOP cassettes that are flanked by loxP and rox sites, respectively. it is also possible to generate conditional knock-out mice by combining Cre/loxP with CRISPR Cas9 systems (REF). Here, expression of Cas9 transgene from the ROSA26 locus is prevented by a loxP-flanked stop cassette that can be excised by Cre recombinase in a cell type-specific manner. Crossing the ROSA26 fl Cas9 mice with Cre mice leads to cell type-specific expression of Cas9. Subsequently, delivery of specific gRNA via adeno-associated viral (AAV) vectors will lead to the compound expression of Cas9 and gRNA in cells of interest, thereby leading to gene inactivation. However, in the CRISPR/Cas9 system, in particular, high expression of both will lead to off-target effects where unspecific cleavage might occur to destabilize the mouse genome or to inactivate other genes. These off-target effects have often been reported, and they cannot be neglected since additional unwanted cleavage of the mouse genome might mask or alter the phenotype of CRISPR/Cas9-mediated knock-out mice. Furthermore, the genetic lesion induced by CRISPR Cas9 (which is only some base pairs) cannot be monitored, as well as that the efficiency of delivery of AAVs carrying the gRNA will depend on the cell type. All these limitations will be excluded when using our novel traffic light system. 1. Off-target effects will be reduced by inactivating sCas9, 2. Gene editing by Cas9 will result in the cell fluorescence switch from red to green (like a traffic light), 3. The inclusion of AAVR into the construct will allow for similar infection efficiencies of all cell types expressing this receptor.

5.2. AAVR Expression May Increase the Probability of ES Cells Being Infected by AAVs.

Moreover, AAV receptor (AAVR) is a universal receptor involved in AAV2 infection. It is like a protein capable of rapid endocytosis from the plasma membrane and trafficking to the trans-Golgi network. In all AAVR-overexpressing cell lines compared to wt, the susceptibility of AAV2 infection increased[73]. Therefore, we inserted AAVR into our sCAS9 tomato construct. Then, we will test it to see if the upgraded ES cells can be infected by the AAV (2a). The generated targeting construct will be inserted into the ROSA26 locus of mouse embryonic stem cells, which will then be injected into blastocysts to generate chimeric mice to acquire germline transmission in the F1 generation ultimately: the R26 fl rx sCas9P2A-AAVR E2tomato mouse strain. This mouse strain will be useful for the scientific community since it enables easy generation of knock out mice via CRISPR Cas9 without off target effects and monitoring of Cas9 gene editing.

5.3. The Cre/Dre Activatable AAV2 (2c) ZsGreen Construct Worked Nicely in Vivo.

Although AAV2s do not infect ES cells, AAV2 (2c) does infect neuron well **(Fig.30 A, B, C)**. Rui Beleza (a postdoc in our lab), used intercrosses of POMC-Dre and Lepr-Cre, and Sox14-Cre and Trh-Dre and performed ICV injections of the AAV2 (2c) virus. As expected from our in vitro data, only neurons expressing both recombinases were green fluorescent indicating that the traffic light system might work soon when R26 fl rx sCas9P2A AAVR E2Atomato mice are available **(Fig.15).**

A

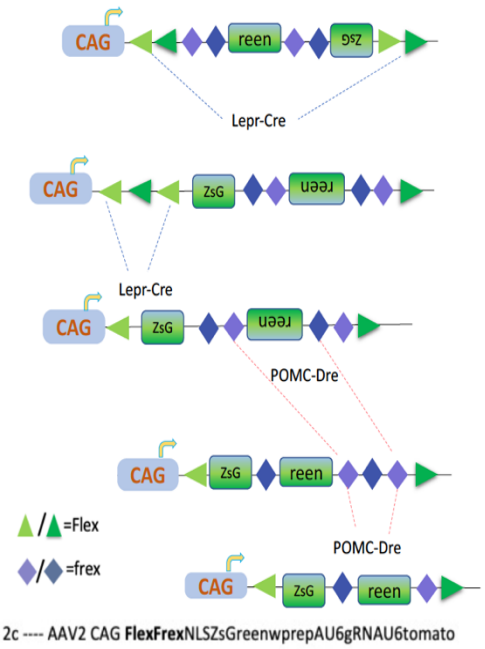

B

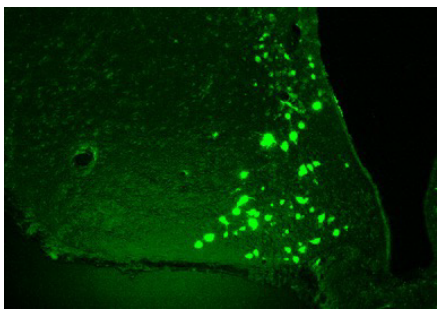

C

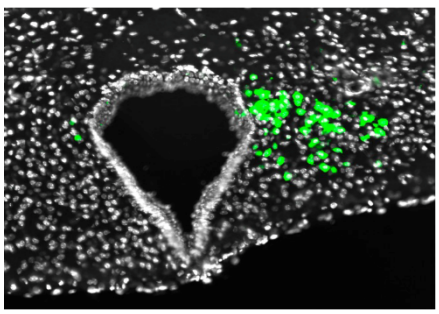

Figure 30 AAV2 (2c) worked in mouse neuron. (A) AAV2 (2c) infected a Lepr-Cre POMC-Dre and a Sox14-Cre Trh-Dre mouse brain (B) A scanning confocal image of Lepr-Cre POMC-Dre mouse brain (C) A scanning electron microscopic image of Sox14-Cre Trh-Dre mouse brain.

5.4. Disruption of Hepatic GH-STAT5 Signaling Causes a Pygmyism, Lipogenic Gene Expression Profile, and Steatosis

Deficiency of STAT5 in the liver leads to depletion of the target gene for IGF-1. Since there is no negative feedback mechanism, endogenous GH levels are high. Following GH stimulation, liver-derived IGF-1 controls postnatal body growth[81, 82]. Our study found a significant reduction in postnatal body growth in STAT5 knock-out mice with reduced IGF- levels in their livers. Similarly, the literature has also reported human patients with STAT5B missense mutations who suffer from severe growth failure[81, 82]. In addition, impaired GH-STAT5 signaling results in complex modifications in lipid and carbohydrate metabolism, resulting in an early onset but stable MASLD-like phenotype.

Our previous study revealed that in NIK knockout mice, STAT5 is activated and can inhibit free fatty acid uptake and lipogenic gene expression and instead induces hepatoprotective gene expression, leading to protection from MASH[68]. According to our experimental data, STAT5 loss and its metabolic stress led to the sensitization of hepatocytes to damage and MASH transformation. Under NCD/ MASH/ MASH-Ctrl fed conditions, compared with $STAT5^{fl/fl}$ mice, the expression of genes related to lipid anabolism such as CD36, Scd1, Fasn, and Pparαγ was elevated in $STAT5^{LKO}$ mice, and subsequent histological sections of $STAT5^{LKO}$ mice liver also showed more lipid deposits and inflammatory cell infiltration. Thus, the data presented here are in line with the work previously published by our lab.

5.5. Hepatocyte-specific STAT5 Deficiency Causes Insulin Resistance, Increased Gluconeogenesis, and Hepatic Collagen Accumulation in CDAA and MASH-diet Mice

Glucose-6-phosphatase is a key enzyme in glucose homeostasis and plays a role in gluconeogenesis and glycogenolysis. G6PC gene expression increased significantly in $STAT5^{LKO}$ mice under CDAA-fed conditions. Its upregulation leads to increased gluconeogenesis, which can cause lactic acidosis, hypertriglyceridemia, and hyperuricemia[83]. This disorder of glycolipid metabolism is likely to be the cause of premature death of CDAA-fed $STAT5^{LKO}$ mice with high triglycerides and hypercholesterolemia **(Fig.26 D)** but rapid weight loss **(Fig.25 D, E)**. Deleting hepatic STAT5 silencing causes extensive lysis of peripheral fat depots and the release of free fatty acids, which are subsequently deposited in hepatocyte lipid droplets. Cx3cr1 and Clec4f are specifically expressed by macrophages/

Kupffer cells. Two new types of research suggest that during short-term high-fat feeding, adipose tissue stem cells can induce macrophages to express a high level of Cx3cr1, thus activating the Stat3-Arg1-polyamine-EIF5a hypusination axis, which enhances autophagy of adipose-derived stem cells (ASCs) and alleviates cell senescence, hence maintaining the normal proliferation ability of adipose tissue. This interaction is disrupted by long-term high-fat feeding[84]. Moreover, Arg1 (arginase 1) is widely present in tumors, and its elevated activity is associated with advanced disease and poor clinical prognosis. Increased expression of Arg1 is a key factor in rapid tumor growth and progression. ARG1, which is derived primarily from tumor-associated macrophages (TAMs), promotes T cell depletion by degrading the expression of arginine immune checkpoints (ICs)[85]. These results are consistent with our findings in CDAA-fed mice **(Fig.27 B)**. In addition, excessive deposition of extracellular matrix (ECM) in the liver is a characteristic change of liver fibrosis. Various factors act on HSC and fiber-forming cells in the liver in different ways, leading to changes in their biology and function and liver fibrosis. Activated hepatic stellate cells (AHSC) are the central link of hepatic fibrosis[86-88]. While synthesizing ECM, HSC also secretes matrix metalloproteinases (MMPs) that degrade ECM and tissue inhibitors of metalloproteinases (TIMPs) that bind to MMPs to inactivate them. After liver injury, the continuous expression of TIMPs inhibited the activity of MMPs, while low expression of MMPs and high levels of TIMPs prevented the degradation of collagen fibers. The key enzyme in collagen fiber degradation is MMP1. Our qPCR results showed that the expressions of pro-fibrotic genes such as Timp1 and Col1as were significantly increased in NCD and MASH-Ctrl STAT5^{LKO} mice, but Timp1, Mmp2 and 9 were significantly down-regulated under CDAA and/or MASH diet conditions, indicating that: in NCD and MASH-Ctrl diet, STAT5^{LKO} mice can inhibit ECM degradation and increase collagen fiber deposition. In addition, the expression of genes that promote and inhibit fibrosis is down-regulated under a high-fat and/or choline deficiency diet (simulating MASH caused by improper diet in humans), which may be the compensatory mechanism of MASH before it progresses to liver sclerosis, which also explains why clinically MASH patients can only show hepatocyte steatosis and chronic inflammation without complicated liver fibrosis.

In general, liver fibrosis is a kind of injury-healing reaction caused by the imbalance of ECM deposition and degradation for various reasons, resulting in the change and increase of liver matrix composition and quantity. The mechanism of liver fibrosis is a complex regulatory system related to parenchymal and non-parenchymal cells and immune cells in the liver. Different causes of liver fibrosis mechanisms are different; only a comprehensive understanding of the formation of various liver fibrosis mechanisms is needed to maintain the dynamic balance of ECM better to delay or even reverse the process of liver fibrosis.

Clinically, the main pathological changes of patients with MASH include hepatic steatosis (large amounts of lipid droplet deposition), hepatocyte ballooning, and lobular inflammation,

fibrosis is not part of the histological definition of MASH. However, the degree of fibrosis (stage) in liver tissue biopsy is used as a prognostic factor, whereas the grade of inflammation and necrosis is not. The disease can persist for years in an asymptomatic stage and may progress to cirrhosis or hepatocellular carcinoma (HCC).

5.6. Hepatocyte-specific STAT5 Deficiency Upregulates the Expression of Clec4f in NCD and MASH-fed Mice.

Kupffer cells (KCs), liver capsule macrophages (LCM), and Lipid-associated Macrophages (LAM) are resident macrophages of a healthy liver. KCs can mediate inflammation or regression by becoming plastic cells responding to stimuli. In any case, how KCs are activated is a question that needs to be answered.

It was found that PCK1 could significantly up-regulate histone H3K9me3 modification of hepatoma cells under the catalysis of methyltransferase SUV39H1 and inhibit the proliferation and migration of hepatoma cells. It was confirmed that low expression of PCK1, low level of H3K9me3 modification, and high expression of S100A11 were closely related to the malignant progression of liver cancer in clinical liver cancer tissues. In a PCK1conditional knockout mouse model of liver cancer, it was verified that SAM supplementation or S100A11 knockout effectively inhibited liver cancer progression.

G6PC is abnormally expressed in a variety of cancers and is involved in tumor proliferation and metastasis.

Clec4f is identified as a specific marker for mouse KC. Still, it is only expressed late in KC development, making it challenging to recognize cells developing into KC, such as monocyte-derived KC (moKC) in the liver with the disease. Moreover, Clec4f is not conserved in humans, so identifying real human KC is still lacking. In the diseased liver, other subtypes of macrophage populations are recruited, including LAM, which is recruited to the diseased area. In two distinct models of liver disease, MASLD/MASH and acetaminophen overdose (APAP), monocytes have been shown to localize to specific damage areas and differentiate into LAM[89]. In MASH, these cells replace dying KCs in areas of steatosis and fibrosis, while the few KCs lost from areas of less steatosis/fibrosis are replaced by MOKCs. In addition to KC death, LAM-like KC phenotypes have also been reported in fibrosis models of MASH, suggesting that KCS may sense the same signals as infiltrating LAM before their death, resulting in a mixed LAM-like KC phenotype. Similarly, LAM-like KC is present around the damaged area of the central vein of APAP, and LAM also develops around the central vein. It may interact with activated fibroblasts, necrotic hepatocytes, and other recruited cells such as neutrophils or CDCS. It is also suggested that LAM can be protective by promoting tissue repair[90]. In our STAT5^{LKO} mice, the expression of Clec4f increased significantly compared with Ctrl mice **(Fig.19 B)**. In conclusion, hepatocyte-specific STAT5 deficiency can significantly decrease body length and weight, causing mild liver hepatocyte damage, steatosis, and a small amount of collagen fiber

hyperplasia. CDAA-fed can easily cause dyslipidemia and insulin resistance. Interestingly, on a high fat, high cholesterol, and high fructose diet (MASH diet), hepatic STAT5 deficiency may promote M1 macrophage polarization, which in turn affects hepatic stellate cells to increase fibrosis. But the absence of hepatic STAT5 in the fibrosis model (CDAA diet) appears to polarize macrophages toward M2, which may alleviate fibrosis. The further pathogenesis and specific cell types will be explored in our next experiments.

In our previous study, the NIK^{HKO} mice were protected from MASH, and NIK^{HKO} mice showed increased STAT5 signaling. NIK^{HKO} mice show upregulation of multiple STAT5-related genes in AHSC and macrophages. Therefore, STAT5 may have a cell-type-specific role in AHSC and macrophages and might be regulated by NIK. In the future, STAT5/ NIK KO in Macrophages (Clec4f-Cre) and STAT5/ NIK KO in AHSC (Lrat-Cre) mice will be performed in our experiment. The function of STAT5 in activated hepatic stellate cells (AHSC) and liver resident macrophages will be investigated to identify the cell type-specific role of NIK and STAT5 during MASH.

Given the limited number of current treatments in MASLD, there is an urgent need to clarify potential therapeutic targets and develop effective drug therapies. As a result of our studies, we will better understand the crosstalk between hepatocytes, macrophages, and AHSCs in glucose and lipid metabolism, as well as how MASH progresses to HCC.

6. REFERENCE

1. Rajewsky K, Gu H, Kuhn R, Betz UA, Muller W, Roes J, et al. Conditional gene targeting. J Clin Invest. 1996;98(3):600-3.
2. Sauer B, Henderson N. Site-specific DNA recombination in mammalian cells by the Cre recombinase of bacteriophage P1. Proc Natl Acad Sci U S A. 1988;85(14):5166-70.
3. O'Neil KT, Hoess RH, DeGrado WF. Design of DNA-binding peptides based on the leucine zipper motif. Science. 1990;249(4970):774-8.
4. Gu H, Zou YR, Rajewsky K. Independent control of immunoglobulin switch recombination at individual switch regions evidenced through Cre-loxP-mediated gene targeting. Cell. 1993;73(6):1155-64.
5. Hall B, Limaye A, Kulkarni AB. Overview: generation of gene knockout mice. Curr Protoc Cell Biol. 2009;Chapter 19:Unit 19 2 2 1-7.
6. Gossen M, Freundlieb S, Bender G, Muller G, Hillen W, Bujard H. Transcriptional activation by tetracyclines in mammalian cells. Science. 1995;268(5218):1766-9.
7. Sprengel R, Hasan MT. Tetracycline-controlled genetic switches. Handb Exp Pharmacol. 2007(178):49-72.
8. Chuang K, Nguyen E, Sergeev Y, Badea TC. Novel Heterotypic Rox Sites for Combinatorial Dre Recombination Strategies. G3 (Bethesda). 2015;6(3):559-71.
9. Li H, Zhang Q, Gu Y, Wu Y, Wang Y, Wang L, et al. Efficient photoactivatable Dre recombinase for cell type-specific spatiotemporal control of genome engineering in the mouse. Proc Natl Acad Sci U S A. 2020;117(52):33426-35.
10. Zambrowicz BP, Imamoto A, Fiering S, Herzenberg LA, Kerr WG, Soriano P. Disruption of overlapping transcripts in the ROSA beta geo 26 gene trap strain leads to widespread expression of beta-galactosidase in mouse embryos and hematopoietic cells. Proc Natl Acad Sci U S A. 1997;94(8):3789-94.
11. Voss AK, Thomas T, Gruss P. Efficiency assessment of the gene trap approach. Dev Dyn. 1998;212(2):171-80.
12. Belgardt BF, Husch A, Rother E, Ernst MB, Wunderlich FT, Hampel B, et al. PDK1 deficiency in POMC-expressing cells reveals FOXO1-dependent and -independent pathways in control of energy homeostasis and stress response. Cell Metab. 2008;7(4):291-301.
13. Petyuk V, McDermott J, Cook M, Sauer B. Functional mapping of Cre recombinase by pentapeptide insertional mutagenesis. J Biol Chem. 2004;279(35):37040-8.
14. Biglari N, Gaziano I, Schumacher J, Radermacher J, Paeger L, Klemm P, et al. Functionally distinct POMC-expressing neuron subpopulations in hypothalamus revealed by intersectional targeting. Nat Neurosci. 2021;24(7):913-29.

15. Tao P, Wu X, Rao V. Unexpected evolutionary benefit to phages imparted by bacterial CRISPR-Cas9. Sci Adv. 2018;4(2):eaar4134.
16. Brouns SJ, Jore MM, Lundgren M, Westra ER, Slijkhuis RJ, Snijders AP, et al. Small CRISPR RNAs guide antiviral defense in prokaryotes. Science. 2008;321(5891):960-4.
17. Richter C, Chang JT, Fineran PC. Function and regulation of clustered regularly interspaced short palindromic repeats (CRISPR) / CRISPR associated (Cas) systems. Viruses. 2012;4(10):2291-311.
18. Hryhorowicz M, Lipinski D, Zeyland J, Slomski R. CRISPR/Cas9 Immune System as a Tool for Genome Engineering. Arch Immunol Ther Exp (Warsz). 2017;65(3):233-40.
19. Hashemi A. CRISPR-Cas9/CRISPRi tools for cell factory construction in E. coli. World J Microbiol Biotechnol. 2020;36(7):96.
20. Bhaya D, Davison M, Barrangou R. CRISPR-Cas systems in bacteria and archaea: versatile small RNAs for adaptive defense and regulation. Annu Rev Genet. 2011;45:273-97.
21. Cong L, Ran FA, Cox D, Lin S, Barretto R, Habib N, et al. Multiplex genome engineering using CRISPR/Cas systems. Science. 2013;339(6121):819-23.
22. Sander JD, Joung JK. CRISPR-Cas systems for editing, regulating and targeting genomes. Nat Biotechnol. 2014;32(4):347-55.
23. Hwang WY, Fu Y, Reyon D, Maeder ML, Tsai SQ, Sander JD, et al. Efficient genome editing in zebrafish using a CRISPR-Cas system. Nat Biotechnol. 2013;31(3):227-9.
24. Adli M. The CRISPR tool kit for genome editing and beyond. Nat Commun. 2018;9(1):1911.
25. Platt RJ, Chen S, Zhou Y, Yim MJ, Swiech L, Kempton HR, et al. CRISPR-Cas9 knockin mice for genome editing and cancer modeling. Cell. 2014;159(2):440-55.
26. Anzalone AV, Randolph PB, Davis JR, Sousa AA, Koblan LW, Levy JM, et al. Search-and-replace genome editing without double-strand breaks or donor DNA. Nature. 2019;576(7785):149-57.
27. Adiego-Perez B, Randazzo P, Daran JM, Verwaal R, Roubos JA, Daran-Lapujade P, et al. Multiplex genome editing of microorganisms using CRISPR-Cas. FEMS Microbiol Lett. 2019;366(8):fnz086.
28. Chu VT, Graf R, Wirtz T, Weber T, Favret J, Li X, et al. Efficient CRISPR-mediated mutagenesis in primary immune cells using CrispRGold and a C57BL/6 Cas9 transgenic mouse line. Proc Natl Acad Sci U S A. 2016;113(44):12514-9.
29. Xu J, Bartolome CL, Low CS, Yi X, Chien CH, Wang P, et al. Genetic identification of leptin neural circuits in energy and glucose homeostases. Nature. 2018;556(7702):505-9.
30. Slaymaker IM, Gao L, Zetsche B, Scott DA, Yan WX, Zhang F. Rationally engineered Cas9 nucleases with improved specificity. Science. 2016;351(6268):84-8.

31. Zarghamravanbakhsh P, Frenkel M, Poretsky L. Metabolic causes and consequences of nonalcoholic fatty liver disease (NAFLD). Metabol Open. 2021;12:100149.
32. Yanai H, Adachi H, Hakoshima M, Iida S, Katsuyama H. Metabolic-Dysfunction-Associated Steatotic Liver Disease-Its Pathophysiology, Association with Atherosclerosis and Cardiovascular Disease, and Treatments. Int J Mol Sci. 2023;24(20):15473.
33. Severson TJ, Besur S, Bonkovsky HL. Genetic factors that affect nonalcoholic fatty liver disease: A systematic clinical review. World J Gastroenterol. 2016;22(29):6742-56.
34. Chan WK, Chuah KH, Rajaram RB, Lim LL, Ratnasingam J, Vethakkan SR. Metabolic Dysfunction-Associated Steatotic Liver Disease (MASLD): A State-of-the-Art Review. J Obes Metab Syndr. 2023;32(3):197-213.
35. Younossi ZM, Koenig AB, Abdelatif D, Fazel Y, Henry L, Wymer M. Global epidemiology of nonalcoholic fatty liver disease-Meta-analytic assessment of prevalence, incidence, and outcomes. Hepatology. 2016;64(1):73-84.
36. Younossi Z, Anstee QM, Marietti M, Hardy T, Henry L, Eslam M, et al. Global burden of NAFLD and NASH: trends, predictions, risk factors and prevention. Nat Rev Gastroenterol Hepatol. 2018;15(1):11-20.
37. Friedman SL, Neuschwander-Tetri BA, Rinella M, Sanyal AJ. Mechanisms of NAFLD development and therapeutic strategies. Nat Med. 2018;24(7):908-22.
38. Kim DY, Park JY. Overview of emerging treatment of non-alcoholic fatty liver disease: more than one drug needed? Hepatobiliary Surg Nutr. 2019;8(5):522-4.
39. Huby T, Gautier EL. Immune cell-mediated features of non-alcoholic steatohepatitis. Nat Rev Immunol. 2022;22(7):429-43.
40. Li H, Zhou Y, Wang H, Zhang M, Qiu P, Zhang M, et al. Crosstalk Between Liver Macrophages and Surrounding Cells in Nonalcoholic Steatohepatitis. Front Immunol. 2020;11:1169.
41. Wilhelm A, Shepherd EL, Amatucci A, Munir M, Reynolds G, Humphreys E, et al. Interaction of TWEAK with Fn14 leads to the progression of fibrotic liver disease by directly modulating hepatic stellate cell proliferation. J Pathol. 2016;239(1):109-21.
42. Pflug KM, Sitcheran R. Targeting NF-kappaB-Inducing Kinase (NIK) in Immunity, Inflammation, and Cancer. Int J Mol Sci. 2020;21(22):8470.
43. Xiao G, Harhaj EW, Sun SC. NF-kappaB-inducing kinase regulates the processing of NF-kappaB2 p100. Mol Cell. 2001;7(2):401-9.
44. Senftleben U, Cao Y, Xiao G, Greten FR, Krahn G, Bonizzi G, et al. Activation by IKKalpha of a second, evolutionary conserved, NF-kappa B signaling pathway. Science. 2001;293(5534):1495-9.
45. Kiu H, Nicholson SE. Biology and significance of the JAK/STAT signalling pathways. Growth Factors. 2012;30(2):88-106.

46. Rampal R, Al-Shahrour F, Abdel-Wahab O, Patel JP, Brunel JP, Mermel CH, et al. Integrated genomic analysis illustrates the central role of JAK-STAT pathway activation in myeloproliferative neoplasm pathogenesis. Blood. 2014;123(22):e123-33.
47. Zitman-Gal T, Einbinder Y, Ohana M, Katzav A, Kartawy A, Benchetrit S. Effect of liraglutide on the Janus kinase/signal transducer and transcription activator (JAK/STAT) pathway in diabetic kidney disease in db/db mice and in cultured endothelial cells. J Diabetes. 2019;11(8):656-64.
48. Romero CJ, Pine-Twaddell E, Sima DI, Miller RS, He L, Wondisford F, et al. Insulin-like growth factor 1 mediates negative feedback to somatotroph GH expression via POU1F1/CREB binding protein interactions. Mol Cell Biol. 2012;32(21):4258-69.
49. Furigo IC, de Souza GO, Teixeira PDS, Guadagnini D, Frazao R, List EO, et al. Growth hormone enhances the recovery of hypoglycemia via ventromedial hypothalamic neurons. FASEB J. 2019;33(11):11909-24.
50. Trifunovic S, Lakic I, Vujovic P, Jevdjovic T, Sosic-Jurjevic B, Milosevic V, et al. Morphofunctional parameters of rat somatotrophes after acute and repeated immobilization or restraint stress. Acta Histochem. 2019;121(1):29-34.
51. Kopchick JJ, Berryman DE, Puri V, Lee KY, Jorgensen JOL. The effects of growth hormone on adipose tissue: old observations, new mechanisms. Nat Rev Endocrinol. 2020;16(3):135-46.
52. Rowland JE, Lichanska AM, Kerr LM, White M, d'Aniello EM, Maher SL, et al. In vivo analysis of growth hormone receptor signaling domains and their associated transcripts. Mol Cell Biol. 2005;25(1):66-77.
53. Held MA, Cosme-Blanco W, Difedele LM, Bonkowski EL, Menon RK, Denson LA. Alterations in growth hormone receptor abundance regulate growth hormone signaling in murine obstructive cholestasis. Am J Physiol Gastrointest Liver Physiol. 2005;288(5):G986-93.
54. Waters MJ, Hoang HN, Fairlie DP, Pelekanos RA, Brown RJ. New insights into growth hormone action. J Mol Endocrinol. 2006;36(1):1-7.
55. Schaefer F, Yoon SA, Nouri P, Tsao T, Tummala P, Deng E, et al. Growth hormone-mediated janus associated kinase-signal transducers and activators of transcription signaling in the growth hormone-resistant potassium-deficient rat. J Am Soc Nephrol. 2004;15(9):2299-306.
56. Hennighausen L, Robinson GW. Interpretation of cytokine signaling through the transcription factors STAT5A and STAT5B. Genes Dev. 2008;22(6):711-21.
57. Lin M, Ku AT, Dong J, Yue F, Jiang W, Ibrahim AA, et al. STAT5 confers lactogenic properties in breast tumorigenesis and restricts metastatic potential. Oncogene. 2022;41(48):5214-22.

58. Santos SJ, Haslam SZ, Conrad SE. Estrogen and progesterone are critical regulators of Stat5a expression in the mouse mammary gland. Endocrinology. 2008;149(1):329-38.
59. Hao P, Waxman DJ. STAT5 Regulation of Sex-Dependent Hepatic CpG Methylation at Distal Regulatory Elements Mapping to Sex-Biased Genes. Mol Cell Biol. 2021;41(2):e00166-20.
60. Aaronson DS, Horvath CM. A road map for those who don't know JAK-STAT. Science. 2002;296(5573):1653-5.
61. Levy DE, Darnell JE, Jr. Stats: transcriptional control and biological impact. Nat Rev Mol Cell Biol. 2002;3(9):651-62.
62. Rani A, Murphy JJ. STAT5 in Cancer and Immunity. J Interferon Cytokine Res. 2016;36(4):226-37.
63. Liu X, Robinson GW, Wagner KU, Garrett L, Wynshaw-Boris A, Hennighausen L. Stat5a is mandatory for adult mammary gland development and lactogenesis. Genes Dev. 1997;11(2):179-86.
64. Barclay JL, Nelson CN, Ishikawa M, Murray LA, Kerr LM, McPhee TR, et al. GH-dependent STAT5 signaling plays an important role in hepatic lipid metabolism. Endocrinology. 2011;152(1):181-92.
65. Sen B, Peng S, Woods DM, Wistuba I, Bell D, El-Naggar AK, et al. STAT5A-mediated SOCS2 expression regulates Jak2 and STAT3 activity following c-Src inhibition in head and neck squamous carcinoma. Clin Cancer Res. 2012;18(1):127-39.
66. Lv Y, Xie X, Zou G, Kong M, Yang J, Chen J, et al. SOCS2 inhibits hepatoblastoma metastasis via downregulation of the JAK2/STAT5 signal pathway. Sci Rep. 2023;13(1):21814.
67. Kaltenecker D, Themanns M, Mueller KM, Spirk K, Suske T, Merkel O, et al. Hepatic growth hormone - JAK2 - STAT5 signalling: Metabolic function, non-alcoholic fatty liver disease and hepatocellular carcinoma progression. Cytokine. 2019;124:154569.
68. Vesting AJ, Jais A, Klemm P, Steuernagel L, Wienand P, Fog-Tonnesen M, et al. NIK/MAP3K14 in hepatocytes orchestrates NASH to hepatocellular carcinoma progression via JAK2/STAT5 inhibition. Mol Metab. 2022;66:101626.
69. Carter-Su C, Rui L, Herrington J. Role of the tyrosine kinase JAK2 in signal transduction by growth hormone. Pediatr Nephrol. 2000;14(7):550-7.
70. Liu J, Wang F, Luo F. The Role of JAK/STAT Pathway in Fibrotic Diseases: Molecular and Cellular Mechanisms. Biomolecules. 2023;13(1):119.
71. Livak KJ, Schmittgen TD. Analysis of relative gene expression data using real-time quantitative PCR and the 2(-Delta Delta C(T)) Method. Methods. 2001;25(4):402-8.
72. Ellis BL, Hirsch ML, Barker JC, Connelly JP, Steininger RJ, 3rd, Porteus MH. A survey of ex vivo/in vitro transduction efficiency of mammalian primary cells and cell lines with Nine

natural adeno-associated virus (AAV1-9) and one engineered adeno-associated virus serotype. Virol J. 2013;10:74.
73. Pillay S, Meyer NL, Puschnik AS, Davulcu O, Diep J, Ishikawa Y, et al. An essential receptor for adeno-associated virus infection. Nature. 2016;530(7588):108-12.
74. Cui Y, Riedlinger G, Miyoshi K, Tang W, Li C, Deng CX, et al. Inactivation of Stat5 in mouse mammary epithelium during pregnancy reveals distinct functions in cell proliferation, survival, and differentiation. Mol Cell Biol. 2004;24(18):8037-47.
75. Kellendonk C, Opherk C, Anlag K, Schutz G, Tronche F. Hepatocyte-specific expression of Cre recombinase. Genesis. 2000;26(2):151-3.
76. Friedbichler K, Themanns M, Mueller KM, Schlederer M, Kornfeld JW, Terracciano LM, et al. Growth-hormone-induced signal transducer and activator of transcription 5 signaling causes gigantism, inflammation, and premature death but protects mice from aggressive liver cancer. Hepatology. 2012;55(3):941-52.
77. Mueller KM, Kornfeld JW, Friedbichler K, Blaas L, Egger G, Esterbauer H, et al. Impairment of hepatic growth hormone and glucocorticoid receptor signaling causes steatosis and hepatocellular carcinoma in mice. Hepatology. 2011;54(4):1398-409.
78. Jiang Y, Tao Y, Zhang X, Wei X, Li M, He X, et al. Loss of STAT5A promotes glucose metabolism and tumor growth through miRNA-23a-AKT signaling in hepatocellular carcinoma. Mol Oncol. 2021;15(2):710-24.
79. Szlachta K, Kuscu C, Tufan T, Adair SJ, Shang S, Michaels AD, et al. CRISPR knockout screening identifies combinatorial drug targets in pancreatic cancer and models cellular drug response. Nat Commun. 2018;9(1):4275.
80. Wei X, Yang J, Adair SJ, Ozturk H, Kuscu C, Lee KY, et al. Targeted CRISPR screening identifies PRMT5 as synthetic lethality combinatorial target with gemcitabine in pancreatic cancer cells. Proc Natl Acad Sci U S A. 2020;117(45):28068-79.
81. Brooks AJ, Waters MJ. The growth hormone receptor: mechanism of activation and clinical implications. Nat Rev Endocrinol. 2010;6(9):515-25.
82. Waters MJ. The growth hormone receptor. Growth Horm IGF Res. 2016;28:6-10.
83. Cao J, Choi M, Guadagnin E, Soty M, Silva M, Verzieux V, et al. mRNA therapy restores euglycemia and prevents liver tumors in murine model of glycogen storage disease. Nat Commun. 2021;12(1):3090.
84. Zhou Z, Zhang H, Tao Y, Jie H, Zhao J, Zang J, et al. CX3CR1(hi) macrophages sustain metabolic adaptation by relieving adipose-derived stem cell senescence in visceral adipose tissue. Cell Rep. 2023;42(5):112424.
85. Lv Y, Li M, Weng L, Huang H, Mao Y, Yang DA, et al. Ginseng-derived nanoparticles reprogram macrophages to regulate arginase-1 release for ameliorating T cell exhaustion in tumor microenvironment. J Exp Clin Cancer Res. 2023;42(1):322.

86. Zhao YQ, Deng XW, Xu GQ, Lin J, Lu HZ, Chen J. Mechanical homeostasis imbalance in hepatic stellate cells activation and hepatic fibrosis. Front Mol Biosci. 2023;10:1183808.
87. Schuppan D, Ruehl M, Somasundaram R, Hahn EG. Matrix as a modulator of hepatic fibrogenesis. Semin Liver Dis. 2001;21(3):351-72.
88. Casari M, Siegl D, Deppermann C, Schuppan D. Macrophages and platelets in liver fibrosis and hepatocellular carcinoma. Front Immunol. 2023;14:1277808.
89. Krenkel O, Hundertmark J, Abdallah AT, Kohlhepp M, Puengel T, Roth T, et al. Myeloid cells in liver and bone marrow acquire a functionally distinct inflammatory phenotype during obesity-related steatohepatitis. Gut. 2020;69(3):551-63.
90. Guilliams M, Scott CL. Liver macrophages in health and disease. Immunity. 2022;55(9):1515-29.